REVIEW OF THE LOWER ORDOVICIAN ELLENBURGER GROUP OF THE PERMIAN BASIN, WEST TEXAS

Robert Loucks

Bureau of Economic Geology
Jackson School of Geosciences
The University of Texas at Austin
Austin, TX

ABSTRACT

The Ellenburger Group of the West Texas Permian Basin is part of a Lower Ordovician carbonate platform sequence that covers a large area of the United States. During the Early Ordovician, the Permian Basin area was located on the southwest edge of the Laurentia plate between 20° and 30° latitude. The equator crossed northern Canada, situating Texas in a tropical to subtropical latitude. The area of Texas was a shallow-water shelf, with deeper water conditions to the south where it bordered the Iapetus Ocean.

Shallow-water carbonates were deposited on the shelf, and deep-water shales and carbonates were deposited on the slope and in the basin. The interior of the shelf produced restricted environments, whereas the outer shelf produced open-marine conditions. Diagenesis of the Ellenburger Group is complex, and the processes that produced the diagenesis spanned millions of years. Three major diagenetic processes strongly affected Ellenburger carbonates: (1) dolomitization, (2) karsting, and (3) tectonic fracturing. Pore networks in the Ellenburger are complex because of the amount of brecciation and fracturing associated with karsting. Networks can consist of any combination of the following pore types, depending on depth of burial: (1) matrix, (2) cavernous, (3) interclast, (4) crackle-/mosaic-breccia fractures, or (5) tectonic-related fractures.

The Ellenburger Group is an ongoing, important exploration target in West Texas. Carbonate depositional systems within the Ellenburger Group are relatively simple; however, the diagenetic overprint is complex, producing strong spatial heterogeneity within the reservoir systems.

INTRODUCTION

The Ellenburger Group of the Permian Basin is part of a Lower Ordovician carbonate platform sequence that covers a large area of the United States (Figures 1, 2) (Ross, 1976; Kerans, 1988, 1990). It is well known for being one of the largest shallow-water carbonate platforms in the geologic record (covering thousands of square miles and as much as 500 mi wide in West Texas), being extensively karsted at the Sauk unconformity, with its widespread hydrocarbon production. Hydrocarbon production ranges from as shallow as 856 ft in West Era field in Cooke County, Texas, to as deep as 25,735 ft in McComb field in Pecos County, Texas. A review of the Ellenburger Group will help explain the sedimentology and diagenesis that have resulted in this widespread producing unit.

The first inclusive studies of the Ellenburger Group were completed by Cloud et al. (1945), Cloud and Barnes (1948, 1957), and Barnes et al. (1959). These studies cover many aspects of the group, ranging from stratigraphy to diagenesis to chemistry. Much has been learned since then about carbonate sedimentology and diagenesis, and these new concepts were integrated into later studies by Kerans (1988, 1989), which cover regional geologic setting, depositional systems, facies analysis, depositional history, diagenesis, and paleokarsting. Many other papers have described the local geology of fields (e.g., Loucks and Anderson, 1980, 1985; Combs et al., 2003) and outcrop areas (e.g., Goldhammer et al., 1992; Lucia, 1995, 1996; Loucks et al., 2004) or have elaborated on paleokarsting (e.g., Lucia, 1971, 1995, 1996; Loucks and Anderson, 1985; Kerans, 1988, 1989, 1990; Candelaria and Reed, 1992; Loucks and Handford, 1992; Loucks, 1999; Loucks et al., 2004; Loucks, 2007; McDonnell et al., 2007).

Major objectives of this paper are to review (1) regional geological setting and general stratigraphy; (2) depositional systems, facies analysis, and depositional history; (3) general regional diagenesis; (4) reservoir characteristics; and (5) the petroleum system. Many of the data are from published literature; however, new insights can be derived by integrating these data.

REGIONAL GEOLOGICAL SETTING

At global plate scale during the Early Ordovician, the West Texas Permian Basin area was located on the southwest edge of the Laurentia plate between 20° and 30° latitude (Figure 1) (Blakey, 2005a, b). The equator crossed northern Canada (Figure 1), situating Texas in a tropical to subtropical latitude (Lindsay and Koskelin, 1993). Much of the United States was covered by a shallow sea. Most of Texas was a shallow-water shelf with deeper water conditions to the south, where it bordered the Iapetus Ocean. The Texas Arch (Figures 2), a large land complex, existed in North Texas and New Mexico.

Ross (1976) and Kerans (1990) pointed out that the main depositional settings within the Permian Basin for the Ellenburger Group were the deeper water slope and the shallower water carbonate platform. Ross (1976) presented the broad Lower Ordovician carbonate platform as having an interior of dolomite and an outer area of limestone (Figure 2). Seaward of the limestone he postulated black shale. Kerans (1990) interpreted Ross's map in terms of depositional settings (Figure 3), the dolomite being a restricted shelf interior and the limestone being an outer rim of more open-shelf deposits. Seaward of the platform was a deeper water slope system (shales), which Kerans (1990) claimed to be represented by the Marathon Limestone. The Ellenburger Group in the south part of Texas, where the deeper water equivalent strata would have been, was strongly affected by the Ouachita Orogeny when the South American plate was thrust against the North American plate (Figure 2). Basinal and slope facies strata were destroyed or extensively structurally deformed. Ellenburger Group facies cannot be traced south of the slope setting in southwest Texas because of the Ouachita Orogeny.

Kerans (1990) recognized that several peripheral structural features affected deposition of Ellenburger sediments in the West Texas New Mexico area (Figure 4); however, most of the platform was relatively flat. Major structural features in the area that formed after Early Ordovician time include the Middle Ordovician Toboas Basin and the Pennsylvanian Central Basin Platform (Galley, 1958).

Structural maps of the top Ellenburger Group (Figure 5) and top Precambrian intervals (Figure 6) show the Ellenburger Group as a structural low in the area of the Permian Basin. In the Midland Basin area, the top of Ellenburger carbonate is as deep as

11,000 ft, shallower over the Central Basin Platform, and as deep as 25,000 ft in the Delaware Basin. Isopach maps (Figure 4) by the Texas Water Development Board (1972), Wilson (1993), and Lindsay and Koskelin (1993) show thickening of the Ellenburger Group into the area of the Permian Basin.

GENERAL STRATIGRAPHY

The Ellenburger Group is equivalent to the El Paso Group in the Franklin Mountains, the Arbuckle Group in northeast Texas and Midcontinent, the Knox Group in the eastern United States, and the Beekmantown Group of the northeastern United States. In West Texas the Ellenburger Group overlies the Cambrian Bliss subarkosic sandstone (Loucks and Anderson, 1980). In the Llano area, Barnes et al. (1959) divided the Ellenburger Group from bottom to top into the Tanyard, Gorman, and Honeycut Formations. Kerans (1990) compared the Llano stratigraphic section to the subsurface stratigraphy of West Texas (Figure 7). A worldwide hiatus appeared at the end of Early Ordovician deposition, creating an extensive second-order unconformity (Sauk-Tippecanoe Supersequence Boundary defined by Sloss [1963]; Figure 7). This unconformity produced extensive karsting throughout the United States and is discussed later in this paper. In West Texas, the upper Middle Ordovician Simpson Group was deposited above this unconformity (Figure 7).

A general second-order sequence stratigraphic framework was proposed by Kupecz (1992) for the Ellenburger Group in West Texas (Figure 8). The contact between the Precambrian and the Lower Ordovician intervals represents a lowstand of sea level of unknown duration; the Bliss Sandstone sediments are partly lowstand erosional deposits (Loucks and Anderson, 1985). The lower second-order transgressive systems tract includes the Bliss Sandstone and the lower Ellenburger alluvial fan to interbedded shallow-subtidal paracycles. The second-order highstand systems tracts include the upper interbedded paracycles of peritidal deposits. The next second-order lowstand produced the Sauk-Tippecanoe sequence boundary.

A detailed sequence stratigraphy of the Lower Ordovician of West Texas (Figure 9) was worked out by Goldhammer et al. (1992), Goldhammer (1996), and

Goldhammer and Lehmann (1996), who worked in the Franklin Mountains in far West Texas and who compared their work to that in other areas, including the Arbuckle Mountains in Oklahoma (Figure 9). They divided the general Lower Ordovician section, which they called the Sauk-C second-order supersequence, into nine third-order sequences (Figure 9) on the basis of higher order stacking patterns. Each third-order sequence had a duration of 1 to 10 million years. Goldhammer et al. (1992) stated that the origin and control of third-order sequences in the Lower Ordovician remain problematic because this period of time lacks evidence of major glaciation.

In the Franklin Mountains, Goldhammer et al. (1992), Goldhammer (1996), and Goldhammer and Lehmann (1996) recognized only the lower seven sequences (Figure 9), and they included the Bliss Sandstone as the lowest sequence. The sequences in this area range from 2 to 6 million years in duration. Within the third-order sequences, these researchers recognized numerous higher order sequences at the scale of fourth- and fifth-order parasequences, which are detailed depositional units that consist of meter-scale aggradational or progradational depositional cycles. This is the stratigraphic architectural scale that is used for flow-unit modeling in reservoir characterization (Kerans et al., 1994).

DEPOSITIONAL FACIES AND DEPOSITIONAL SYSTEMS

Ellenburger Platform Systems

Loucks and Anderson (1980, 1985) presented depositional models (Figures 10, 11) of the Ellenburger section in Puckett field, Pecos County, West Texas. Their data consist of two cores that provide ~1,700 ft of overlapping, continuous coverage of the section (Figure 12). They defined the lower Ellenburger section as being dominated by alluvial fan/coastal sabkha paracycles, the middle Ellenburger as subtidal paracycles, and the upper Ellenburger as supratidal/intertidal paracycles. Numerous fourth- and fifth-order cycles occur within this Puckett Ellenburger section. These researchers recognized many solution-collapsed zones that they attributed to exposure surfaces of different duration (Figure 12).

Kerans (1990) completed the most detailed and complete regional Ellenburger depositional systems and facies analysis on the basis of wireline-log and core material. Much of the rest of this section is a summary of Kerans' work. **(**See Kerans [1990] for complete description and interpretation of facies**.)** He recognized six general lithofacies (Figure 7):

(1) Litharenite: fan delta – marginal marine depositional system
(2) Mixed siliciclastic-carbonate packstone/grainstone: lower tidal-flat depositional system
(3) Ooid and peloid grainstone: high-energy restricted-shelf depositional system
(4) Mottled mudstone: low-energy restricted-shelf depositional system
(5) Laminated mudstone: upper tidal-flat depositional system
(6) Gastropod-intraclast-peloid packstone/grainstone: open shallow-water-shelf depositional system

Fan Delta – Marginal Marine Depositional System

Description: Kerans (1990) noted that this system contains two prominent facies: cross-stratified litharenite and massive to cross-stratified pebbly sandstone to conglomerate. Sedimentary structures include thick trough and tabular crossbeds, parallel current lamination, and graded and massive beds. Clastic grains are composed of granite and quartzite rock fragments, feldspar, and quartz.

Interpretation: According to Kerans (1990) this unit was deposited as a fan delta – marginal marine depositional system. It is a basal retrogradational clastic deposit where the Ellenburger Group onlaps the Precambrian basement. Loucks and Anderson (1985) presented a similar interpretation of a fan-delta complex prograding into a shallow subtidal environment (Figure 11).

Lower Tidal-Flat Depositional System

Description: Kerans (1990) stated that the dominant facies are mixed siliciclastic-peloid packstone-grainstone, intraclastic breccia, stromatolitic boundstone containing

silicified nodular anhydrite, ooid grainstone, and carbonate mudstone. These facies are mostly dolomitized. Kerans (1990) noted that the siliciclastic content is related to distribution of the sandstone below. Sedimentary structures include relict cross-stratification, scour channels, stromatolites, flat cryptalgal laminites, and silica-replaced evaporate nodules.

Interpretation: According to Kerans (1990) this unit was deposited in a lower tidal-flat depositional system in close association with the fan-delta depositional system (Figure 10). Upward in the section carbonate tidal flats override the fan deltas. Kerans (1990) presented the idealized cycle within this system as an upward-shoaling succession. Tidal-flat complexes prograded across subtidal shoals and intervening lagoonal muds (Figure 10). The relict evaporate nodules indicate an arid sabkha climate (Loucks and Anderson, 1985; Kerans, 1990). Kerans (1990) pointed out that thin siliciclastic sand laminae in tidal-flat laminites represent eolian deposits, whereas thicker sand units represent periodic sheetflood deposits from adjacent alluvial fans. Loucks and Anderson (1985) also recognized quartz sandstone units in the algal laminae.

High-Energy Restricted-Shelf Depositional System

Description: Kerans (1990) noted that this system is characterized by ooid grainstone; ooid-peloid packstone-grainstone; laminated, massive, and mottled mudstone; and minor cyanobacterial boundstone. It also contains coarse-crystalline white chert and rare gastropod molds. Coarse dolomite fabric is common. Depositional structures include cross-stratification, intraclastic breccias, small stromatolites, cryptalgal mats, and silicified relict nodular anhydrite.

Interpretation: According to Kerans (1990) this unit was deposited in a high-energy restricted-shelf depositional system. He stated that this system represents the period of maximum marine inundation during the Ellenburger transgression. He noted that extensive ooid shoals dominated the shelf and bioturbated mudstones formed in protected settings between shoals (Figure 11). Cryptalgal laminites and mudstones (tidal flats) with relict evaporate nodules may mark local shoaling cycles or more extensive upward-shoaling events. Kerans (1990) noted that the lack of fauna suggests restricted

circulation on the shelf produced by shoal-related restriction or by later destruction by dolomitization.

Low-Energy Restricted-Shelf Depositional System

Description: Kerans (1990) described this widespread system as a "remarkably homogeneous sequence of gray to dark-gray, fine- to medium-crystalline dolomite containing irregular mottling and lesser parallel-laminated mudstone and peloid wackestone." He noted sparse fauna of a few gastropods and nautiloids. The facies is highly dolomitized.

Interpretation: According to Kerans (1990) this unit was deposited in a low-energy restricted-shelf depositional system (Figure 11). The mottling is considered to be the result of bioturbation. It is a restricted shelf deposit ranging from subtidal mudstones to shoaling areas with tidal flats. Kerans (1990) noted that seaward this system interfingers with the open-marine, shallow-water shelf depositional system, fitting the model of Ross (1976) (Figure 2).

Upper Tidal-Flat Depositional System

Description: Kerans (1990) noted that the dominant facies in this system is smooth and parallel or irregular and crinkled laminated dolomite. Other facies include mottled mudstone, current-laminated dolostone, and beds of intraclastic breccia. Sedimentary structures include desiccation cracks, current laminations, nodular chert (relict evaporates?), and stromatolites.

Interpretation: According to Kerans (1990) this unit was deposited in an upper tidal-flat depositional system. A common cycle is composed of a basal bioturbated mudstone passing through current-laminated mudstone and into cryptalgal laminated mudstone, with desiccation structures and intraclastic breccias (Figure 11). Kerans (1990) noted that the mottled and current-laminated mudstones intercalated with the laminites are low-energy shelf deposits and intercalated ooid-peloid grainstone beds are storm deposits transported from high-energy shoals offshore (Figure 11). Kerans (1990)

suggested that the upper tidal-flat depositional system consisted of a broad tidal-flat environment situated landward of the lagoon-mud shoal complex. This model is similar to that presented by Loucks and Anderson (1985) (Figure 11). The depositional system occurs near the top of the Ellenburger succession.

Open Shallow-Water-Shelf Depositional System

Description: Kerans (1990) noted that the rocks in this system are mainly limestone, which is in contrast to many of the other sections of the Ellenburger interval. Facies include peloid and ooid grainstones, mollusk-peloidal packstones, intraclastic breccias, cryptalgal laminated mudstones, digitate stromatolitic boundstones, bioturbated mudstones, and thin quartzarenite beds. Again, in general contrast to the other depositional systems, this system has abundant fossils, including sponges, trilobites, gastropods, bivalves, and cephalopods. Kerans (1990) described the grainstones and packstones as massive or displaying parallel current laminations. He noted abundant desiccation cracks in the laminites, as well as fenestral fabric.

Interpretation: According to Kerans (1990) this unit was deposited in an open, shallow-water-shelf depositional system. He described the depositional setting as a complex mosaic of tidal-flat subenvironments, shallow-water subtidal carbonate sand bars, and locally thin stromatolite bioherms and biostromes (Figure 11). He interpreted the greater diversity of fauna, lack of evaporate evidence, and presence of high-energy grainstones and packstones as suggesting a moderate-current energy environment with open-marine circulation. He speculated that this system may have occurred close to the shelf edge or slope break.

Marathon Limestone Deeper Water System

The Marathon Limestone is the time-equivalent, deeper water slope facies of the Ellenburger shallow-water-platform facies (Berry, 1960; Young, 1968; Ross, 1982; Kerans, 1990). In West Texas, it occurs in the Marathon Basin (Young, 1968) and on the west margin of the Diablo Platform (Lucia, 1968, 1969).

Description: Kerans (1990) described the unit as containing graptolite-bearing shale, siliciclastic siltstone, lime grainstone and lime mudstone, and debris-flow megabreccia. Sedimentary structures consist of graded beds, horizontal laminations, sole marks, flute casts, and soft-sediment deformation structures (slump folds).

Interpretation: According to Kerans (1990) this unit was deposited in a more basinal setting than the laterally equivalent Ellenburger depositional systems. He defined the setting as a distally steepened ramp. He recognized that the thin-bedded shale, siltstone, and lime grainstone-mudstone packages are Bouma turbidite sequences produced by turbidity currents on a deeper water slope. Both Young (1968) and Kerans (1990) interpreted the massively bedded megabreccias as deeper water debris-flow deposits.

General Depositional History of the Ellenburger Group

Kerans (1990) summarized the depositional history of the Ellenburger Group in four stages (Figure 13).

Stage 1: Marked by retrogradational deposition of fan delta – marginal marine depositional system continuous with Early Cambrian transgression (Kerans, 1990). Kerans (1990) described interfingering of the basal siliciclastics with overlying tidal-flat and shallow-water subtidal deposits of the lower tidal-flat depositional system. This transition represents initial transgression and associated retrogradational sedimentation. Kerans (1990) noted that this stage was followed by regional progradation and aggradation of peritidal carbonate facies. This stage of deposition filled in existing paleotopography resulting in a low-relief platform.

Stage 2: Kerans (1990) documented rapid transgression and widespread aggradational deposition of the high-energy, restricted-shelf depositional system across much of West and Central Texas during this stage. He noted that the transgression produced an extensive carbonate sand sheet over much of the platform. He interpreted a moderately hypersaline setting on the basis of rare macrofauna, evidence of evaporites, and abundance of ooids.

Stage 3: Kerans (1990) stated that upward transition from the high-energy, restricted-shelf depositional systems to the low-energy, restricted-shelf depositional systems is evidence of a second regression across the Ellenburger shelf. Progradation during this stage is marked by transition of landward upper tidal flats to more seaward, low-energy, restricted subtidal to intertidal facies to farthest seaward, open-marine, shallow-water-shelf facies. Kerans (1990) recognized that laminated mudstones of the upper tidal-flat depositional system represent maximum regression across the Ellenburger inner shelf.

Stage 4: Near the end of the Early Ordovician there was a worldwide eustatic lowstand, the timing of which is reported to be Whiterockian in age (Sloss, 1963; Ham and Wilson, 1967), and whose length of exposure covered several million years. Throughout the United States, an extensive karst terrain formed on the Ellenburger platform carbonates (Kerans, 1988, 1989, 1990). During this long period of exposure, thick sections of cave developed, resulting in extensive paleocave collapse breccias within the Ellenburger section (Lucia, 1971; Loucks and Anderson, 1980, 1985; Kerans, 1988, 1989, 1990; Wilson et al., 1992; Loucks 1999). The time-equivalent, slope-deposited Marathon Limestone was not exposed during this sea-level drop (Kerans, 1990). The area appears to have had continuous deposition from the Early Ordovician through the Middle Ordovician.

GENERAL REGIONAL DIAGENESIS

Diagenesis of the Ellenburger Group is complex, and the processes that produced the diagenesis covered millions of years (e.g., Folk, 1959; Lucia, 1971; Loucks and Anderson, 1985; Lee and Friedman, 1987; Kerans, 1988, 1989, 1990; Kupecz and Land, 1991; Amthor and Friedman, 1991; Loucks, 1999, 2003). Several studies have presented detailed diagenetic analysis of the Ellenburger (Kerans, 1990; Kupecz and Land, 1991; Amthor and Friedman, 1991). A paragenetic chart is presented in Figures 14. Three major diagenetic processes are important to discuss: (1) dolomitization, (2) karsting, and (3) tectonic fracturing. Other diagenetic features are present but do not impact the appearance or reservoir quality of the Ellenburger as much as these three do. In the

following discussion of these diagenetic processes, only an overview will be presented, and the reader is referred to literature on Ellenburger diagenesis for a complete and detailed discussion.

Understanding Diagenesis in the Ellenburger Group

As stated earlier, diagenesis of the Ellenburger Group is complex. Detailed diagenesis can be worked out for any location, but trying to explain the complete diagenetic history for the entire Ellenburger carbonate section in West Texas may be beyond our reach because of relatively sparse subsurface data, length of time (±20 million years), thick stratigraphic section (possibly as many as six third-order sequences), and the large area involved. Remember that carbonates generally undergo diagenesis early in their history, especially if they are subjected to meteoric water. With the number of third-order sequences in the section and the time represented by each sequence (2 to 5 million years), extensive early and shallow diagenesis probably occurred but was later masked by intense dolomitization.

At the end of Early Ordovician time, a several-million-year hiatus occurred, exposing the Ellenburger Group and subjecting it to meteoric karst processes. Several authors have demonstrated that the karst affected strata at least 300 to 1,000 ft beneath the unconformity (e.g., Kerans 1988, 1989; Lucia, 1995; Loucks, 1999). With the occurrence of Ouachita thrusting from the Mississippian through the Pennsylvanian, vast quantities of hydrothermal fluids moved though available permeable pathways within the Ellenburger, producing late-stage diagenesis (e.g., Kupecz and Land, 1991). Following lithification, different parts of the Ellenburger Group were subjected to tectonic stresses, producing fractures and more late-stage diagenesis, which probably affected local areas (e.g., Loucks and Anderson, 1985; Kearns, 1990; Loucks, 2003).

Loucks (2003) presented an overview of the origins of fractures in Ordovician strata and concluded that in order to explain the complex diagenesis in these strata, one must sort all events into a well-documented paragenetic sequence—the most reliable method of delineating timing of events and features. He demonstrated that karsting and paleocave collapse breccias and related fractures and some tectonic fractures had

occurred before the hydrothermal events that had produced saddle dolomite. But first he had to establish well-documented paragenetic relationships.

Dolomitization

Of the several authors (Kerans, 1990; Kupecz and Land, 1991; Amthor and Friedman, 1991) that have attempted to understand the regional dolomite history, Kupecz and Land (1991) appear to have made the most progress. This section will mainly address findings of Kupecz and Land (1991) but will still include observations and conclusions from the other authors. Kupecz and Land's (1991) paragenetic sequence is presented in Figure 14. Their study covered a large area of West Texas, as well as the Llano Uplift area in Central Texas. They used both cores and outcrop as a data source and combined petrography with carbon, oxygen, and strontium isotopes.

Kupecz and Land (1991) recognized five general stages of dolomitization (Figure 14). Generations of dolomite were separated into early-stage dolomitization, which predated the Sauk unconformity, and late-stage dolomitization, which postdated the Sauk unconformity. They attributed 90% of the dolomite as early stage and 10% as late stage.

Kupecz and Land (1991) Dolomite Types:

(1) Stage 1 prekarstification early-stage dolomite (Dolomite E1)

a. Description: Crystal size ranges from 5 to 700 μ but varies by facies. In cryptalgal laminites crystal sizes range from 5 to 100 μ. These euhedral crystals have planar interfaces. In millimeter-laminated facies crystal size ranges from 5 to 70 μ, and in the bioturbated mudstones crystal size ranges from 5 to 700 μ. Kupecz and Land (1991) thought that some of the coarser crystals were a product of later recrystallization.

b. Interpretation: Kupecz and Land (1991) documented that this dolomite replaced lime mud or mudstone and that the dolomite predated karstification because it is found in nonkarsted rock as well as in clasts created by karsting. Therefore, it must have formed before karsting for it

to have been brecciated. Probable source of Mg for dolomitization is seawater (Kupecz and Land, 1991).

(2) Stage 2 postkarstification late-stage dolomite (Dolomite L1)

a. Description: This replacement dolomite consists of coarse-crystalline euhedral rhombs with crystal size ranging from 200 to 2,000 μ. Its homogeneous cathodoluminescence and homogeneous backscattered imaging suggest that this dolomite type has undergone recrystallization (Kupecz and Land, 1991). This stage of dolomitization is a regional event and is related to hydrothermal fluids.

b. Interpretation: Late-stage origin is based on coarse-crystal size (Kupecz and Land, 1991).

(3) Stage 3 postkarstification late-stage dolomite (Dolomite L2)

a. Description: Crystals have planar interfaces, sizes range from 100 to 3,500 μ, and crystals have subhedral to anhedral shapes. Extinction ranges from straight to undulose.

b. Interpretation: This stage is a replacement type of dolomite (Kupecz and Land, 1991). Late origin is based on relationship to a later stage chert and its replacement of early-stage dolomite E1. Much of the grainstone facies is replaced by this stage of dolomitization, which is related to hydrothermal fluids. Probable source of Mg for dolomitization is dissolution of previously precipitated dolomite (Kupecz and Land, 1991).

(4) Stage 4 postkarstification late-stage dolomite (Dolomite C1)

a. Description: Crystals are subhedral with undulose extinction (saddle/baroque dolomite), and sizes range from 100 to 5,000 μ.

b. Interpretation: Pore-filling cement (Kupecz and Land, 1991). Paragenetic sequence is established by the fact that Dolomite C1 postdates Dolomite L2 and was corroded before Dolomite C 2 was precipitated. Probable source of Mg for dolomitization is dissolution of previously precipitated dolomite (Kupecz and Land, 1991). This stage of dolomitization is a regional event and is related to hydrothermal fluids.

(5) Stage 5 postkarstification late-stage dolomite (Dolomite C2)

a. Description: Subhedral white crystals with moderate to strong undulose extinction (saddle/baroque dolomite), and crystal sizes range from 100 to 7,500 μ. Contain abundant fluid inclusions.
b. Interpretation: Pore-filling cement (Kupecz and Land, 1991). Occurred after corrosion of Dolomite C1. Probable source of Mg for dolomitization is dissolution of previously precipitated dolomite (Kupecz and Land, 1991). This stage of dolomitization is related to hydrothermal fluids.

Kupecz and Land (1991) provided the only integrated analysis of fluid-flow pathways and sources of Mg for the different dolomitizing events. Early-stage prekarstification dolomite is associated with muddier rocks, and the source of Mg was probably seawater. Kerans (1990) similarly attributed these finer crystalline dolomites to penecontemporaneous replacement of mud in tidal flats and to regionally extensive reflux processes during deposition.

Late-stage postkarstification dolomites are attributed by Kupecz and Land (1991) to warm, reactive fluids, which were expelled from basinal shales during the Ouachita Orogeny. The fluids are thought to have been corrosive, as evidenced by corroded dolomite rhombs (Kupecz and Land, 1991). This corrosion provided the Mg necessary for dolomitization. The warm, overpressured fluids were episodically released and migrated hundreds of miles from the foldbelt toward New Mexico (Figure 15). These fluids migrated through high-permeability aquifers of the Bliss Sandstone, basal subarkose facies of the Ellenburger, as well as grainstone facies and paleocave breccia zones. Figure 15 from Kupecz and Land (1991) shows the regional isotopic composition of late-stage Dolomite L2. The pattern of lighter to heavier delta-O^{18} away from the foldbelt to the south suggests movement and cooling of fluids to the northwest. Kupecz and Land's (1991) regional dolomitization model is displayed in Figure 15. Figure 16 shows the tectonic setting that produced the hydrothermal fluids.

Kerans (1990) defined three major styles of dolomitization:

(1) Very fine crystalline dolomite that he considered as a replacement product penecontemporaneous with deposition in a tidal-flat setting.
(2) Fine- to medium-crystalline dolomite appearing in all facies and that contributed to regionally extensive reflux processes during Ellenburger deposition.

(3) Coarse-crystalline replacement mosaic dolomite and saddle (baroque) dolomite associated with burial.

Kerans' first two types of dolomite are probably equivalent to Kupecz and Land's (1991) early-stage Dolomite E1. His coarse-crystalline replacement mosaic dolomite and saddle dolomite are equivalent to Kupecz and Land's (1991) late-stage dolomites.

Amthor and Friedman (1991) also recognized early- to late-stage dolomitization of the Ellenburger Group (Figures 17, 18). Similar to Kerans (1990) and Kupecz and Land (1991), Amthor and Friedman (1991) described early-stage, low-temperature, fine-crystalline dolomites associated with lime muds, where the Mg was supplied by diffusion from overlying seawater. Amthor and Friedman (1991) also described medium- to coarse-crystalline dolomite that replaced grains and matrix in the depth range of 1,500 to 6,000 ft. These dolomites are postkarstification and are probably replacement Dolomite L1 and L2 of Kupecz and Land (1991). Amthor and Friedman's (1991) last stage of dolomite is assigned a deep-burial origin (>6,000 ft) and consists of coarse-crystalline saddle dolomite. Its occurrence is both pore filling and replacive, and it is Dolomite L2, C1, and C2 of Kupecz and Land (1991). Amthor and Friedman (1991) also noticed extensive corrosion of previously precipitated dolomite, and they invoked a fluid-flow model similar to that of Kupecz and Land (1991), in which fluids were associated with the Ouachita Orogeny.

Overall, much of the Ellenburger is dolomitized. Dolomitization favors preserving open fractures and pores because it is mechanically and chemically more stable than limestone. Pores within dolomites are commonly preserved to deeper burial depths and higher temperatures than those of pores in limestone. Also, limestone breccia clasts tend to undergo extensive pressure solution at their boundaries and lose all interclast pores (Loucks and Handford, 1992), whereas dolomite breccia clasts are more chemically and mechanically stable with burial.

Karsting

Karsting is a complex, large-scale diagenetic event that strongly affected the Ellenburger Group. The process may affect only the surface of a carbonate terrain,

forming *terra rosa,* or extensively dissolve the carbonate surface, creating karst towers (Figure 19). It can also produce extensive subsurface dissolution in the form of dolines, caves, etc. (Figure 19). The next several paragraphs are meant to provide a background on karst systems that are seen in the Ellenburger Group.

Review of Caves and Paleocaves

Loucks (1999) provided a review of paleocave carbonate reservoirs. He stressed that to understand the features of paleocave systems, an understanding of how paleocave systems form is necessary. The best approach to such an understanding is to review how modern cave systems form at the surface and evolve into coalesced, collapsed-paleocave systems in the subsurface. Loucks (1999) described this evolutionary process, and the review presented here is mainly from that investigation.

To describe the features or elements of both modern and ancient cave systems, Loucks (1999) proposed a ternary classification of breccias and clastic deposits in cave systems based on relationships between crackle breccia, chaotic breccia, and cave-sediment fill (Figure 20). Crackle breccias have thin fractures separating breccia clasts. Individual clasts can be fitted back together. Mosaic breccias are similar to crackle breccias, but displacement between clasts is greater and some clast rotation is evident. Chaotic breccias are characterized by extensive rotation and displacement of clasts. The clasts can be derived from multiple horizons, producing polymictic breccias. Chaotic breccias grade from matrix-free, clast-supported breccias to matrix-supported breccias.

Loucks (1999) also showed that paleocave systems have complex histories of formation (Figure 21). They are products of near-surface cave development, including dissolutional excavation of passages, breakdown of passages, and sedimentation in cave passages. These are followed by later-burial cave collapse, compaction, and coalescence.

Phreatic or vadose-zone dissolution creates cave passages (Figures 19, 21). Passages are excavated where surface recharge is concentrated by preexisting pore systems, such as bedding planes or fractures (Palmer, 1991), that extend continuously between groundwater input, such as sinkholes, and groundwater output, such as springs (Ford, 1988).

Cave ceilings and walls are under stress from the weight of overlying strata. A tension dome—a zone of maximum shear stress—is induced by the presence of a cavity (White, 1988), and stress is relieved by collapse of the rock mass within the stress zone, which commonly starts in the vadose zone. In the phreatic zone, water supplies 40% of the ceiling support through buoyancy (White and White, 1968). Removal of this support in the vadose zone weakens the ceiling and can result in its collapse. Major products of collapsed ceiling and walls are chaotic breakdown breccia on the floor of the cave passage (Figures 19, 21). In addition, stress release around cave passages produces crackle breccias in cave-ceiling and cave-wall host rocks (Figures 19, 21).

Near-surface dissolutional excavation and cave sedimentation terminate as cave-bearing strata are buried into the subsurface. Extensive mechanical compacting begins, resulting in collapse of remaining passages and further brecciation of blocks and slabs (Figure 21). Multiple stages of collapse occur over a broad depth range, and foot-scale bit drops (cavernous pores) are not uncommon at depths of 6,000 to 7,000 ft (Loucks, 1999). The areal cross-sectional extent of brecciation and fracturing after burial and collapse is greater than that of the original passage (Figure 21). Collapsed, but relatively intact, strata over the collapsed chamber are fractured and form burial cave-roof crackle and mosaic breccias with loosely to tightly fitted clasts (Figure 21). Sag feature and faults (suprastratal deformation) can occur over collapsed passages (Figure 21) (Lucia, 1971, 1995, 1996; Kerans, 1988, 1989, 1990; Hardage et al., 1996; Loucks, 1999, 2003, 2007; McDonnell et al., 2007).

Development of a large collapsed paleocave reservoir is the result of several stages of development (Figure 22). The more extensive coalesced, collapsed-paleocave system originated at composite unconformities, where several cave systems may overprint themselves during several million years of exposure to karst processes (Figure 22) (Esteban 1991; Lucia, 1995; Loucks, 1999). As the multiple-episode cave system subsides into the deeper subsurface, wall and ceiling rock adjoining open passages collapses and forms breccias that radiate from the passage and may intersect with fractures from other collapsed passages and older breccias within the system. This process forms coalesced, collapsed-paleocave systems and associated reservoirs that are hundreds to thousands of feet across, thousands of feet long, and tens to hundreds of feet

thick. Internal spatial complexity is high, resulting from the collapse and coalescing of numerous passages and cave-wall and cave-ceiling strata. These breccias and fractures are commonly major reservoirs in the Ellenburger Group. The reader is referred to Kerans (1988, 1989, 1990), Loucks and Handford (1992), Hammes et al. (1996), and Loucks (1999, 2001, 2003) for discussions about paleocave systems in the Ellenburger Group.

Loucks and Mescher (2001) developed a classification of paleocave facies (Figure 23, Table 1). Six basic cave facies are recognized in a paleocave system and are classified by rock textures, fabrics, and structures: (1) undisturbed strata (undisturbed host rock), (2) disturbed strata (disturbed host rock), (3) highly disturbed strata (collapsed roof and wall rock), (4) coarse chaotic breccia (collapsed-breccia cavern fill), (5) fine chaotic breccia (transported-breccia cavern fill), and (6) sediment fill (cave-sediment cavern fill). Each paleocave facies can be distinct and adjoin sharply with adjacent facies, or they may show gradation into adjacent facies within the coalesced, collapsed-paleocave system. Pore networks associated with paleocave reservoirs can consist of cavernous pores, interclast pores, crackle- and mosaic-breccia fractures, tectonic fractures, and, less commonly, matrix pores. The paleocave facies classification, in conjunction with burial-history data, can be used to describe the complex geology expressed in coalesced, collapsed-paleocave systems and can be used to explain and predict pore-type distribution and magnitude of reservoir quality.

Table 1. Summary of general paleocave facies. From Loucks and Mescher (2001).

Cave Facies	Interpretation	Description	Pore System/ Reservoir Quality
Undisturbed strata	Undisturbed host rock	Excellent bedding continuity for hundreds to thousands of feet.	Minor matrix and fracture pores. Ø < 3% to 5% K < few millidarcys
Disturbed strata	Disturbed host rock	Bedding continuity is high but folded and offset by small faults. Commonly overprinted with crackle and mosaic brecciation.	Minor matrix pores and crackle to mosaic fracture pores. Ø < 5% K is as much as tens of millidarcys
Highly disturbed Strata	Collapsed host rock (cave-roof and cave-wall rock) over passages	Highly disturbed, very discontinuously bedded strata with pockets and layers of chaotic breccia. Small-scale folding and faulting are common. Commonly overprinted with crackle and mosaic brecciation.	Localized pockets or layers of breccia might have porosities in the range of 5% to 15% and permeabilities in the tens to hundreds of millidarcys.
Coarse chaotic breccia	Collapsed-breccia cavern fill	Mass of very poorly sorted, granule- to boulder-sized chaotic breccia clasts 1 to 10 ft long. Commonly clast supported but can contain matrix material. Ribbon- to tabular-shaped body as much as 45 ft across and hundreds of meters long.	Abundant interclast pores. Porosity can exceed 20%, and permeability can be in the darcys.
Fine chaotic breccia	Transported-breccia cavern fill	Mass of clast-supported, moderately sorted, granule- to cobble-sized clasts with varying amounts of matrix. Clasts can be imbricated or graded. Ribbon- to tabular-shaped body as much as 45 ft across and hundreds of feet long.	Abundant interclast pores. Porosity can exceed 20%, and permeability can be in the darcys.
Sediment fill	Cave-sediment cavern fill	Carbonate and/or siliciclastic debris commonly with sedimentary structures.	Siliciclastic fill is commonly tight. Carbonate fill might be permeable.

Ellenburger Karsting

In the Ellenburger Group, extensive cave systems formed at a composite unconformity (Sauk unconformity) that lasted several million years to several tens of million years. Many authors have recognized this karsting and associated features in the Ellenburger Group. Barnes et al. (1959) recognized solution collapse in the Ellenburger Group, stating that "… a matrix composed of material foreign to the formation indicates

breccia formed by solution and collapse probably related to an erosional unconformity." Lucia (1971) was the first to promote that the extensive brecciation seen in the El Paso Group (equivalent to the Ellenburger Group) was associated with karst dissolution and was not the result of tectonic brecciation. Loucks and Anderson (1980, 1985) in Puckett field in Pecos County also realized that many of the breccias in the Ellenburger Group were related to solution collapse (Figure 11). They associated them with exposed diagenetic terrains. Kerans (1988, 1989, 1990) strongly established karsting and cave development in the Ellenburger Group. He proposed paleocave models (Figure 24) that were immediately accepted and applied.

Lucia's (1971, 1995, 1996) work in the El Paso Group in the Franklin Mountains of far West Texas presents an excellent outcrop analog for coalesced, collapsed-paleocave systems. He mapped a large paleocave system that was developed in the upper 1,000 ft of the El Paso Group during a 33-m.y. time gap (Figures 25, 26). Large fracture systems and collapse-breccia zones 1,000 ft thick, 1,500 ft wide, and >1 mi long mark the collapsed-paleocave system. Lucia (1995) noted that the cavernous porosity could have been as high as 30% before infilling with cave-sediment fill and cement.

Within the southern Franklin Mountains, Lucia (1995) described the Great McKelligon Sag in McKelligon Canyon along the eastern face (Figure 27). The sag, ~1,500 ft wide and ~150 ft deep, formed by collapse of paleocaves in the El Paso section after the Montoya and Fusselman units were deposited, buried, and lithified. It is an important feature that paints a complete picture of a coalesced, collapsed-paleocave system (Loucks, 1999). Hardage et al. (1996), Loucks (2003), and McDonnell et al. (2007) all stressed that collapse of a coalesced-paleocave system not only affects the karsted unit, but also strongly affects the units above (Figure 22). Loucks (2003) called the deformation of younger lithified units "suprastratal deformation." Besides the example of suprastratal deformation shown in the Great McKelligon Sag, examples of suprastratal deformation from seismic in the Ellenburger Group can be seen in Hardage et al. (1996), Loucks (1999, 2003), and McDonnell et al. (2007) and from wireline-log cross sections by Kerans (1989) (his Figure 25).

Kerans (1988, 1989, 1990) presented an excellent overview of paleokarst in the Ellenburger Group. His paleocave models (Figure 24) were the first to define paleocave

floor, paleocave sediment fill, and paleocave roof. Figures 28 through 32 present several cores and associated core slabs from collapsed-paleocave systems, which emphasize Kerans' paleocave model. Paleocave terrigenous-bearing sediment fill is strikingly apparent from gamma-ray, spontaneous potential, and resistivity logs (Kerans, 1988, 1989, 1990). Paleocave fabrics can also be recognized on electrical imaging tools (Hammes, 1997). Kerans (1988, 1989) discussed several breccia types, including (1) a laterally persistent breccia association formed in the upper phreatic zone (water table) karst and (2) a laterally restricted breccia association formed by deep phreatic dissolution and collapse.

Kerans (1990), in his sequence of diagenetic events (his Figure 37), noted that the Ellenburger section had been subjected to karsting during several periods of time. The main karst event was at the Early Ordovician Sauk-Tippecanoe Supersequence boundary. In local areas it was karsted several more times. In the Llano area of Texas, Kupecz and Land (1991) showed that the Ellenburger stayed near the surface until deep burial during Later Pennsylvanian subsidence (Figure 33A). Loucks et al. (2000) recognized conodonts in cave-sediment fill from paleocaves in the Llano that would indicate exposure during the Middle to Late Ordovician, Late Devonian, and Earliest Mississippian times. Also, they established other strong periods of karsting during Pennsylvanian, Cretaceous, and Tertiary times. Combs et al. (2003) noted a second period of karsting in the Ellenburger interval in Barnhart field in Reagan County, where the Wolfcamp clastic overlies the Ellenburger Group. Their burial-history diagram (Figure 33B) displays the two periods of karsting.

Tectonic Fracturing

In the past there has been controversy on the origin of many of the breccias and fractures in the Ellenburger Group. Some workers (e.g., Ijirighoi and Schreiber, 1986) wanted to assign most, if not all, fractures and breccias to a tectonic origin. They thought that faulting could produce these widespread breccias. The extensive size and shape of most Ellenburger breccias and the inclusion of cave-sediment fill, speleothems, and younger conodonts preclude a simple tectonic origin (Loucks, 2003).

However, several authors have noted tectonic fractures in the Ellenburger section (e.g., Loucks and Anderson, 1985; Kerans, 1989; Holtz and Kerans, 1992; Combs et al., 2003). Each of these authors recognized that tectonic fractures cut across lithified breccias. Kerans (1989) noted the fractures cutting late saddle dolomite and suggested that the Pennsylvanian foreland deformation that affected much of West and Central Texas, as described by Budnik (1987), probably produced many tectonic-related fractures. However, as pointed out by many authors, paleocave collapse can also produce fractures that are not associated with tectonic events. Kerans (1990), Lucia (1996), and Loucks (1999, 2003) showed that suprastratal deformation above collapsing paleocave systems can create sags, faults, and numerous fractures (Figure 22).

Kerans (1989) pointed out several distinct ways to separate karst-related fractures from tectonic-related fractures:

(1) Tectonic fractures are commonly the youngest fractures in the core and generally crosscut karst-related fractures.
(2) Tectonic fractures postdate saddle dolomite. In the Llano area, however, saddle dolomite fills in a well-developed Pennsylvanian fracture set (Loucks, 2003).
(3) Karst-related fractures are generally near the top of the Ellenburger section, whereas tectonic-related fractures can occur throughout the Ellenburger section.

Loucks and Mescher (1998) presented additional criteria for separating karst-related fractures from tectonic-related fractures:

(1) Tectonic fractures generally show a strong relationship to regional stress patterns and have well-defined, oriented sets of fractures, whereas karst-related fractures respond to near-field stresses and fracture orientation is more random than tectonic fractures.
(2) Regional tectonic fractures are generally spaced at >1-inch scale and commonly at 1-ft or larger scale. Karst-related fractures (crackle-breccia fractures) can be closely spaced—only a fraction of an inch apart.
(3) Breccias associated with tectonic-derived faults commonly form a narrow band around the fault only a few feet wide but may be tens of feet wide. Karst-related breccias can be thousands of feet wide and hundreds of feet thick, contain a large

range of clast sizes, and show hydrodynamic sedimentary structures in the sediment fill.

(4) Tectonic faults are linear or curved in map view. Karst-related faults are linear, curved, or cylindrical (Hardage et al., 1996; Loucks, 1999, McDonnell et al., 2007) in map view.

Tectonic- and karst-related fractures are both present in the Ellenburger section. Detailed analysis of the fractures can commonly define their origin.

RESERVOIR CHARACTERISTICS

Pore Types

Pore networks in the Ellenburger are complex because of the amount of dolomitization, brecciation, and fracturing associated with karsting and regional tectonic deformation. Pore networks can consist of any combination of the following pore types, depending on depth of burial (Loucks, 1999): (1) matrix, (2) cavernous, (3) interclast, (4) crackle-/mosaic-breccia fractures, or (5) tectonic-related fractures.

Loucks (1999) presented an idealized plot of how karst-related Ellenburger pore networks probably change with depth (Figure 34). Relative abundance of pore types and relative depth of burial are estimates based on review of near-surface modern cave systems and buried paleocave systems (see Table 2 in Loucks, 1999). Large voids may be preserved down to 8,000 to 9,000 ft of burial, but they eventually collapse, forming smaller interclast pores and fractures associated with crackle and mosaic breccias. Coarse-interclast pores between large clasts are reduced by rotation of clasts to more stable positions and by rebrecciation of clasts to smaller fragments (Figure 21). As passages and large interclast pores in the cave system collapse, fine-interclast pores first increase and then decrease, whereas fracture pore types become more abundant. Cave-sediment fill is commonly cemented tight during burial diagenesis in the Ellenburger carbonates, especially if it is terrigenous sediment or it has a terrigenous sediment component. In the Ellenburger carbonates, matrix porosity is generally low (<5%), consisting of common matrix pore types such as interparticle, moldic, intercrystalline, or

micropores. See Table 1 (Loucks and Mescher, 2001) for a general estimate of reservoir quality by paleocave facies types.

Three-Dimensional Architecture of an Ellenburger Coalesced, Collapsed-Paleocave System

The three-dimensional, interwell-scale architecture of a Lower Ordovician Ellenburger coalesced, collapsed-paleocave system was constructed through integration of 7.8 mi of ground-penetrating radar (GPR), 29 shallow cores (~50 ft long), and outcrop data within a large quarry (McMechan et al., 1998, 2002; Loucks et al., 2000; Loucks et al., 2004). Data were collected near Marble Falls in Central Texas over an area (~2,600 × ~3,300 ft) that could cover several oil-well locations (~160 ac) typical of a region such as West Texas (Figure 35). Integration of core-based facies descriptions with GPR-reflection response identified several paleocave facies that could be deciphered and mapped using GPR data alone (Figure 36): (1) continuous reflections image the undisturbed strata, (2) relatively continuous reflections (more than tens of feet) characterized by faults and folds image the disturbed strata, and (3) chaotic reflections having little to no perceptible continuity image heterogeneous cave-related facies recognized in core that cannot be individually resolved with GPR data. These latter facies include highly disturbed strata, coarse-clast chaotic breccia, fine-clast chaotic breccia, and cave-sediment fill.

The three-dimensional architecture of the coalesced, collapsed-paleocave system based on core and GPR data indicates that trends of brecciated bodies are as much as 1,100 ft wide, >3300 ft long, and tens of feet high (Figures 37, 38). These brecciated bodies are coalesced, collapsed paleocaves. Between the brecciated bodies are areas of disturbed and undisturbed host rock that are jointly as much as 660 ft wide. Representative cores from the study are presented in Figure 39.

As a cave system is buried, many structural features form by mechanical compaction, and these features, including folds, sags, and faults, were documented in the study by McMechan et al. (1998, 2002) and Loucks et al. (2004). Folds and sags measure from ~10 ft to several hundred feet wide. Collapse-related faults are numerous and can

have several feet of throw. Most are normal faults, but some reverse faults also occur. See Figures 40 to 43 for examples of collapsed-paleocave features from GPR and outcrop data.

Megascale Architecture

Coalesced, collapsed-paleocave systems are megascale geologic features that can have dimensions of hundreds to thousands of square miles laterally and several thousand feet vertically (Loucks, 1999, 2003). Strata above and below the unconformity are affected by late collapse in the subsurface (Figure 22).

A coalesced, collapsed-paleocave system can be divided into two parts (Loucks, 2007): (1) a lower section of karsted strata that contains collapsed paleocaves and (2) an upper section of strata that is deformed to various degrees (suprastratal deformation) by the collapse and compaction of the lower section of paleocave-bearing strata (Figure 22). The collapse and compaction of cave systems provide the potential for development of large-scale fracture/fault systems that can extend from the collapsed interval upward several thousand feet. These fracture/fault systems are not related to regional tectonic stresses.

Both Kerans (1990) and Loucks (1999, 2007) speculated that the regional pattern of karsted Ellenburger reservoirs probably follows a rectilinear pattern as a result of regional fractures controlling cave development. Loucks (1999) presented data from subsurface seismic and from mining areas that express the rectilinear pattern of paleocave systems (Figure 44). Lucia (1995) presented a map of the paleocave system in the El Paso Group that also displays a rectilinear pattern (Figure 26). The coalesced brecciated bodies mapped by Loucks et al. (2004) in the Marble Falls area are rectilinear (Figure 37). At a larger scale, Canter et al. (1993) showed a regional isopach map of Ellenburger paleocave sediments over tens of square miles (Figure 45) having a strong rectilinear pattern. Also, a modified map of Hardage et al. (1996) of rectilinear suprastratal deformation trends, associated with Ellenburger subsurface paleocave collapse, in Wise County, Texas, lines up in a rectilinear pattern (Figure 46). A later study of this area by McDonnell et al. (2007) presents this pattern as well, but in more detail. Strong evidence therefore suggests that coalesced, collapsed-paleocave systems have rectilinear patterns that may

be associated with regional fracture systems. However, at present no definitive study has shown an actual regional paleofracture system that has controlled these rectilinear patterns.

HYDROCARBON PRODUCTION

Holtz and Kerans (1992) estimated that the original in-place oil in the Lower Ordovician strata had been ~11 million barrels of oil equivalent (MMboe), 3.8 MMboe of which had been produced at the time of their article. Production from the Ellenburger since 1970 from Railroad Commission of Texas files has been 488.5 million barrels (MMbbl) of oil and 13.5 trillion cubic feet (Tcf) of gas (personal communication from Romulo Briceno, Bureau of Economic Geology). Total hydrocarbons produced are 2, 249 billion barrels of oil equivalent (Bboe).

Holtz and Kerans (1992) tabulated 149 oil and/or gas reservoirs that each has produced >1 MMbbl of oil equivalent. According to Railroad Commission of Texas files, there are approximately 700 fields of various sizes within the Ellenburger Group in Texas (personal communication from Romulo Briceno, Bureau of Economic Geology).

Holtz and Kerans (1992) divided Ellenburger reservoirs into three groups (Figure 47):

(1) Karst-modified reservoirs: Reservoirs formed in the inner-ramp depositional setting and affected by extensive dolomitization and karsting. Karst-related fractures and interclast pores are the main pore types, with tectonic fractures secondary. These reservoirs are characterized by moderately thick net pay, low porosity, moderate permeability, low initial water saturation, and moderate residual oil saturation.

(2) Ramp carbonates: Reservoirs formed in middle- to outer-ramp depositional settings and dolomitized to various degrees. Predominant pores types are intercrystalline and interparticle, with tectonic and karst fractures being secondary. These reservoirs are characterized by thinnest net pay, highest porosity, moderate permeability, highest initial water saturation, and highest residual oil saturation.

(3) Tectonically fractured dolomites: Reservoirs formed in the inner-ramp depositional environment, subsequently extensively dolomitized, karsted, and, lastly, extensively tectonically fractured. Tectonic-related fractures are the dominant pore type, and the other pore types are commonly fractures. These reservoirs are characterized by the thickest net pay, lowest porosity, lowest permeability, and lowest initial water saturation.

Tables 2 and 3 from Holtz and Kerans (1992) summarize geologic and reservoir traits of each group. Note that Ellenburger reservoirs generally have low porosities (a few percent) and fair permeabilities (one to a few hundred millidarcys). The low porosities and fair permeabilities are the result of permeability being related to fracture-type pores. Figure 48 shows field averages of porosity and permeability for a number of Ellenburger fields. Average porosities are low, whereas permeabilities are fair. This relationship is the result of karst-related fracture pores. Figure 49 is a histogram of productive (past and present) wells drilled into the Ellenburger Group. Producing wells show a range from 856 ft (Originala Petroleum #1 Gensler well in Archer County, Texas) to 25,735 ft (Exxon Mobil McComb Gas Unit B well in Pecos County, Texas). A recent review of Texas oil fields by Dutton et al. (2005) states that the Karst-Modified Reservoir play had produced ~1.5 Bbbl of oil and the Ellenburger Ramp Carbonate play had produced ~164 MMbbl of oil as of 2005.

Figure 50 by Katz et al. (1994) is an event chart for the Simpson-Ellenburger petroleum system, showing the temporal relationships of essential elements and processes. Even though the source of the petroleum system is problematic, these workers thought that the source rocks are shales within the Simpson Group. However, where the Simpson is absent, Ellenburger oil appears to be sourced from the Woodford Shale or younger strata (Pennsylvanian or Permian) (Kvenvolden and Squires, 1967). Katz et al. (1994) mentioned that the level of organics within the Ellenburger section is too lean (<0.5% total organic carbon [TOC]) to be capable of generating commercial quantities of hydrocarbons. The Simpson has >1% TOC. These workers' ideas about reservoir rock type in Ellenburger carbonates come from articles cited earlier in this paper, and these reservoir rocks within this petroleum system are buried between 8,530 and 13,240 ft

(Central Basin Platform area). Katz et al. (1994) stated that trap development was associated with the collisional event that subdivided the Permian Basin into its major structural units ~290 m.y.a. Traps are predominately faulted anticlines (Figure 51). Seal rocks are Simpson shales in the Central Basin Platform area. Traps formed about 50 m.y. before peak generation at ~245 m.y.a. (Figure 50). Katz et al. (1994) mentioned that API oil gravity ranges from 35° to 50°, thus allowing a recovery factor of 40%.

Table 2. Geologic characteristics of the three Ellenburger reservoir groups. From Holtz and Kerans (1992).

	Karst Modified	**Ramp Carbonate**	**Tectonically Fractured Dolostone**
Lithology	Dolostone	Dolostone	Dolostone
Depositional setting	Inner ramp	Mid- to outer ramp	Inner ramp
Karst facies	Extensive sub-Middle Ordovician	Sub-Middle Ordovician, sub-Silurian/Devonian, sub-Mississippian, sub-Permian/ Pennsylvanian	Variable intra-Ellenburger, sub-Middle Ordovician
Fault-related fracturing	Subsidiary	Subsidiary	Locally extensive
Dominant pore type	Karst-related fractures and interbreccia	Intercrystalline in dolomite	Fault-related fractures
Dolomitization	Pervasive	Partial, stratigraphic and fracture-controlled	Pervasive

Table 3. Petrophysical parameter of the three Ellenburger reservoir groups. From Holtz and Kerans (1992).

Parameter	**Karst Modified**	**Ramp Carbonate**	**Tectonically Fractured Dolostone**
Net pay (ft)	Avg. = 181, Range = 20 - 410	Avg. = 43 Range = 4 - 223	Avg. = 293, Range = 7 - 790
Porosity (%)	Avg. = 3 Range = 1.6 - 7	Avg. = 14 Range = 2 - 14	Avg. = 4 Range = 1 - 8
Permeability (md)	Avg. = 32 Range = 2 - 750	Avg. = 12 Range = 0.8 - 44	Avg. = 4 Range = 1 - 100
Initial water saturation (%)	Avg. = 21 Range = 4 - 54	Avg. = 32 Range = 20 - 60	Avg. = 22, Range = 10 - 35
Residual oil saturation (%)	Avg. = 31 Range = 20 - 44	Avg. = 36 Range = 25 - 62	NA

COMMENTS ON APPROACHES TO EXPLORATION AND FIELD DEVELOPMENT

Exploration

The vast majority of Ellenburger fields are trapped in anticlinal or faulted anticlinal structures (Figure 51). Because Ellenburger reservoirs are mainly structural plays, seismic is needed to define these structural prospects. Complexities of the structure must be delineated to focus on correct trapping geometry. Stratigraphic trapping in the highly karsted and fractured Ellenburger carbonate is probably not common because some level of communication is generally within the carbonate, although poor. After a structure is defined, fault compartmentalization of the structure must be mapped. If 3-D seismic analysis is able to display the sag features produced by collapse of the cave system (Loucks, 1999), these collapsed zones may contain the highest reservoir quality (Purves et al., 1992).

Many wells testing the Ellenburger section penetrate only the top of the interval to prevent water from being encountered when drilling too deep (Kerans, 1990). Caution must be taken to ensure that the full prospective section is tested and that any vertical permeability barriers are penetrated (Loucks and Anderson, 1985; Kerans, 1990). Kerans (1990) provided an excellent example from University Block 13 field in Andrews County, Texas, where a series of wells drilled into the very top of the Ellenburger section were produced and then later deepened (Figure 52). The deepened wells encountered new hydrocarbons that had been separated from the upper unit by paleocave fill and tight carbonate. The cave-fill-prone intervals are distinctive on wireline logs. Note that a cave fill by itself cannot be a laterally continuous permeability barrier because its limited lateral extent is controlled by the size of the original cave itself (Loucks, 1999, 2001).

Kerans (1990), Loucks and Handford (1992), Hammes et al. (1996), and Loucks (1999) all stressed that karsted reservoirs can have stacked porous brecciated zones (Figure 29). These stacked reservoir zones are results of multiple cave passages forming during base-level drop while a cave system is developing (Figure 19). Commonly each of the paleocave passage levels will be in contact with one another because of cave collapse

and associated fracturing. However, as Kerans (1990) showed for University Block 13 field, this is not always the case.

In any test of the Ellenburger section, a core or image log is necessary to evaluate the section properly. Commonly porosity will be low (<5%) as calculated from wireline logs; however, permeability from karst-related fracturing may be in the hundreds of millidarcys. Core will provide a proper reservoir quality analysis, and image logs will provide a description of the fractured pore network in the rock (Hammes, 1997).

Field Development

Field development of paleocave reservoirs should be based on integrated studies that include data from 3-D seismic surveys, cores, borehole image logs, conventional wireline logs, and engineering data (Loucks, 1999). In some cases it might be possible to identify cavernous or intraclast porosity from 3-D seismic data (Bouvier et al., 1990). Cores and borehole image logs are necessary to recognize and describe paleocave reservoir facies (Hammes, 1997). Whole-core data are recommended over core-plug data because of the scale and complexity of pore systems in paleocave reservoirs. Sags associated with cave collapse should be mapped because they may indicate location of the best coalesced reservoirs (Purves et al., 1992; Lucia, 1996; Loucks, 1999). Different cave passage levels of the paleocave system need to be identified and analyzed to determine whether they are separate reservoirs or in vertical communication with one another (Kerans, 1988, 1990). Because of the significant spatial complexity within coalesced paleocave systems, horizontal wells may be an option for improving recovery. Kerans (1988) stated that in the Mobil Block 36 lease of the Emma Ellenburger reservoir, "Adjacent wells in this 40-acre-spaced reservoir have varied in production, one to the other, anywhere from 0 to 900,000 barrels of oil from the lower collapse zone." He noted that this variability is probably related to changes in paleocave facies. The detailed paleocave system maps provided by Loucks et al. (2004) would support this conclusion. Kerans (1988) listed other fields, such as Shafter Lake and Big Lake fields, as showing strong lateral reservoir heterogeneity. Other workers that addressed different aspects of exploration and development are Kerans (1990), Wright et al. (1991), Mazzullo and

Mazzullo (1992), Hammes et al. (1996), Lucia (1996), Mazzullo and Chilingarian (1996), and Loucks (1999).

CONCLUSIONS

The Ellenburger Group of the Permian Basin is part of a Lower Ordovician carbonate platform succession that covered large areas of the United States. During the Early Ordovician, the West Texas Permian Basin area was located on the southwest edge of the Laurentia plate between 20° and 30° latitude. The equator crossed northern Canada, situating Texas in a tropical to subtropical latitude. Texas was a shallow-water shelf with deeper water conditions to the south where it bordered the Iapetus Ocean. The Ellenburger Group in the south part of the Permian Basin, where the deeper water equivalent strata would have been, was strongly affected by the Ouachita Orogeny. The basinal and slope facies strata were destroyed or extensively structurally deformed. A worldwide hiatus appeared at the end of Early Ordovician deposition, creating an extensive second-order unconformity (Sauk-Tippecanoe Supersequence Boundary). This unconformity produced extensive karsting throughout the United States, including Texas.

The general depositional history of the Ellenburger was defined by Kerans (1990) as (1) Marked by retrogradational deposition of a fan delta – marginal marine depositional system continuous with the Early Cambrian transgression. This stage was followed by regional progradation and aggradation of peritidal carbonate facies. (2) Rapid transgression and widespread aggradational deposition of the high-energy restricted-shelf depositional system across much of West and Central Texas during this stage. It has been interpreted as a moderately hypersaline setting, given the rare macrofauna, evidence of evaporites, and abundance of ooids. (3) Upward transition from the high-energy restricted shelf depositional system to the low-energy restricted-shelf depositional systems as evidenced by a second regression across the Ellenburger shelf. Progradation during this stage is marked by transition of landward upper tidal flats to more seaward, low-energy restricted subtidal to intertidal facies to farthest seaward open-marine, shallow-water shelf facies. (4) Near the end of the Early Ordovician there was a

worldwide eustatic lowstand—the exposure spanned several million years and exposed the Ellenburger Platform in West Texas, producing an extensive karst terrain.

Diagenesis of the Ellenburger Group is complex, and the processes that produced it spanned millions of years. Three major diagenetic processes are important to recognize: (1) dolomitization, (2) karsting, and (3) tectonic fracturing. Five general stages of dolomitization were recognized by Kupecz and Land (1991). Generations of dolomite were separated into early-stage dolomitization, which predated the Sauk unconformity, and late-stage dolomitization, which postdated the Sauk unconformity. They attributed 90% of the dolomite to prekarstification, early-stage dolomite, and 10% of the dolomite to postkarstification, late-stage dolomite. Early-stage prekarstification dolomite is associated with muddier rocks, and the source of Mg was probably seawater. Late-stage postkarstification dolomites are attributed to warm, reactive fluids, which were expelled from basinal shales during the Ouachita Orogeny. Fluids are thought to have been corrosive, as evidenced by corroded dolomite rhombs. This corrosion provided the Mg necessary for dolomitization. The fluids migrated through high-permeability aquifers of the Bliss Sandstone, basal subarkose facies of the Ellenburger, as well as grainstone facies and paleocave breccia zones. In the Ellenburger Group, extensive cave systems formed at a composite unconformity (Sauk unconformity) that lasted several million years to several tens of million years. These cave systems collapsed with burial, creating widespread brecciated and fractured carbonate bodies that form many of the Ellenburger reservoirs. As much as 1,000 ft of section can be affected, but more commonly only the top 300 ft is affected. Lithified strata above the karsted Ellenburger are also affected by suprastratal deformation. The West Texas area has been periodically tectonically active following Ellenburger deposition, producing faults and fractures associated with these tectonic periods.

Pore networks in the Ellenburger are complex because of the amount of brecciation and fracturing associated with karsting. Pore networks can consist of any combination of the following pore types, depending on depth of burial (Loucks, 1999): (1) matrix, (2) cavernous, (3) interclast, (4) crackle-/mosaic-breccia fractures, or (5) tectonic-related fractures. The pore network evolved with burial and diagenesis.

Coalesced, collapsed-paleocave systems are megascale geologic features that can have dimensions of hundreds to thousands of square miles laterally and several thousand feet vertically. Strata above and below the unconformity are affected by late collapse in the subsurface. A coalesced, collapsed-paleocave system can be divided into (1) a lower section of karsted strata that contains collapsed paleocaves and (2) an upper section of strata that is deformed to various degrees (suprastratal deformation) by the collapse and compaction of the lower section of paleocave-bearing strata. The regional pattern of karsted Ellenburger reservoirs probably follows a rectilinear pattern as a result of regional fractures controlling original cave-system development.

The Ellenburger Group is an ongoing important exploration target in West Texas. The structural play covers a depth interval of >25,000 ft. Carbonate depositional systems within the Ellenburger Group are relatively simple; however, the diagenetic overprint is complex and it is this complex diagenetic overprint that produces strong spatial heterogeneity within the reservoir systems.

ACKNOWLEDGMENT

Publication authorized by the Director, Bureau of Economic Geology. Special thanks are given to Lana Dieterich for editing the manuscript. Funding for this study came from the State of Texas Advanced Resource Recovery Program.

REFERENCES

Amthor, J. E., and Friedman, G. M., 1991, Dolomite-rock textures and secondary porosity development in Ellenburger Group carbonates (Lower Ordovician), West Texas and southeastern New Mexico: Sedimentology, v. 38, p. 343–362.

Barnes, V. E., Cloud, P. E., Jr., Dixon, L. P., Folk, R. L., Jonas, E. C., Palmer, A. R., and Tynan, E. J., 1959, Stratigraphy of the pre-Simpson Paleozoic subsurface rocks of Texas and southeast New Mexico: University of Texas, Austin, Bureau of Economic Geology Publication 5924, 294 p.

Berry, W. B. N., 1960, Graptolite faunas of the Marathon region, West Texas: University of Texas, Austin, Bureau of Economic Geology Publication 6005, 179 p.

Blakey, R., 2005a, Regional paleogeographic views of earth history; paleogeographic globes: http://jan.ucc.nau.edu/~rcb7/RCB.html.

Blakey, R., 2005b, Paleogeography and geologic evolution of North America; Images that track the ancient landscapes of North America: http://jan.ucc.nau.edu/~rcb7/RCB.html.

Bouvier, J. D., Gevers, E. C.A., and Wigley, P. L., 1990, #-D seismic interpretation and lateral prediction of the Amposta Marino field (Spanish Mediterranean Sea): Geologie en Mijnbouw, v. 69, p. 105–120.

Budnik, T. T., 1987, Left-lateral intraplate deformation along the Ancestral Rocky Mountains: implications for late Paleozoic plate motions: Tectonophysics, v. 132, p. 195–214.

Candelaria, M. P., and Reed, eds., C. L., 1992, Paleokarst, karst related diagenesis and reservoir development: Examples from Ordovician-Devonian age strata of West Texas and the Mid-Continent: Permian Basin Section, Society of Economic Paleontologists and Mineralogists Publication No. 92-33, 202 p.

Canter, K. L., Stearns, D. B., Geesaman, R. C., and Wilson, J. L., 1993, Paleostructural and related paleokarst controls on reservoir development in the Lower Ordovician Ellenburger Group, Val Verde Basin, *in* Fritz, R. D., Wilson, J. L., and D. A. Yurewicz, D. A., eds., Paleokarst related hydrocarbon reservoirs: SEPM Core Workshop No. 18, New Orleans, April 25, p. 61–101.

Cloud, P. E., and Barnes, V. E., 1948, The Ellenburger Group of Central Texas: University of Texas, Austin, Bureau of Economic Geology Publication 4621, 473 p.

Cloud, P. E., and Barnes, V. E., 1957, Early Ordovician sea in Central Texas: Geological Society of American Memoir 67, p. 163–214.

Cloud, P. E., Barnes, V. E., and Bridge, J. 1945, Stratigraphy of the Ellenburger Group in Central Texas—a progress report: University of Texas, Austin, Bureau of Economic Geology Publication 4301, p. 133–161.

Combs, D. M., Loucks, R. G., and Ruppel, S. C., 2003, Lower Ordovician Ellenburger Group collapsed paleocave facies and associated pore network in the Barnhart field, Texas, *in* Hunt, T. J., and Lufholm, P. H., The Permian Basin: back to basics: West Texas Geological Society Fall Symposium: West Texas Geological Society Publication #03-112, p. 397–418.

Custer, M. A., 1957, Polar field, Kent County, Texas, *in* Heard, F. A., ed., Occurrence of oil and gas in West Texas: University of Texas, Austin, Bureau of Economic Geology Publication No. 5716, p. 200–282.

Dutton, S. P., Kim, E. M., Broadhead, R. F., Breton, C. L., Raatz, W. D., Ruppel, S. C., and Kerans, Charles, 2005, Play analysis and digital portfolio of major oil reservoirs in the Permian Basin: The University of Texas at Austin, Bureau of Economic Geology Report of Investigations No. 271, 287 p., CD-ROM.

Entzminger, D. J., 1994, Shafter Lake (Ellenburger), *in* Oil & gas fields in West Texas: West Texas Geological Society Publication 94-96, v. 4, p. 247–250.

Folk, R. L., 1959, Thin-section examination of Pre-Simpson Paleozoic rocks, *in* Barnes, V. E., Cloud, P. E., Jr., Dixon, L. P., Folk, R. L., Jonas, E. C., Palmer, A. R., and Tynan, E. J., Stratigraphy of the pre-Simpson Paleozoic subsurface rocks of Texas and southeast New Mexico: University of Texas, Austin, Bureau of Economic Geology Publication. 5924, p. 95–130.

Ford, D. C., 1988, Characteristics of dissolutional cave systems in carbonate rocks, *in* James, N. P., and Choquette, P. W., eds., Paleokarst: Springer-Verlag, p. 25–57.

Esteban, M., 1991, Palaeokarst: practical applications, *in* Wright, V. P., Esteban, M., and Smart, P. L., eds., Palaeokarst and palaeokarstic reservoirs: Postgraduate Research for Sedimentology, University of Reading, PRIS Contribution No. 152, p. 89–119.

Galley, J. E., 1958, Oil and geology in the Permian Basin of Texas and New Mexico, *in* Weeks, W. L., ed., Habitat of oil: American Association of Petroleum Geologists Special Publication, p. 395–446.

Goldhammer, R. K., 1996, Facies architecture, cyclic and sequence stratigraphy: the Lower Ordovician El Paso Group, West Texas, *in* Stoudt, E. L., ed., Precambrian-Devonian geology of the Franklin Mountains, West Texas—Analogs for

exploration and production in Ordovician and Silurian karsted reservoirs in the Permian basin: West Texas Geological Society Annual Field Trip Guidebook, WTGS Publication No. 96-100, p. 71–98.

Goldhammer, R. K., and Lehmann, P. J., 1996, Chaos in El Paso, *in* Stoudt, E. L., ed., Precambrian-Devonian geology of the Franklin Mountains, West Texas—Analogs for exploration and production in Ordovician and Silurian karsted reservoirs in the Permian basin: West Texas Geological Society 1996 Annual Field Trip Guidebook: WTGS Publication No. 96-100, p. 125–140.

Goldhammer, R. K., Lehmann, P. J., and Dunn, P. A., 1992, Third-order sequence boundaries and high frequency cycle stacking pattern in Lower Ordovician platform carbonates, El Paso Group (Texas): Implications for carbonate sequence stratigraphy, *in* Candelaria, M. P., and Reed, C. L., eds., Paleokarst, karst related diagenesis and reservoir development: examples from Ordovician-Devonian age strata of West Texas and the Mid-Continent: Permian Basin Section, SEPM (Society for Sedimentary Geology), Publication No. 92–33, p. 59–92.

Ham, W. E., and Wilson, J. L., 1967, Paleozoic epeirogeny and orogeny in the central United States: American Journal of Science, v. 265, no, 5, p. 332–407.

Hammes, U., 1997, Electrical imaging catalog: microresistivity images and core photos from fractured, karsted, and brecciated carbonate rocks: The University of Texas at Austin, Bureau of Economic Geology Geological Circular 97-2, 40 p.

Hammes, Ursula, Lucia, F. J., and Kerans, Charles, 1996, Reservoir heterogeneity in karst-related reservoirs: Lower Ordovician Ellenburger Group, West Texas, *in* Stoudt, E. L., ed., Precambrian–Devonian geology of the Franklin Mountains, West Texas—analogs for exploration and production in Ordovician and Silurian karsted reservoirs in the Permian Basin: West Texas Geological Society, Publication No. 96-100, p. 99–117.

Hardage, B. A., Carr, D. L., Lancaster, D. E., Simmons, J. L., Jr., Elphick, R. Y., Pendleton, V. M., and Johns, R. A., 1996, 3-D seismic evidence of the effects of carbonate karst collapse on overlying clastic stratigraphy and reservoir compartmentalization: Geophysics, v. 61, p. 1336–1350.

Hardwick, J. V., 1957, Block 32 field, Crane County, Texas, *in* Heard, F. A., ed., Occurrence of oil and gas in West Texas: The University of Texas at Austin, Bureau of Economic Geology Publication No. 5716, p. 40–46.

Holland, R. R., 1966, Puckett, Ellenburger, Pecos County, Texas, *in* Oil and gas fields in West Texas—A symposium: West Texas Geological Society Publication 66-52, p. 291–295.

Holtz, M. H., and Kerans, C., 1992, Characterization and categorization of West Texas Ellenburger reservoirs, *in* Candelaria, M. P., and Reed, C. L., eds., Paleokarst, karst related diagenesis and reservoir development: examples from Ordovician-Devonian age strata of West Texas and the Mid-Continent: Permian Basin Section SEPM Publication No. 92-33, p. 31–44.

Ijirighoi, B. T., and Schreiber, J. F., Jr., 1986, Origin and classification of fractures and related breccia in the Lower Ordovician Ellenburger Group, West Texas: West Texas Geological Society Bulletin, v. 26, p. 9–15.

Katz, B. J., Dawson, W. C., Robison, V. D., and Elrod, L. W., 1994, Simpson—Ellenburger(.) petroleum system of the Central Basin Platform, West Texas, U.S.A., *in* Magoon, L. B. and Dow, W. G., eds., The petroleum system—from source to trap: AAPG Memoir 60, p. 453–461.

Kerans, Charles, 1988, Karst-controlled reservoir heterogeneity in Ellenburger Group carbonates of West Texas: reply: AAPG Bulletin, v. 72, p. 1160–1183.

Kerans, Charles, 1989, Karst-controlled reservoir heterogeneity and an example from the Ellenburger Group (Lower Ordovician) of West Texas: The University of Texas at Austin, Bureau of Economic Geology Report of Investigations No. 186, 40 p.

Kerans, Charles, 1990, Depositional systems and karst geology of the Ellenburger Group (Lower Ordovician), subsurface West Texas: The University of Texas at Austin, Bureau of Economic Geology Report of Investigations No. 193, 63 p., 6 pl.

Kerans, Charles, Lucia, F. J., and Senger, R. K., 1994, integrated characterization of carbonate ramp reservoirs using Permian San Andres outcrop analogs: AAPG Bulletin, v. 78, p. 181–216.

Kvenvolden, K. A., and Squires, R. M., 1967, Carbon isotopic composition of crude oils from Ellenburger Group (Lower Ordovician), Permian basin, West Texas and eastern New Mexico: AAPG Bulletin, v. 51, p. 1293–1303.

Kupecz, J. A., 1992, Sequence boundary control on hydrocarbon reservoir development, Ellenburger Group, Texas, *in* Candelaria, M. P., and Reed, C. L., eds., Paleokarst, karst related diagenesis and reservoir development: examples from Ordovician-Devonian age strata of West Texas and the Mid-Continent: Permian Basin Section, (Society for Sedimentary Geology), Publication No. 92–33, p. 55–58.

Kupecz, J. A., and L. S. Land, 1991, Late-stage dolomitization of the Lower Ordovician Ellenburger Group, West Texas: Journal of Sedimentary Petrology, v. 61, p. 551–574.

Lee, I. Y., and Friedman, G. M., 1987, Deep-burial dolomitization in the Ordovician Ellenburger Group carbonates, West Texas and southeastern New Mexico—Reply: Journal of Sedimentary Petrology, v. 58, p. 910–913.

Lindsay, R. F., and Koskelin, K. M., 1993, Arbuckle Group (Late Cambrian-early Ordovician) shallowing-upward parasequences and sequences, southern Oklahoma, *in* Keller, D. R., and Reed, C. L., eds., Paleokarst, karst related diagenesis and reservoir development: examples from Ordovician-Devonian age strata of West Texas and the Mid-Continent: Permian Basin Section SEPM Publication No. 92-33, p. 45–65.

Loucks, R. G., 1999, Paleocave carbonate reservoirs: origins, burial-depth modifications, spatial complexity, and reservoir implications: AAPG Bulletin, v. 83, p. 1795–1834.

Loucks, R. G., 2001, Modern analogs for paleocave-sediment fills and their importance in identifying paleocave reservoirs: Gulf Coast Association of Geological Societies Transactions, v. 46, p. 195–206.

Loucks, R. G., 2003, Understanding the development of breccias and fractures in Ordovician carbonate reservoirs, *in* Hunt, T. J., and Lufholm, P. H., The Permian Basin: back to basics: West Texas Geological Society Fall Symposium: West Texas Geological Society Publication No. 03-112, p. 231–252.

Loucks, R. G., 2007, A review of coalesced, collapsed-paleocave systems and associated suprastratal deformation: Acta Carsologica, v. 36, no. 1, p. 121–132.

Loucks, R. G., and Anderson, J. H., 1980, Depositional facies and porosity development in Lower Ordovician Ellenburger dolomite, Puckett Field, Pecos County, Texas, *in* Halley, R. B. and Loucks, R. G., eds., Carbonate reservoir rocks: SEPM Core Workshop No. 1, p. 1–31.

Loucks, R. G., and Anderson, J. H., 1985, Depositional facies, diagenetic terrains, and porosity development in Lower Ordovician Ellenburger Dolomite, Puckett Field, West Texas, *in* Roehl, P. O., and Choquette, P. W., eds., Carbonate petroleum reservoirs: Springer-Verlag, p. 19–38.

Loucks, R. G., and Handford, R. H., 1992, Origin and recognition of fractures, breccias, and sediment fills in paleocave-reservoir networks, *in* Candelaria, M. P., and Reed, C. L., eds., Paleokarst, karst related diagenesis and reservoir development: examples from Ordovician-Devonian age strata of West Texas and the Mid-Continent: Permian Basin Section, SEPM (Society for Sedimentary Geology), Publication No. 92–33, p. 31–44.

Loucks, R. G., and Mescher, P. A, 1998, Origin of fractures and breccias associated with coalesced collapsed paleocave systems (abs.), *in* Rocky Mountain Association Symposium on Fractured Reservoirs: Practical Exploration and Development Strategies, unpaginated.

Loucks, R. G., and Mescher, P., 2001, Paleocave facies classification and associated pore types, *in* American Association of Petroleum Geologists, Southwest Section, Annual Meeting, Dallas, Texas, March 11–13, CD-ROM, 18 p.

Loucks, R. G., Mescher, P., and McMechan, G. A., 2000, Architecture of a coalesced, collapsed-paleocave system in the Lower Ordovician Ellenburger Group, Dean Word Quarry, Marble Falls, Texas: Final report prepared for the Gas Research Institute, GRI-00/0122, CD-ROM.

Loucks, R. G., Mescher, P. K., and McMechan, G. A., 2004, Three-dimensional architecture of a coalesced, collapsed-paleocave system in the Lower Ordovician Ellenburger Group, Central Texas: AAPG Bulletin, v. 88, no. 5, p. 545–564.

Lucia, F. J., 1971, Lower Paleozoic history of the western Diablo Platform, West Texas and south-central New Mexico, *in* Cys, J. M., ed., Robledo Mountains and Franklin Mountains—1971 Field Conference Guidebook: Permian Basin Section, SEPM, p. 174–214.

Lucia, F. J., 1968, Sedimentation and paleogeography of the El Paso Group, *in* Stewart, W. J., ed., Delaware basin exploration: West Texas Geological Society Guidebook No. 68-55, p. 61–75.

Lucia, F. J., 1969, Lower Paleozoic history of the western Diablo Platform of West Texas and south-central New Mexico, *in* Seewald, K., and Sundeen, D., eds., The geologic framework of the Chihuahua tectonic belt: West Texas Geological Society, p. 39–56.

Lucia, F. J., 1995, Lower Paleozoic cavern development, collapse, and dolomitization, Franklin Mountains, El Paso, Texas, *in* Budd, D. A., Saller, A. H., and Harris, P. M., eds., Unconformities and porosity in carbonate strata: AAPG Memoir 63, p. 279–300.

Lucia, F. J., 1996, Structural and fracture implications of Franklin Mountains collapse brecciation, *in* Stoudt, E. L., ed., Precambrian-Devonian geology of the Franklin Mountains, West Texas—Analogs for exploration and production in Ordovician and Silurian karsted reservoirs in the Permian basin: West Texas Geological Society 196 Annual Field Trip Guidebook, WTGS Publication No. 96-100, p. 117–123.

Mazzullo, S. J., and G. V. Chilingarian, 1996, Hydrocarbon reservoirs in karsted carbonate rocks, *in* Chilingarian, G. V., Mazzullo, S. J., and Rieke, H. H., eds., Carbonate reservoir characterization: a geologic-engineering analysis, Part II: Elsevier, p. 797–685.

Mazzullo, S. J., and Mazzullo, L. J., 1992, Paleokarst and karst-associated hydrocarbon reservoirs in the Fusselman Formation, West Texas, Permian basin, *in* Candelaria, M. P., and Reed, C. L., eds., Paleokarst, karst related diagenesis and reservoir development: examples from Ordovician-Devonian age strata of West Texas and the Mid-Continent: Permian Basin Section, SEPM (Society for Sedimentary Geology), Publication No. 92–33, p. 110–120.

McDonnell, Angela, Loucks, R. G., and Dooley, Tim, 2007, Quantifying the origin and geometry of circular sag structures in northern Fort Worth Basin, Texas: paleocave collapse, pull-apart fault systems, or hydrothermal alteration? AAPG Bulletin, v. 91, no. 9, p. 1295–1318.

McMechan, G. A., Loucks, R. G., Mescher, P. A., and Zeng, Xiaoxian, 2002, Characterization of a coalesced, collapsed paleocave reservoir analog using GPR and well-core data: Geophysics, v. 67, no. 4, p. 1148–1158.

McMechan, G. A., Loucks, R. G., Zeng, X., and Mescher, P. A., 1998, Ground penetrating radar imaging of a collapsed paleocave system in the Ellenburger dolomite, Central Texas: Journal of Applied Geophysics, v. 39, p. 1–10.

Palmer, A. N., 1991, Origin and morphology of limestone caves: Geological Society of America Bulletin, v. 103, p. 1–21.

Purves, W. J., E. B. Burnitt, L. R. Weathers, and L. K. Wipperman, 1992, Cave/pillar definition in the Ordovician Ellenburger reservoir by 3-D seismic, Pegasus field, Midland and Upton counties, Texas (abs.): AAPG Annual Meeting Program and Abstracts, p. 108.

Ross, R. J., Jr., 1976, Ordovician sedimentation in the western United States, *in* Bassett, M. G., ed., The Ordovician System: Proceedings of a Paleontological Association Symposium: Birmingham, p. 73–105.

Ross, R. J., Jr., 1982, The Ordovician System in the United States—correlation chart and explanatory note: International Union of Geological Sciences Publication 12, 73 p.

Ruppel, S. C., Jones, R. H., Breton, C. L., and Kane, J. A., 2005, Preparation of maps depicting geothermal gradient and Precambrian structure in the Permian Basin: The University of Texas at Austin, Bureau of Economic Geology, contract report prepared for the U.S. Geological Survey under order no. 04CRSA0834 and requisition no. 04CRPR01474, 23 p. + CD-ROM.

Sloss, L. L., 1963, Sequences in the cratonic interior of North America: Geological Society of America Bulletin, v. 74, p. 93–114.

Texas Water Development Board, 1972, A survey of the subsurface saline water of Texas: Austin, TWDB, v. 1, 113 p.

White, W. B., 1988, Geomorphology and hydrology of karst terrains: New York, Oxford University Press, 464 p.

White, E. L., and White, W. B., 1968, Dynamics of sediment transport in limestone caves: National Speleothem Society Bulletin, v. 30, 115–129.

Wilson, J. L., Medlock, R. L., Fritz, R. D., Canter, K. L., and Geesaman, R. G., 1992, A review of Cambro-Orodovician breccias in North America, *in* Keller, D. R., and. Reed, C. L, eds., Paleokarst, karst related diagenesis and reservoir development: examples from Ordovician-Devonian age strata of West Texas and the Mid-Continent: Permian Basin Section SEPM Publication No. 92-33, p. 19–29.

Wright, V. P., Esteban, M., and Smart, P. L., eds., 1991, Palaeokarst and palaeokarstic reservoirs: Postgraduate Research for Sedimentology, University, PRIS Contribution No. 152, 158 p.

Young, L. M., 1968, Sedimentary petrology of the Marathon Formation, (Lower Ordovician), Trans-Pecos Texas: The University of Texas at Austin at Austin, Ph.D. dissertation, 234 p.

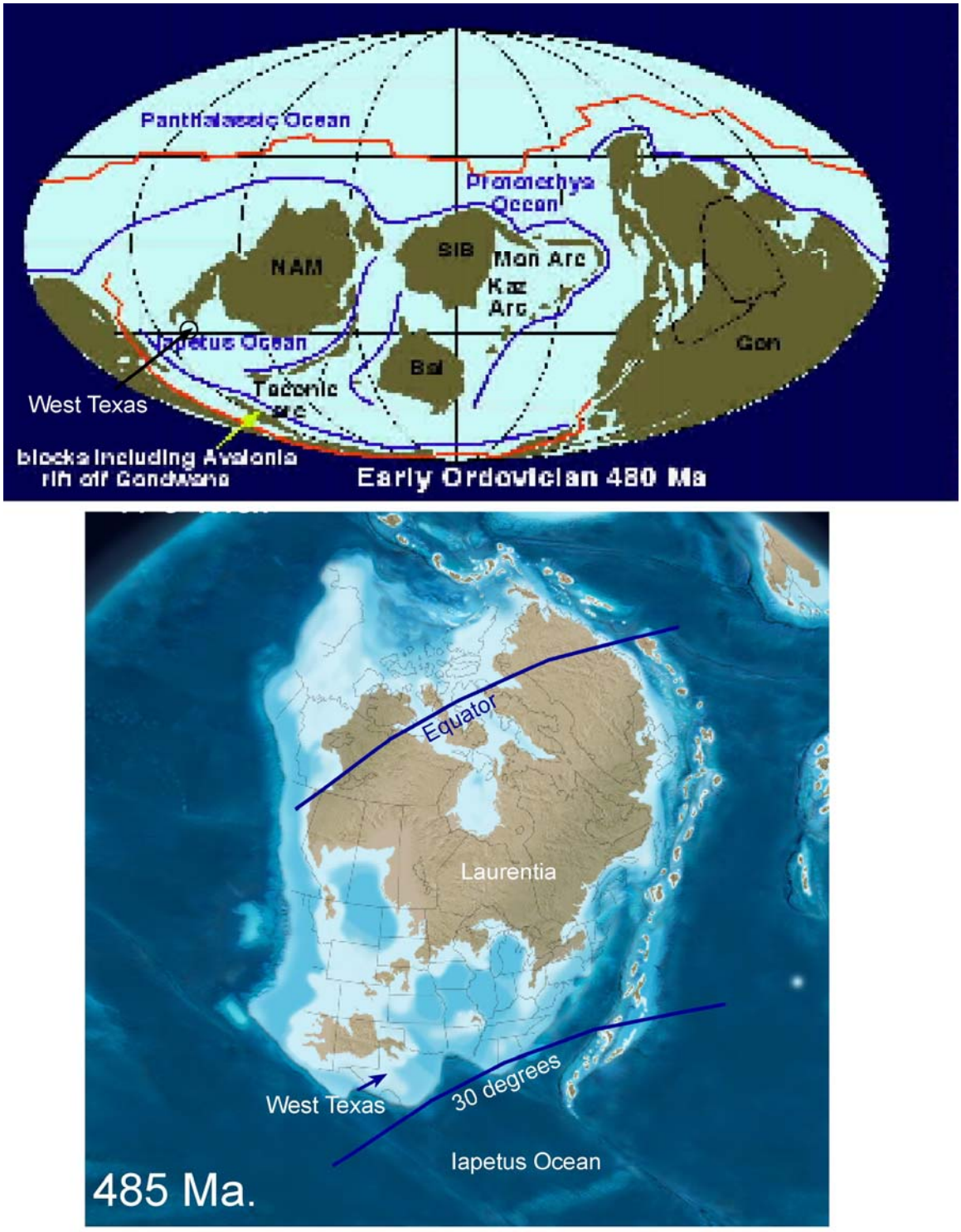

Figure 1. Reconstruction of Laurenia Plate for the Lower Ordovician (480 Ma at top and 485 Ma at bottom). West Texas was located at the southwest edge of the continent bordering the deep Iapetus Ocean. Upper map is from Blakey (2005a) and lower map is from Blakey (2005b). The lower map is slightly modified by present author. The location of the equator and 30 degrees latitude are estimated from the upper global diagram.

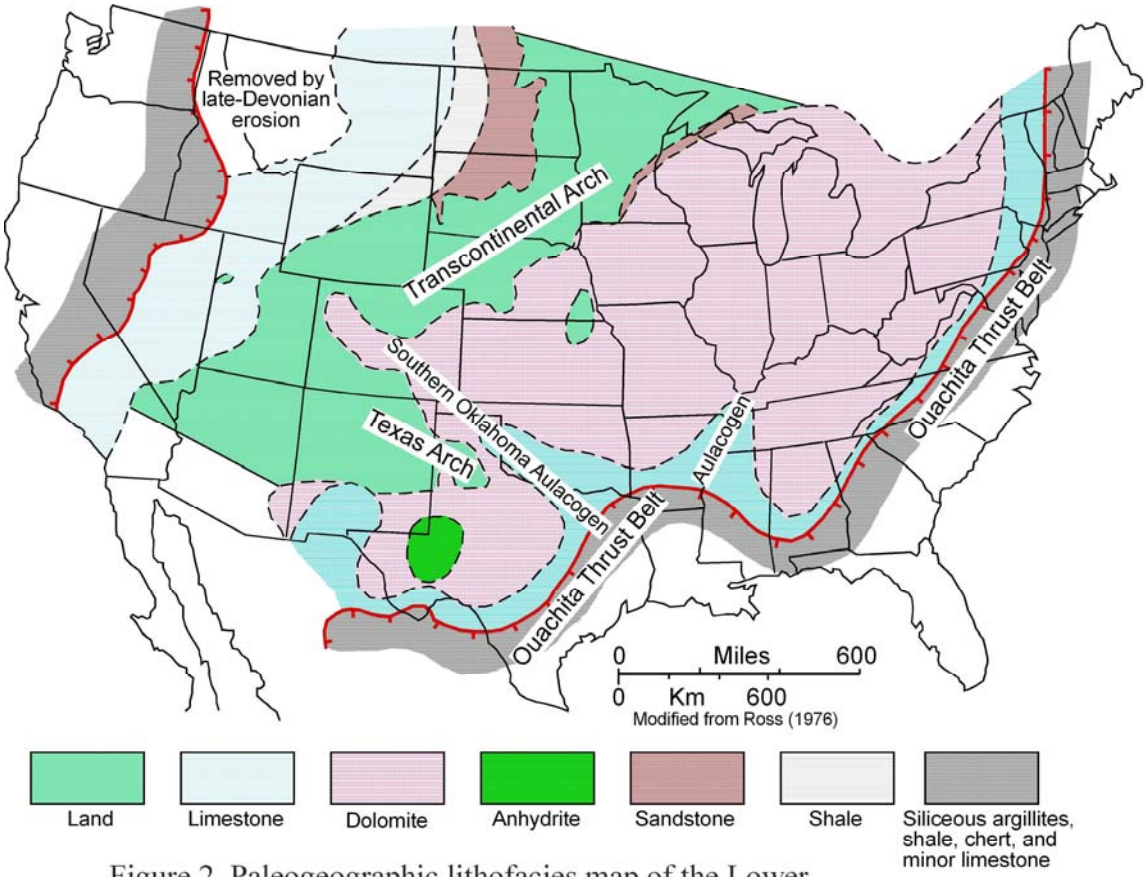

Figure 2. Paleogeographic lithofacies map of the Lower Ordovician section in the United States. From Ross (1976).

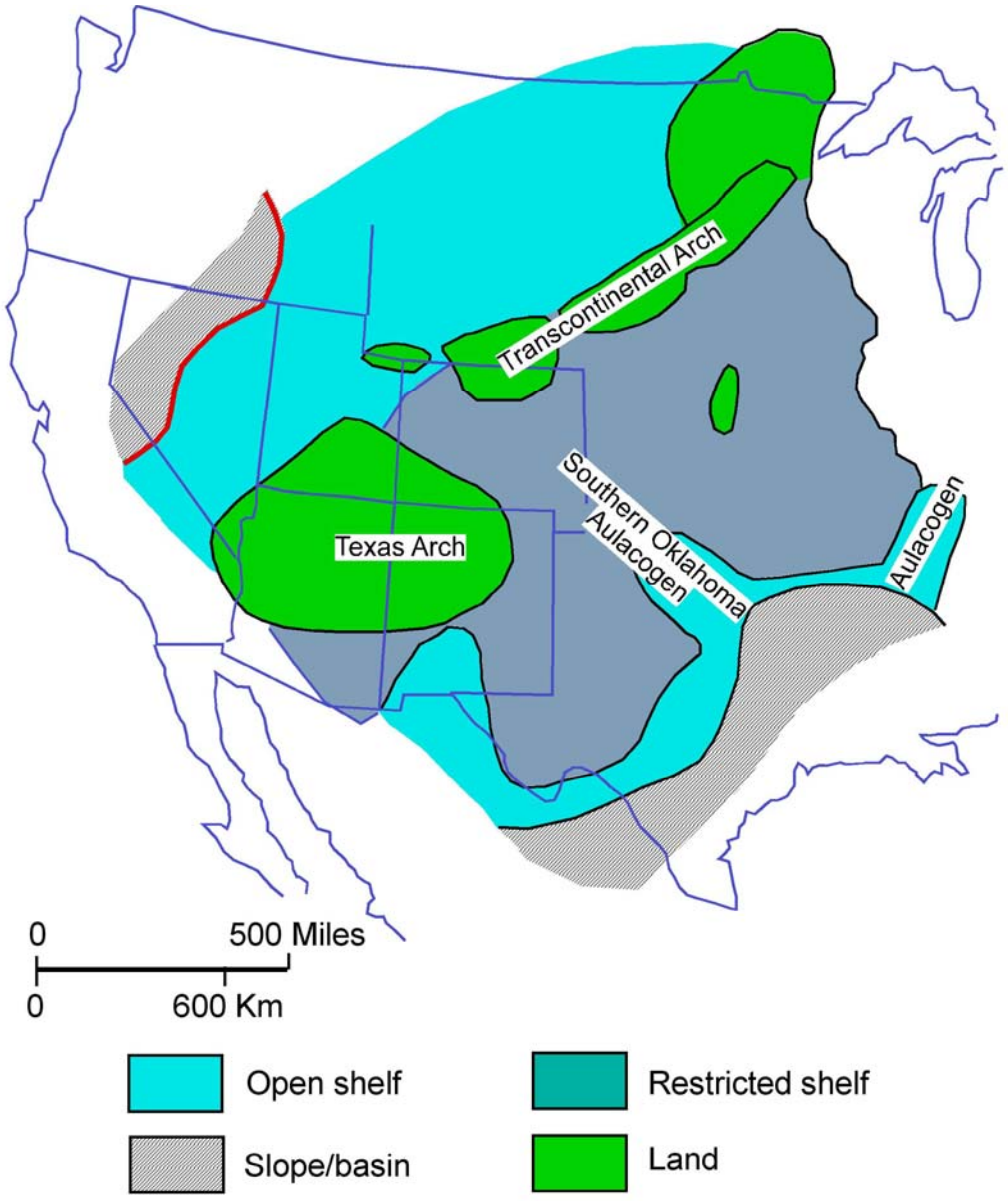

Figure 3. Interpreted regional depositional setting during Early Ordovician time. After Ross (1976) and Kerans (1990).

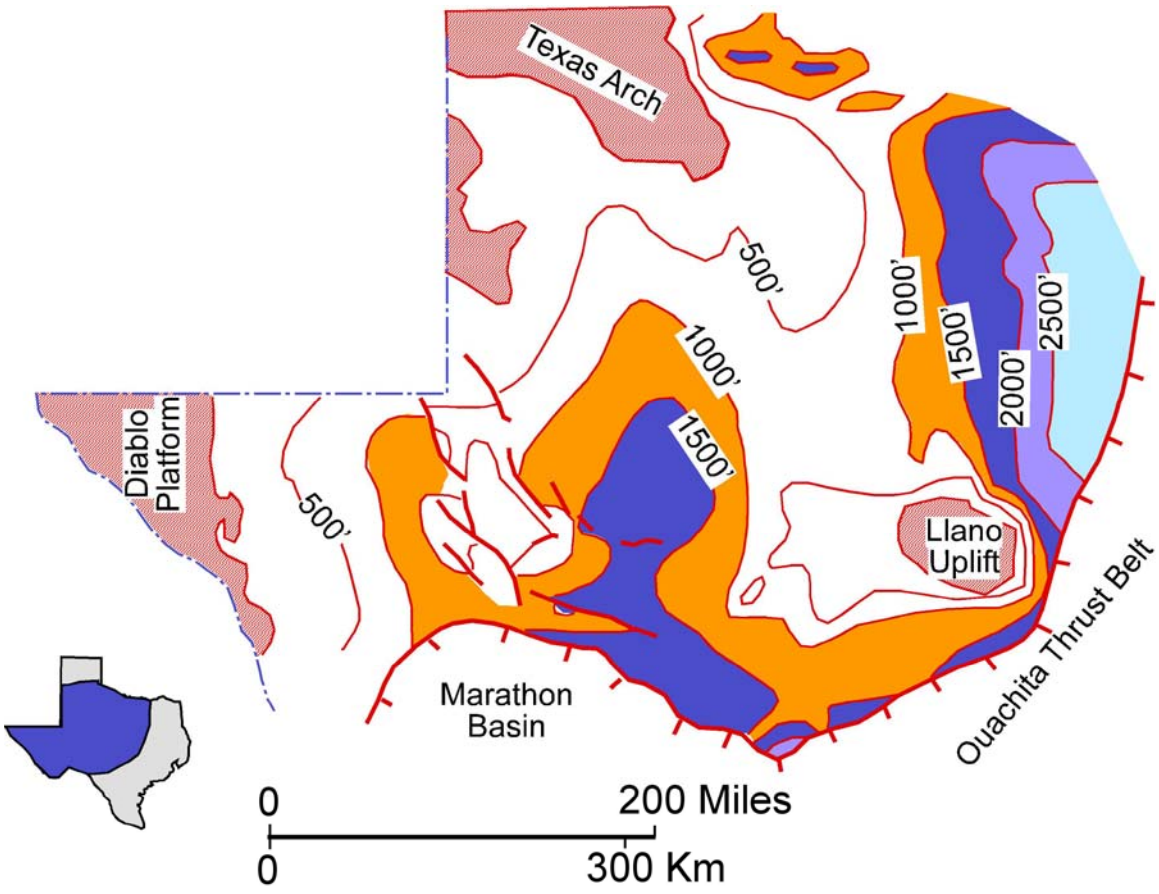

Figure 4. Generalized isopach map of the Ellenburger Group in West Texas. Thickest areas are colored. After Kerans (1989) who modified Texas Water Development Board (1972) figure.

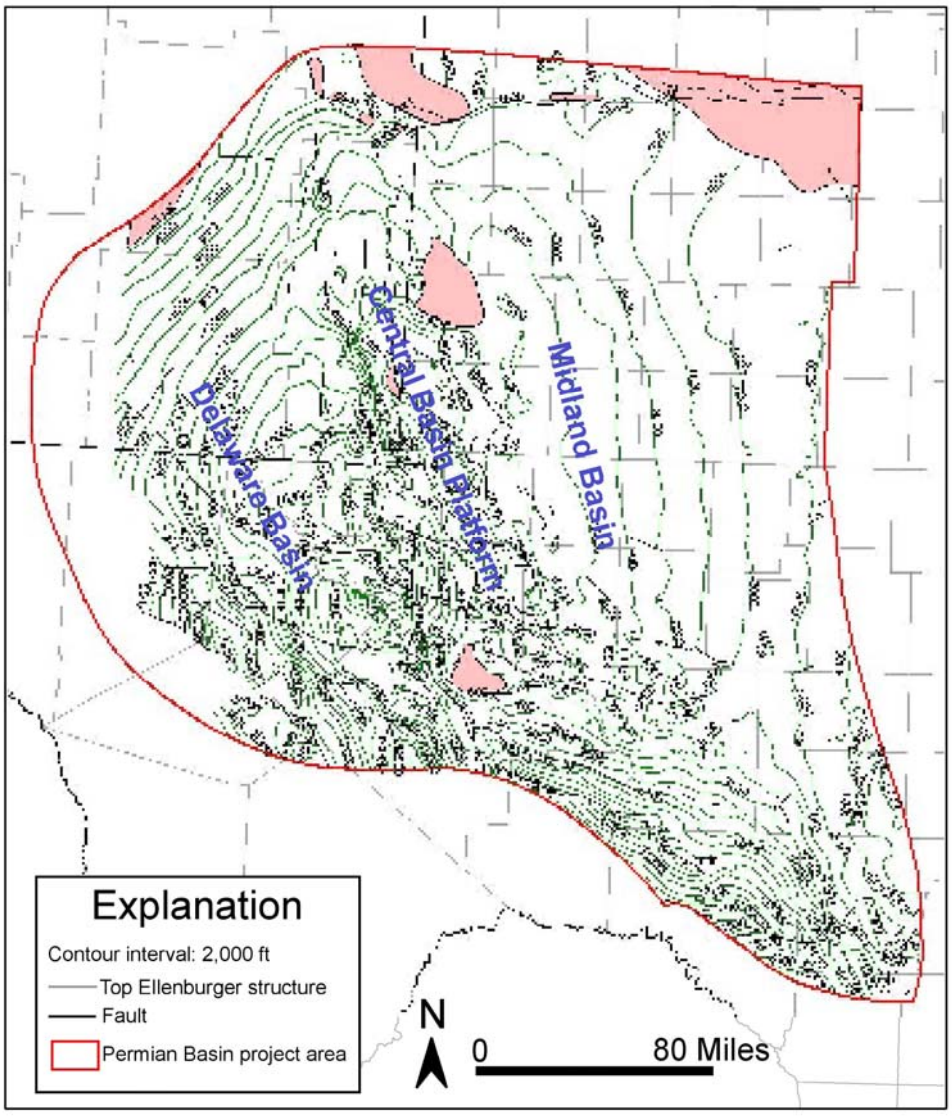

Figure 5. Structure map on top of Ellenburger Group from Ruppel et al. (2005). Contours are subsea depths.

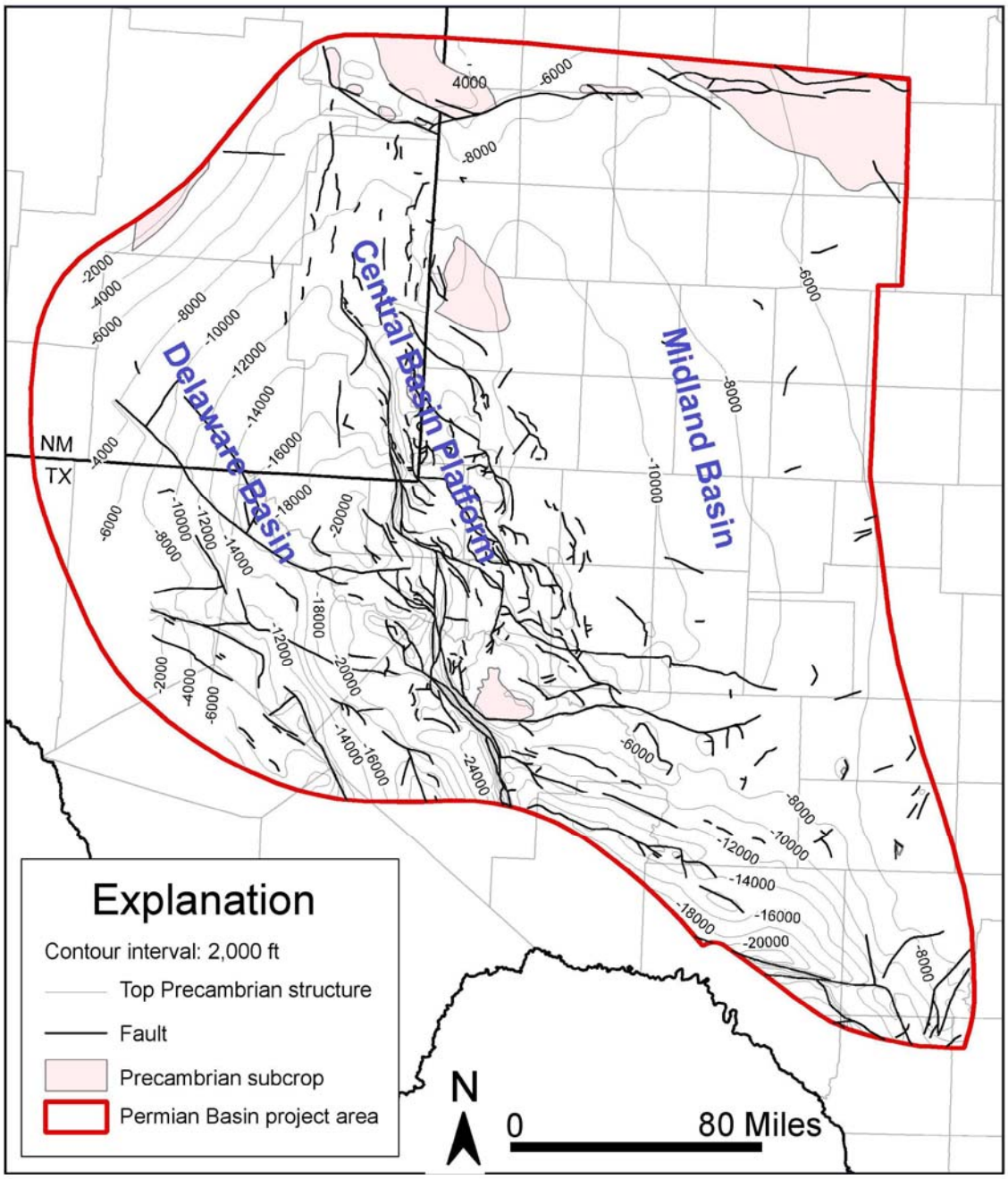

Figure 6. Structure map on top of Precambrian strata from Ruppel et al. (2005). Contours are subsea depths.

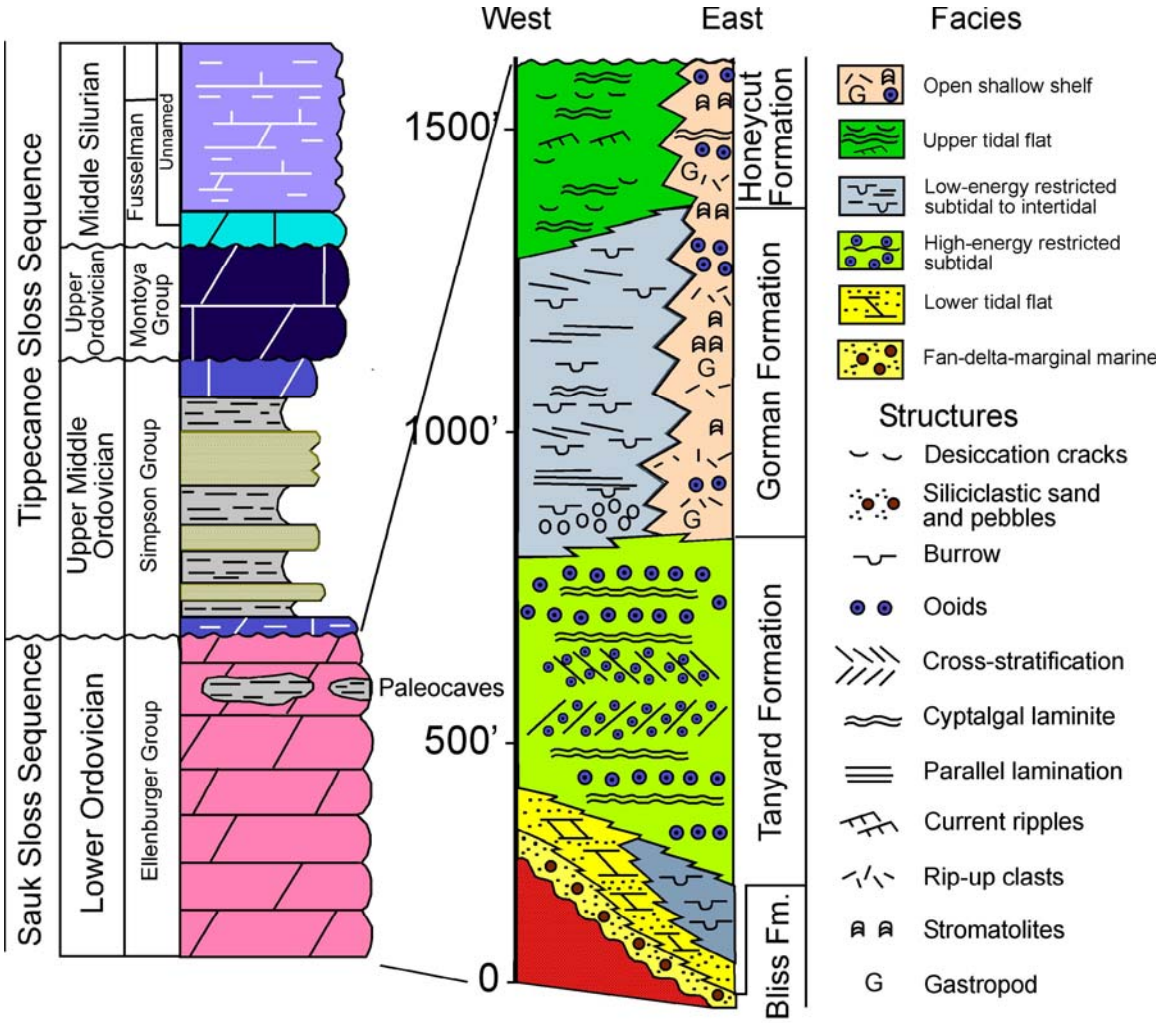

Figure 7. Schematic representation of Ellenburger depositional systems in West Texas compared with formalized Ellenburger stratigraphic units in the Llano area. Thickness of descriptive Ellenburger section is approximate. From Kerans (1990) with minor additions.

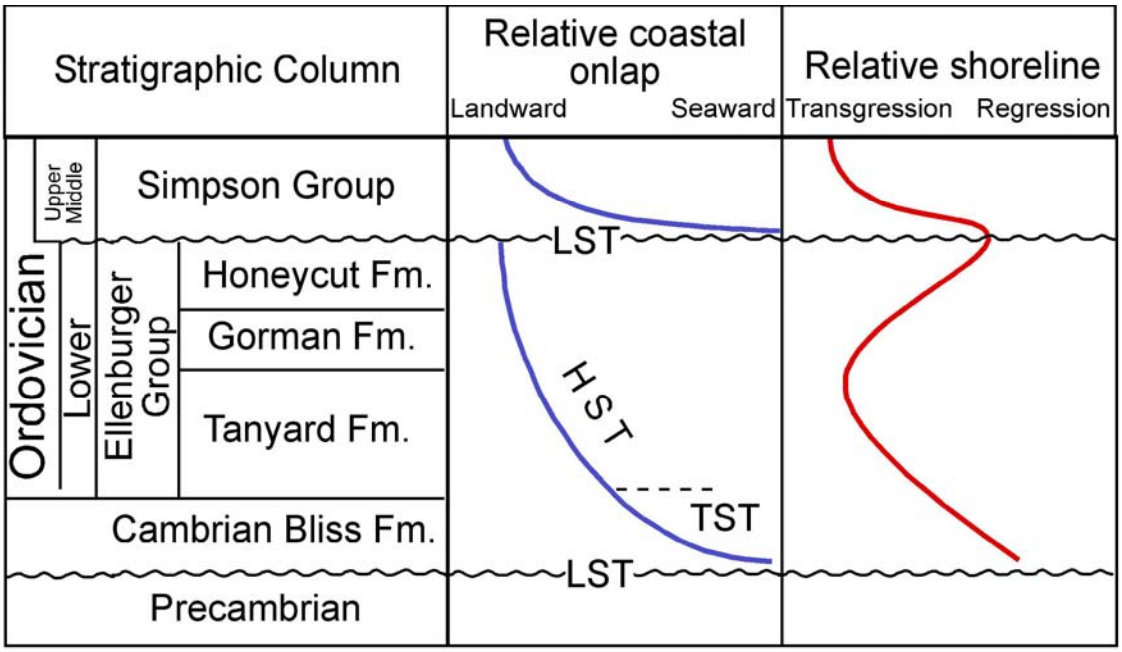

Figure 8. Interpretation of the second-order relative coastal and relative shoreline curves for the Ellenburger Group. Modified from Kupecz (1992).

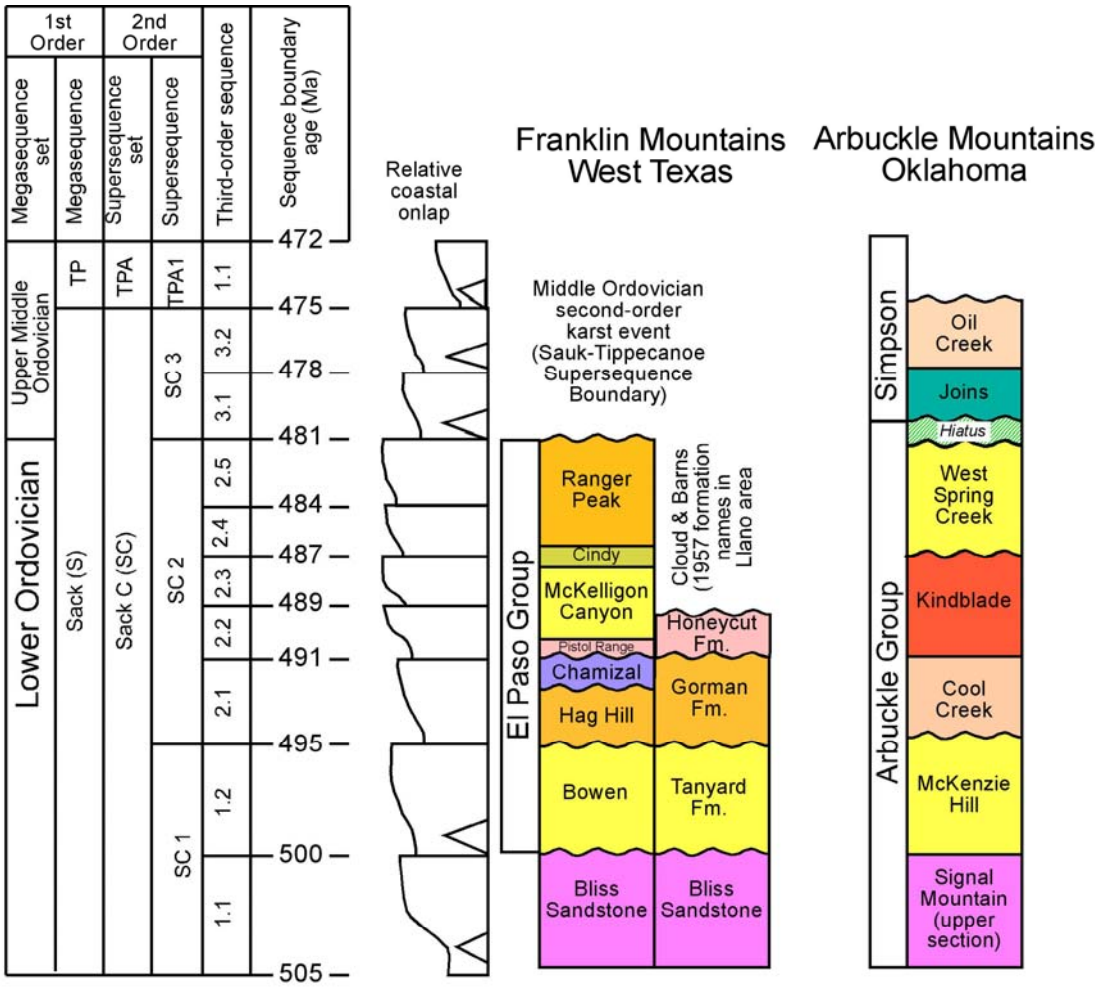

Figure 9. Chronostratigraphic summary of third-order depositional sequences in the Franklin Mountains of West Texas. Modified from Goldhammer et al. (1992).

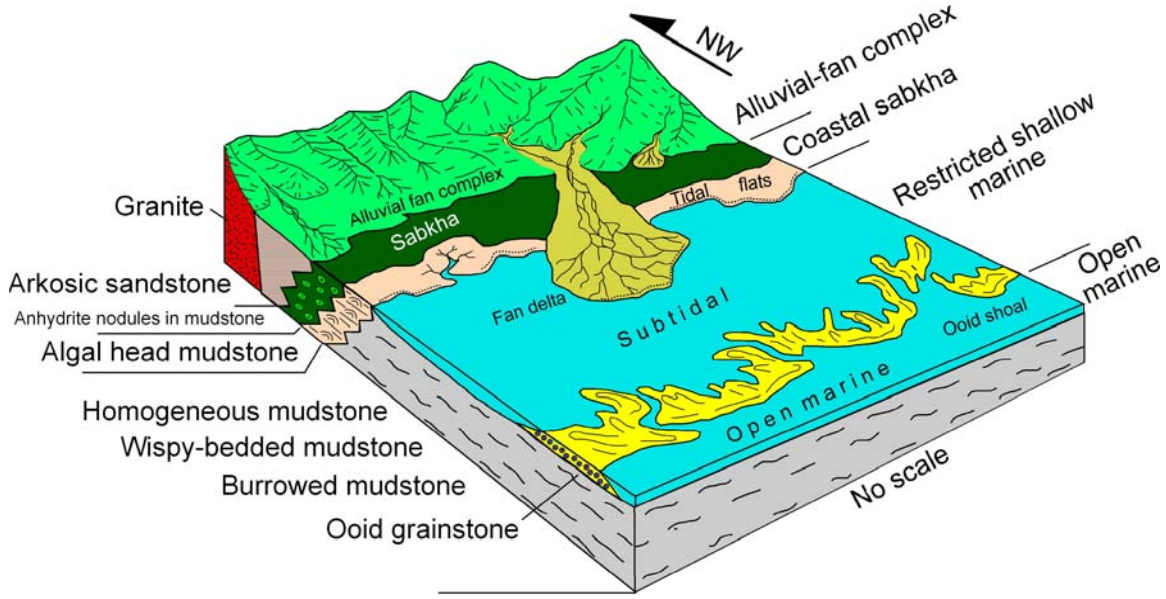

Figure 10. Depositional model for the Bliss and lower Ellenburger sections. Modified slightly from Loucks and Anderson (1985).

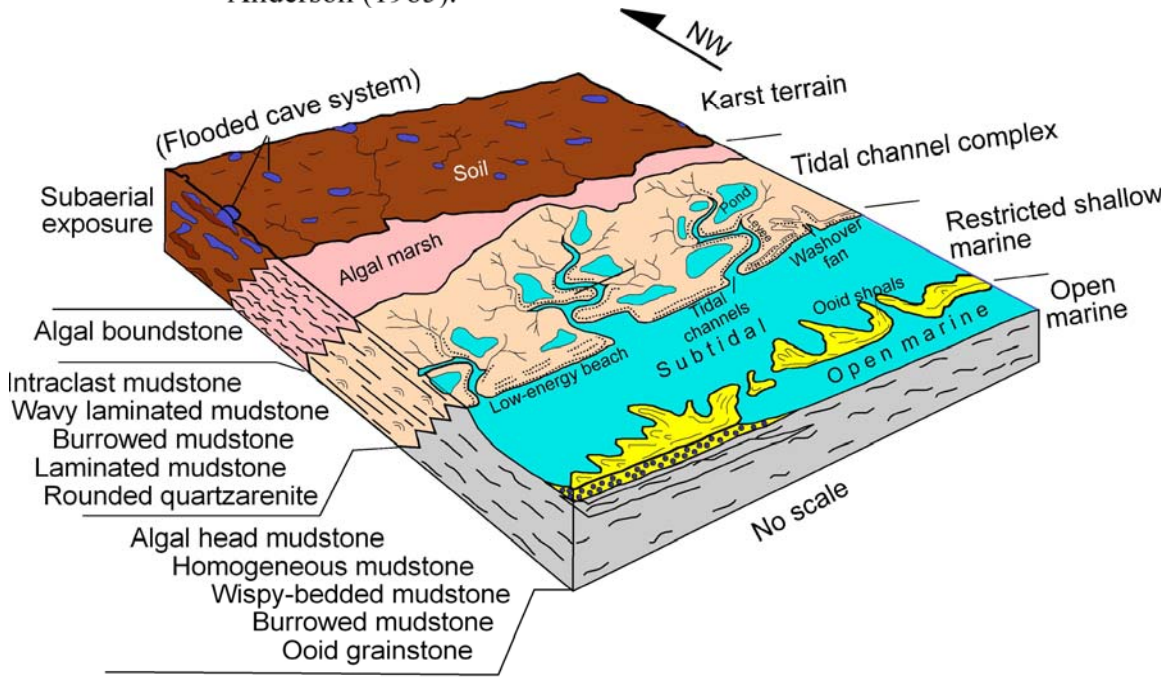

Figure 11. Depositional model for the middle and upper Ellenburger sections. Modified slightly from Loucks and Anderson (1985).

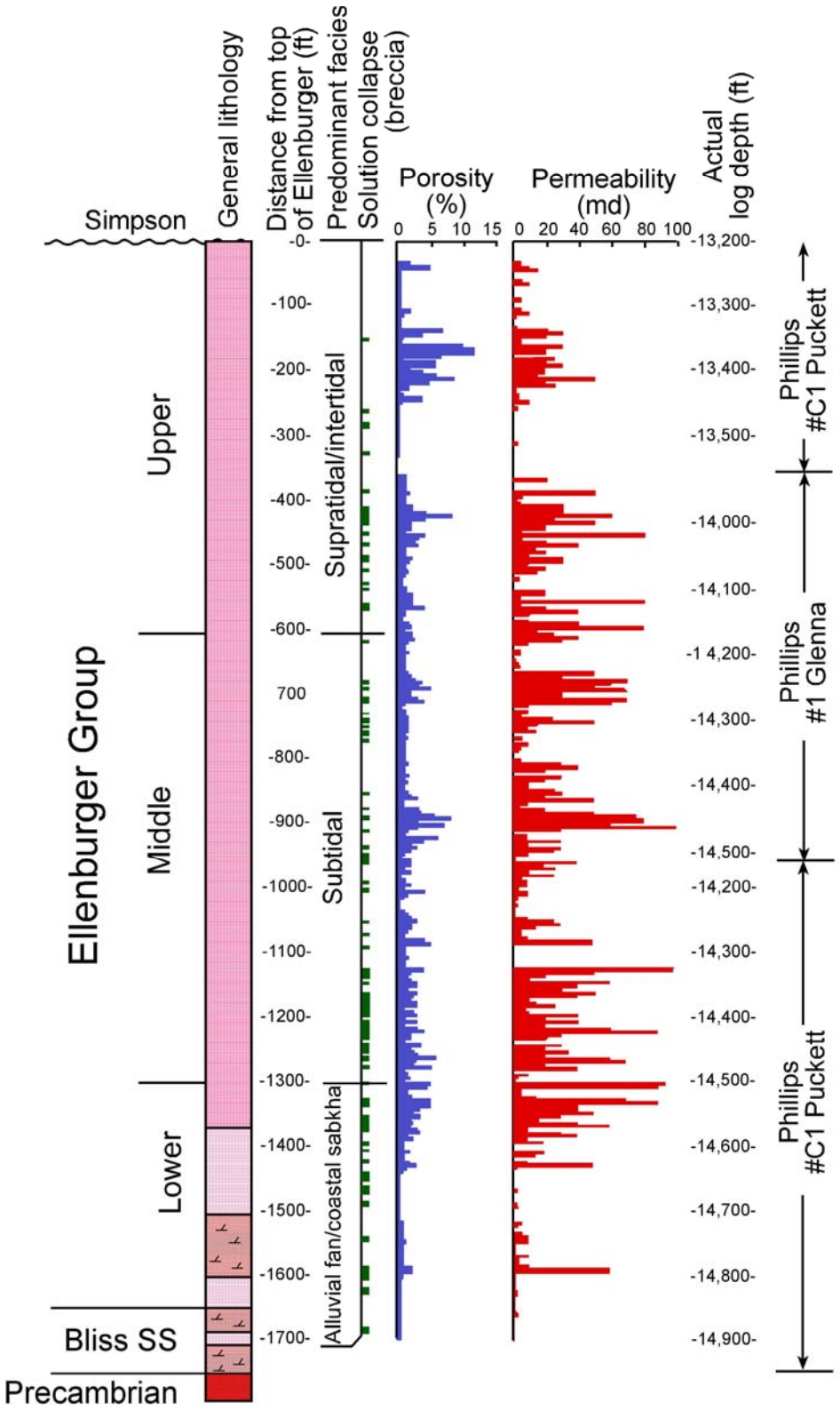

Figure 12. Profiles of porosity and permeability versus depth in the Phillips #C1 Puckett and #1 Glenna wells. Both well-log depths and depth below top of Ellenburger section are shown. "Predominant facies" refers to the facies comprising largest proportions of individual cycles. From Loucks and Anderson (1980, 1985).

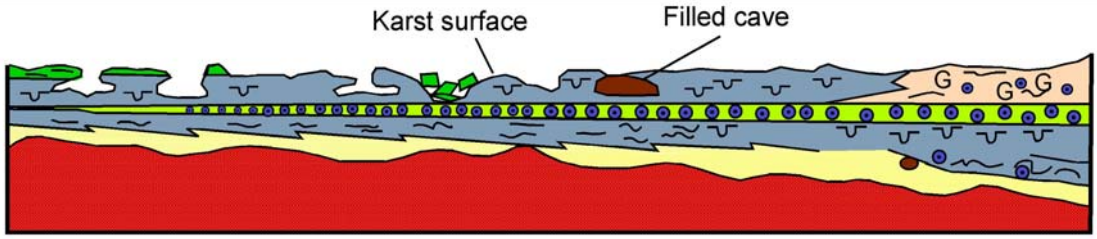

Stage 4. Exposure and erosion of the Ellenburger Group before the Middle Ordovician transgression formed a karst terrain.

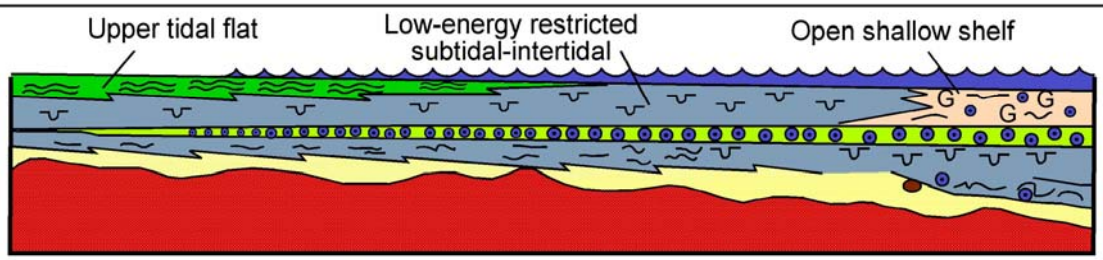

Stage 3. Regressive sedimentation with low-energy restricted-shelf and upper tidal-flat depositional systems prograding across the Ellenburger shelf, from northwest to east, southeast, and south. The open shallow-water shelf depositional system was deposited where more normal marine conditions prevailed, along the southern and eastern portions of the shelf.

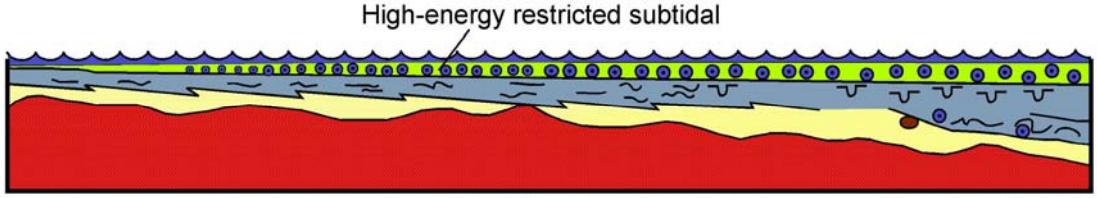

Stage 2. Rapid transgression and widespread aggradational deposition of the high-energy restricted-shelf depositional system across much of West and Central Texas.

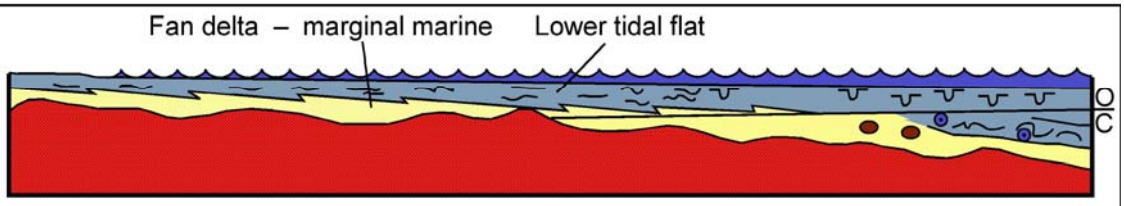

Stage 1. Regional deposition of fan delta – marginal marine depositional system continuous with Early Cambrian transgression. Progradation of lower tidal-flat depositional system followed.

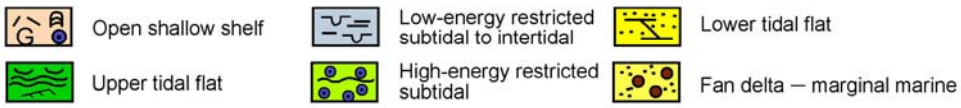

Figure 13. General depositional history of Ellenburger Group by stages. From Kerans (1990). Description of stages is taken directly from Kerans original figure caption.

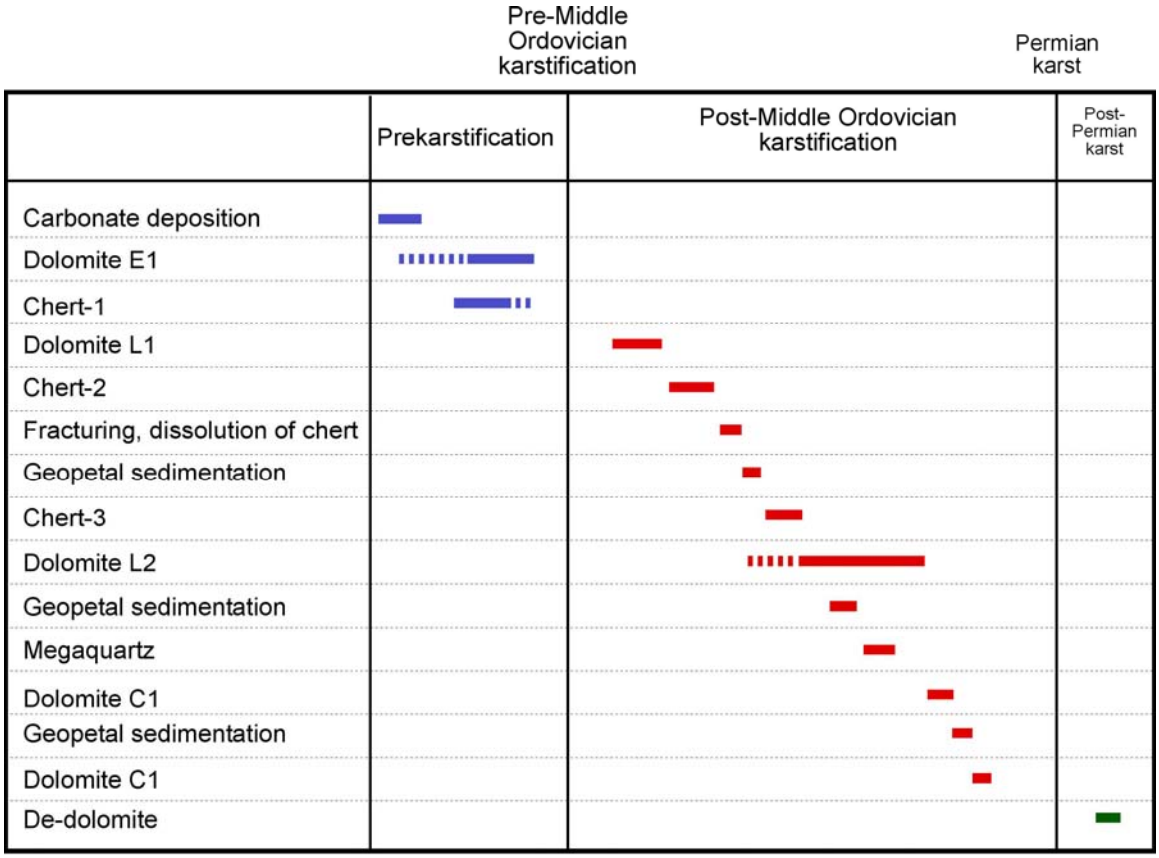

Figure 14. Paragenetic sequence of regional Ellenburger diagenesis by Kupecz and Land (1991). Figure from Kupecz and Land (1991).

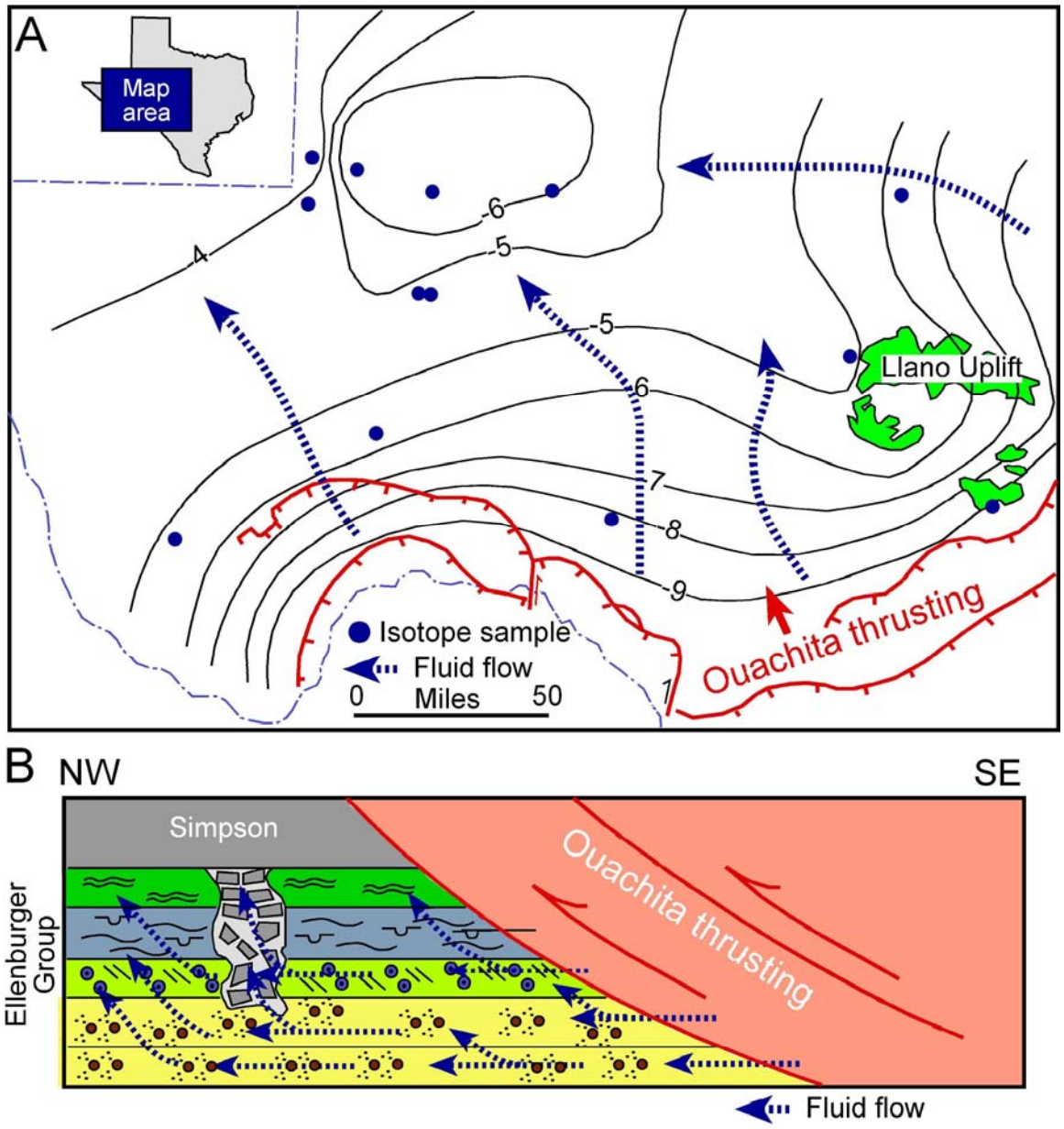

Figure 15. Fluid-flow model of Kupecz and Land (1991) for late-stage replacement Dolomite-L2. Figures from Kupecz and Land (1991). (A) Contour map of delta O^{18} isotopes of the late-stage replacement Dolomite-L2. Hypothetical fluid pathway-flow lines added by present author. The map indicates that hydrothermal fluids moved from the Ouachita Orogeny front in the southeast toward New Mexico to the northwest. (B) Schematic diagram showing the pathways for the hydrothermal fluids expelled by thrusting during the Ouachita Orogeny. The fluids moved along permeable faults, fractures, karst-breccia zones, and matrix pore-rich units.

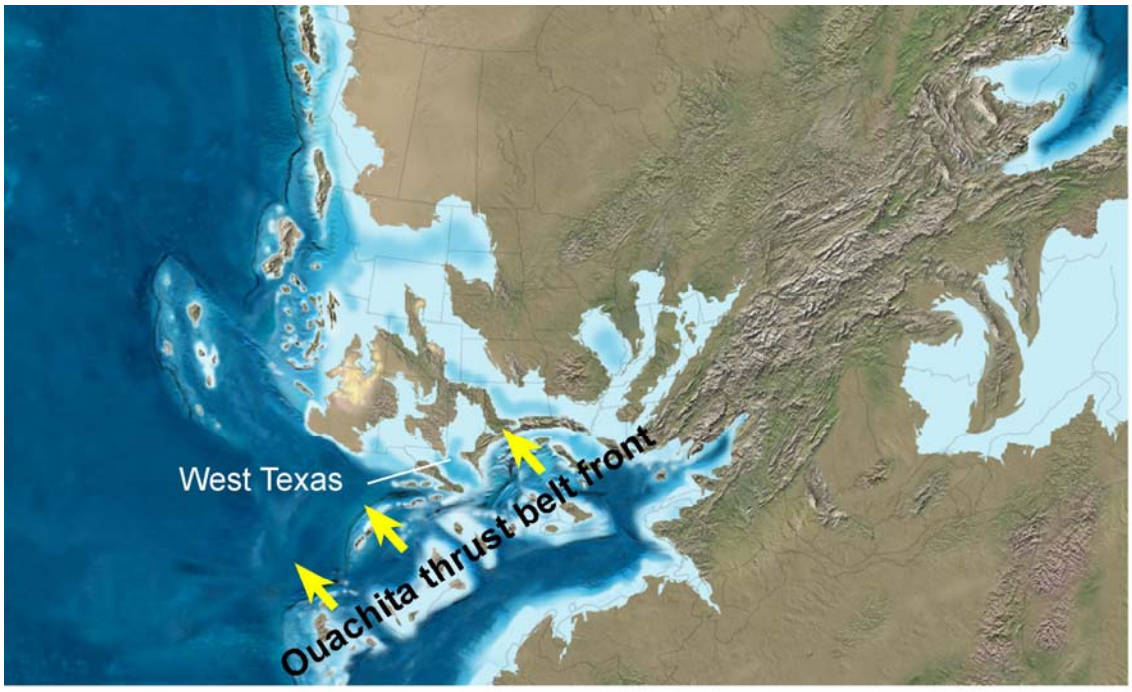

Figure 16. Plate reconstruction map of Early Pennsylvanian (315 Ma) by Blakey (2005b). The Ouachita thrusting injected dolomitizing fluids into the Ellenburger Group in the Central and West Texas areas. The yellow arrows indicate direction of thrust-fault movement.

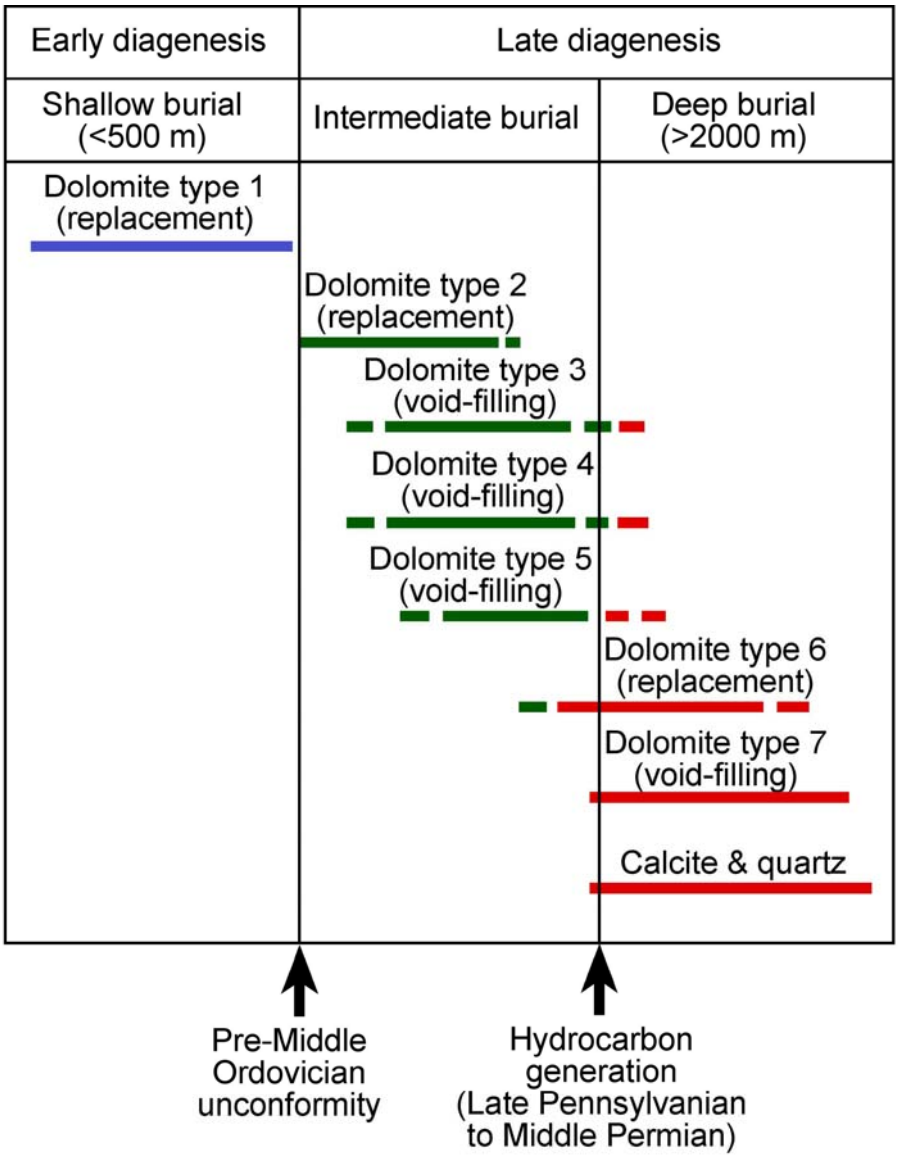

Figure 17. Paragenetic sequence of Amthor and Friedman (1991) for Ellenburger regional diagenetic study. Figure from Amthor and Friedman (1991).

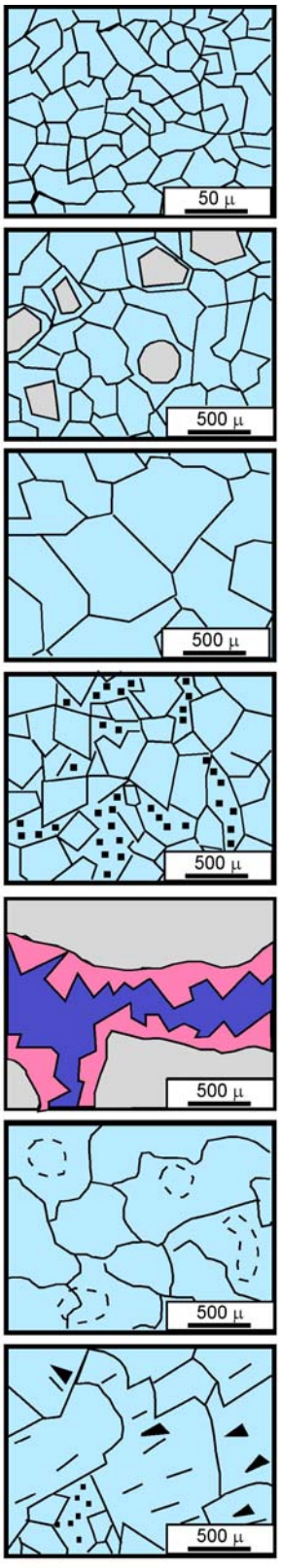

Dolomite type 1: Unimodal, very fine to fine-crystalline planar-s mosaic dolomite; dense, dark mosaics, replacing lime mud, preserving sedimentary structures.

Dolomite type 2: Unimodal, medium- to coarse-crystalline planar-s mosaic dolomite; milky white to clear or cloudy core, clear rim texture, nonmimic replacement of grains.

Dolomite type 3: Coarse- to very coarse crystalline planar-s dolomite; milky to clear crystals; no replacement features; fills void space and fractures.

Dolomite type 4: Medium- to coarse-crystalline planar-e mosaic dolomite; clear or cloudy core, clear rim texture; not replacement features; occurs in mottles orbreccias or near stylolites.

Dolomite type 5: Medium- to coarse-crystalline planar-e dolomite; clear crystals lining void space and fractures filled by late dolomite and/or calcite.

Dolomite type 6: Coarse- to very coarse crystalline nonplanar-a dolomite; dark, inclusion-rich crystals, with serrated, irregular, curved, or otherwise distinct boundaries; undulose extinction; vague nonmimic replacement of grains.

Dolomite type 7: Coarse- to very coarse crystalline nonplanar-c dolomite milky white to clear crystals with undulose extinction and curved crystal faces (saddle dolomite); void filling; associated with authigenic quartz and late calcite.

Figure 18. Dolomite textures described by Amthor and Friedman (1991). Figure from Amthor and Friedman (1991).

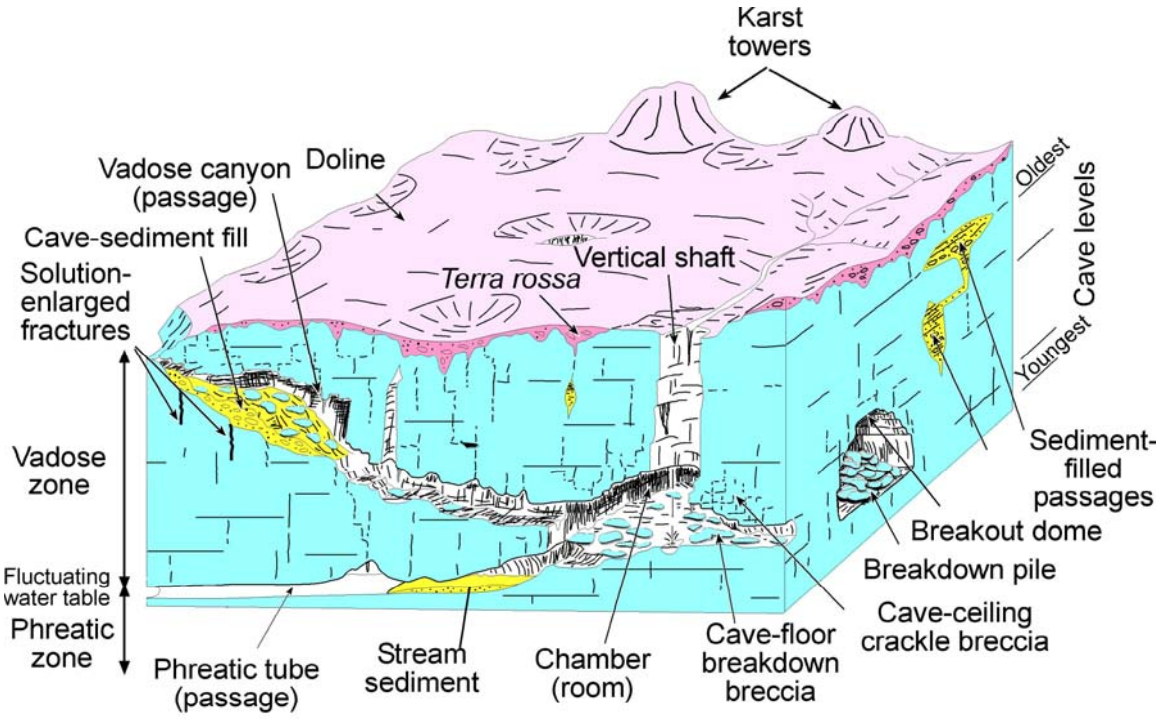

Figure 19. Block diagram of a near-surface modern karst system. The diagram depicts four levels of cave development (upper right corner of block model), with some older passages (shallowest) having sediment fill and chaotic breakdown breccias. Breccia and fracture development begin in a cave system while it is at the surface. As the water table drops, increased stress develops around caverns promoting brecciation and fracturing. Modified from Loucks (1999).

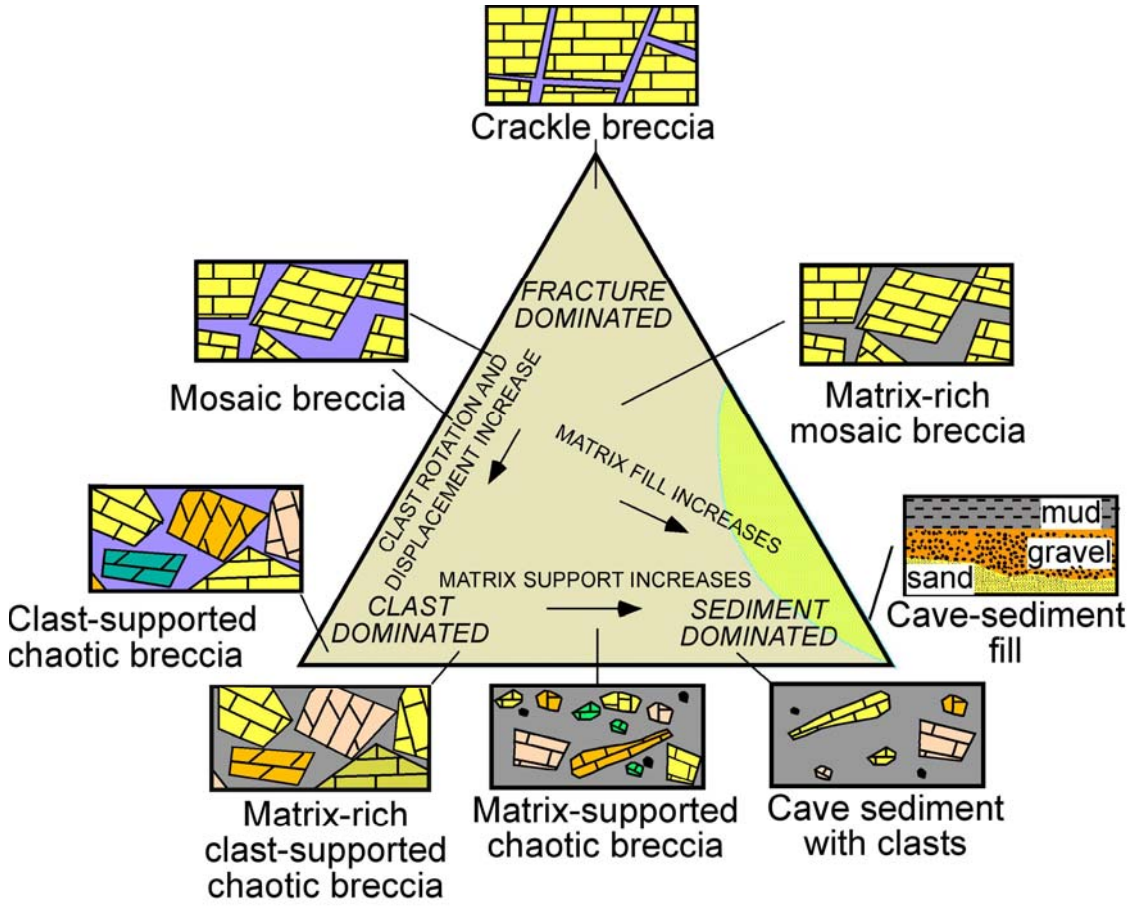

Figure 20. Classification of breccias and cave-sediment fills. Shaded area in the lower right of the diagram indicates that no cave features plot in this area. Cave-sediment fills and breccias can be separated into three end members: crackle breccia, chaotic breccia, and cave-sediment fill. Crackle breccias show slight separation and displacement. Mosaic breccias display some displacement, but they can be fitted back together. Chaotic breccias are composed of displaced clasts that cannot be fitted back together, and they can be composed of clasts of different origins (polymictic). Cave-sediment fill can form a matrix within the breccia, as well as support individual clasts. The best reservoir quality is in the matrix-free breccias. From Loucks (1999).

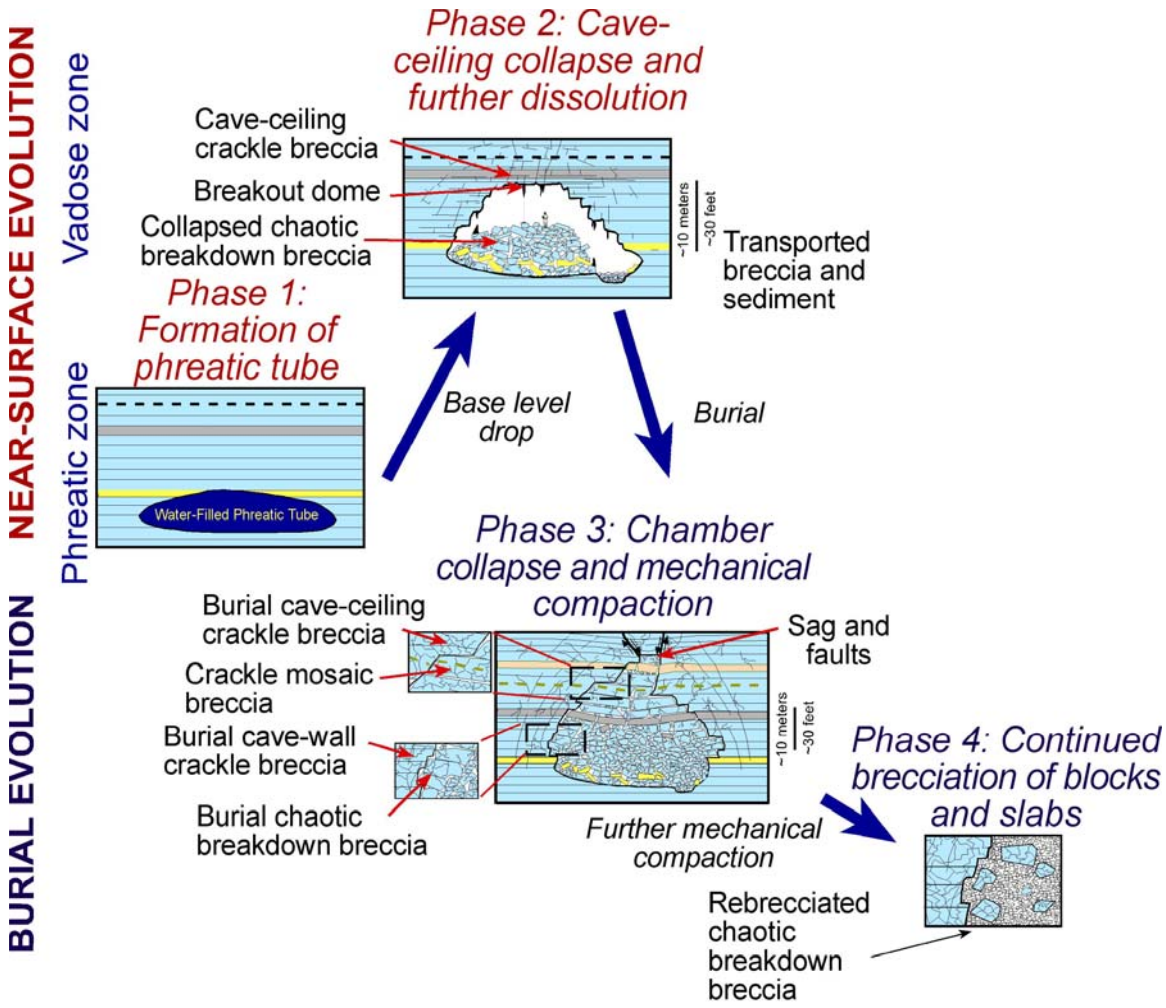

Figure 21. Schematic diagram showing evolution of a single cave passage from its formation in the phreatic zone of a near-surface karst environment to burial in the deeper subsurface. In the near-surface, excavation and associated breakdown are major processes. Many near-surface cave passages contain abundant breccias and cave-sediment fill. Crackle breccia fracturing affects the wall and ceiling rock early in the history of the cave. Excavation solution and cave sedimentation terminate as the cave-bearing strata subside into the subsurface. Mechanical compaction increases and restructures the existing breccias and remaining cavities. Most large voids collapse after several thousand feet of burial, forming more chaotic breakdown breccia. Some large interclast pores may be preserved. Differentially compacted but relatively intact strata over the collapsed chamber are fractured and form burial cave-roof crackle and mosaic breccias with loosely to tightly fitted clasts. Continued burial leads to more extensive mechanical compaction of the previously formed breakdown, thus causing blocks with large void spaces between them to fracture and pack more closely together. The resulting product is a rebrecciated chaotic breakdown breccia composed of smaller clasts. Many of the clasts are overprinted by crackle fracture brecciation.

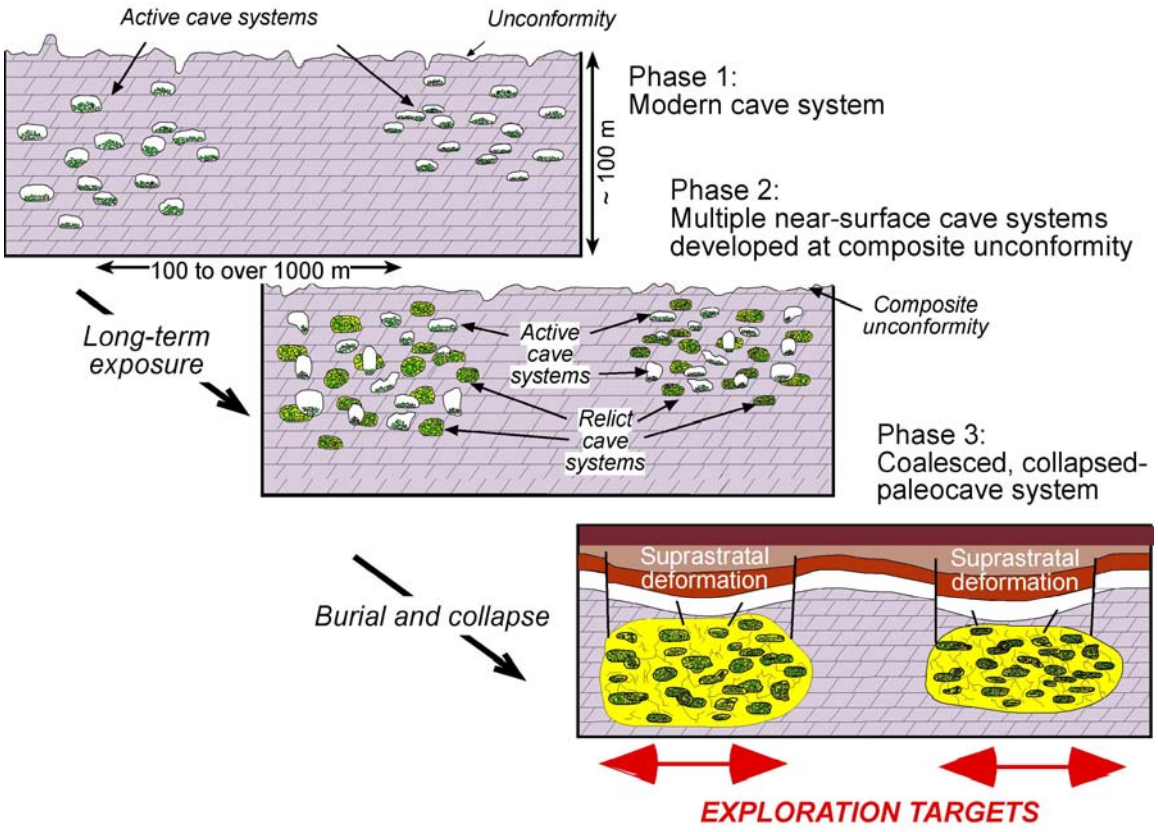

Figure 22. Schematic diagram showing the stages of development of a coalesced, collapsed-paleocave system. The development of a large collapsed-paleocave reservoir is the result of several stages of development. Multiple cave-system development at a composite unconformity may be necessary in order to produce a high density of passages. As the multiple-episode cave system subsides into the deeper subsurface, wall and ceiling rocks adjoining open passages collapse and form breccias that radiate out from the passage, and may intersect with fractures from other collapsed passages and older breccias within the system. The result is the coalescing of the cave system into a spatially complex reservoir system. The resulting coalesced breccia/fractured bodies can be thousands of feet of across, thousands of feet long, and hundreds of feet thick. Strata above the collapsed cave system are deformed by brecciation, faulting, and sagging (suprastratal deformation) Modified from Loucks (1999).

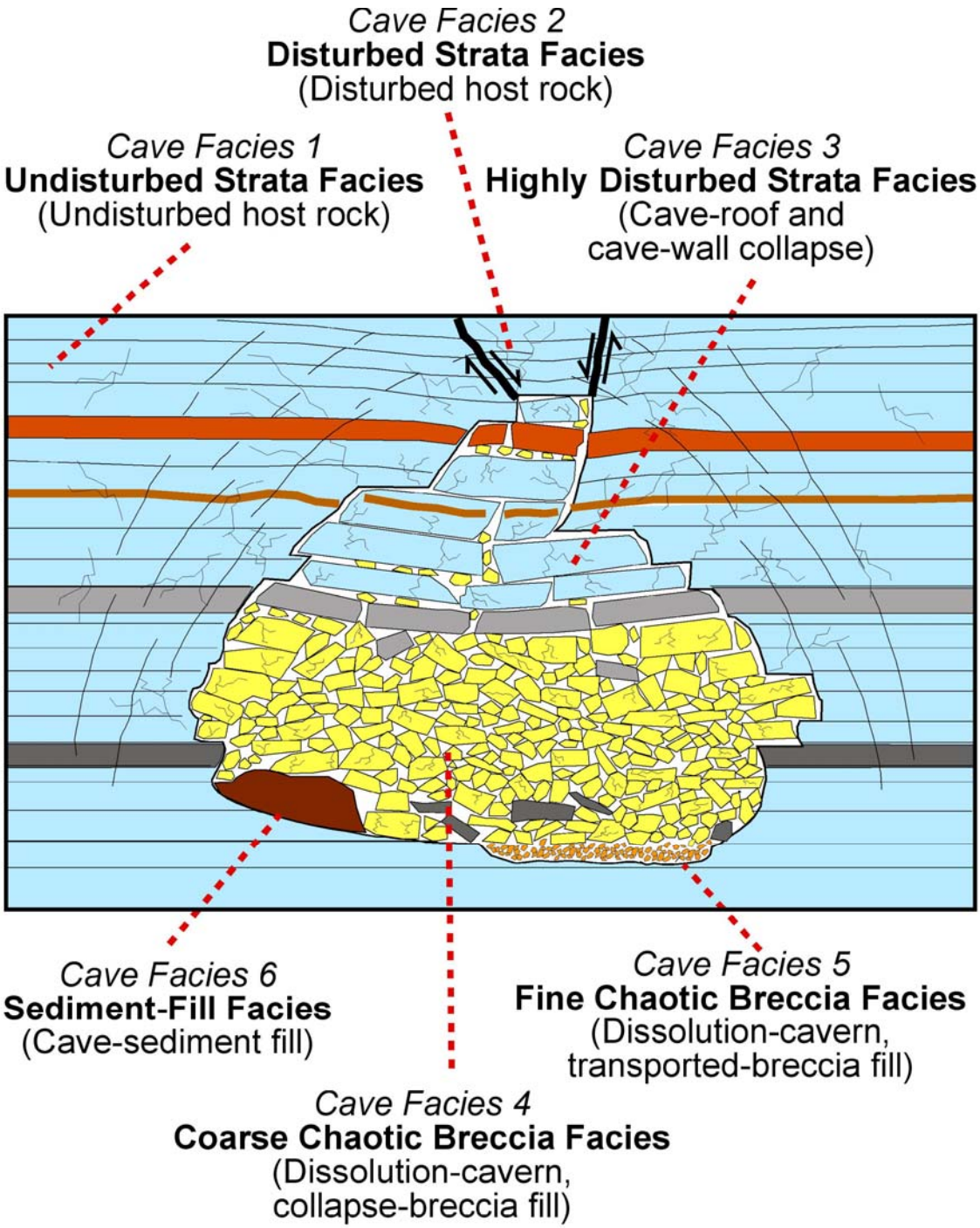

Figure 23. Paleocave facies classification by Loucks and Mescher (2001). See Table 1 for details.

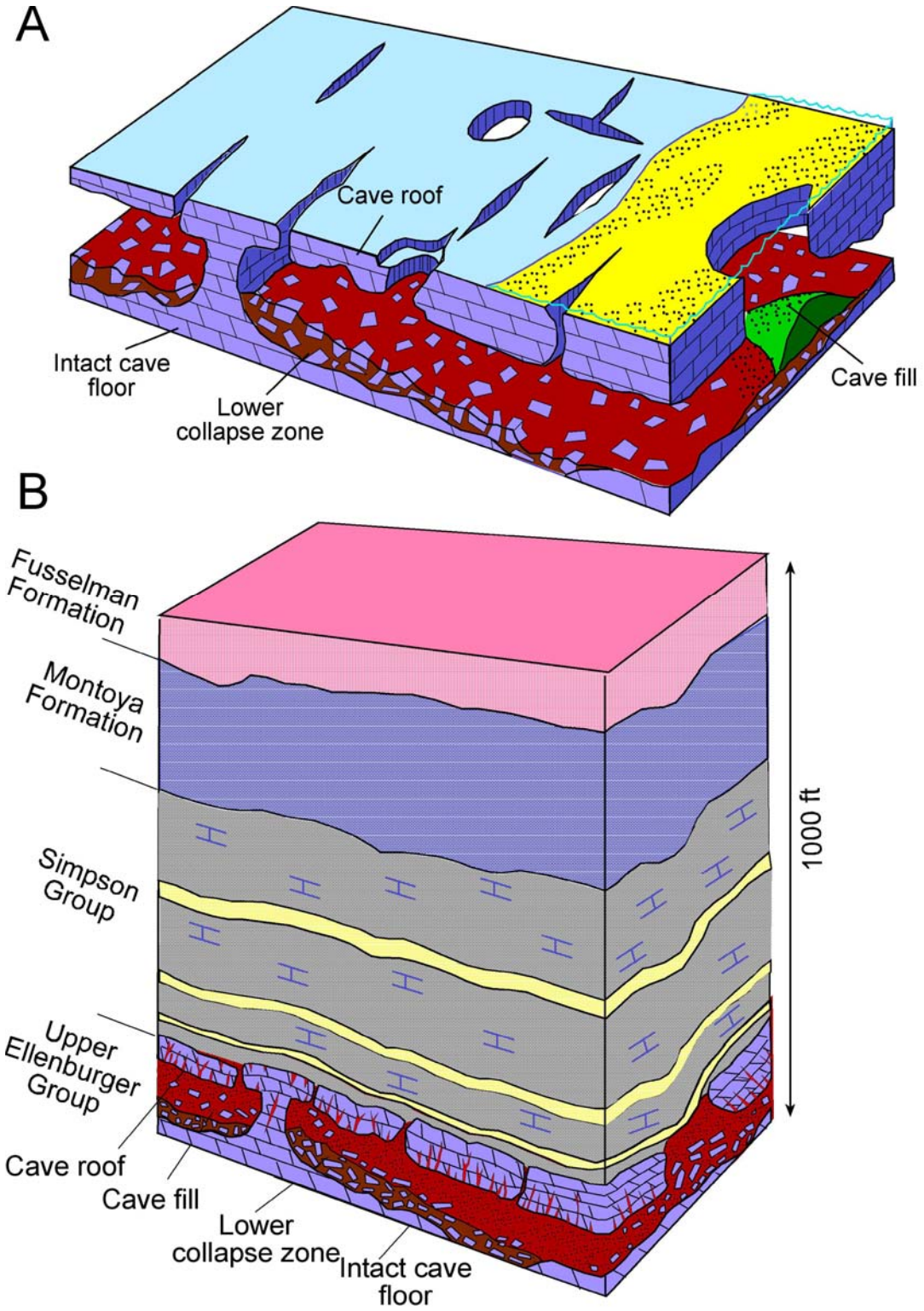

Figure 24. Paleocave models of Kerans (1988, 1989). (A) Schematic block diagram of a cave in the Lower Ordovician of West Texas showing cave floor, cave roof, cave-sediment fill, and collapsed breccia. Simpson siliciclastic material is filling cave during later transgression. (B) Schematic block model showing the collapsed Ellenburger paleocave system buried by successive Ordovician and Silurian deposits. Burial resulted in fracture brecciation of the roof and sagging of later units.

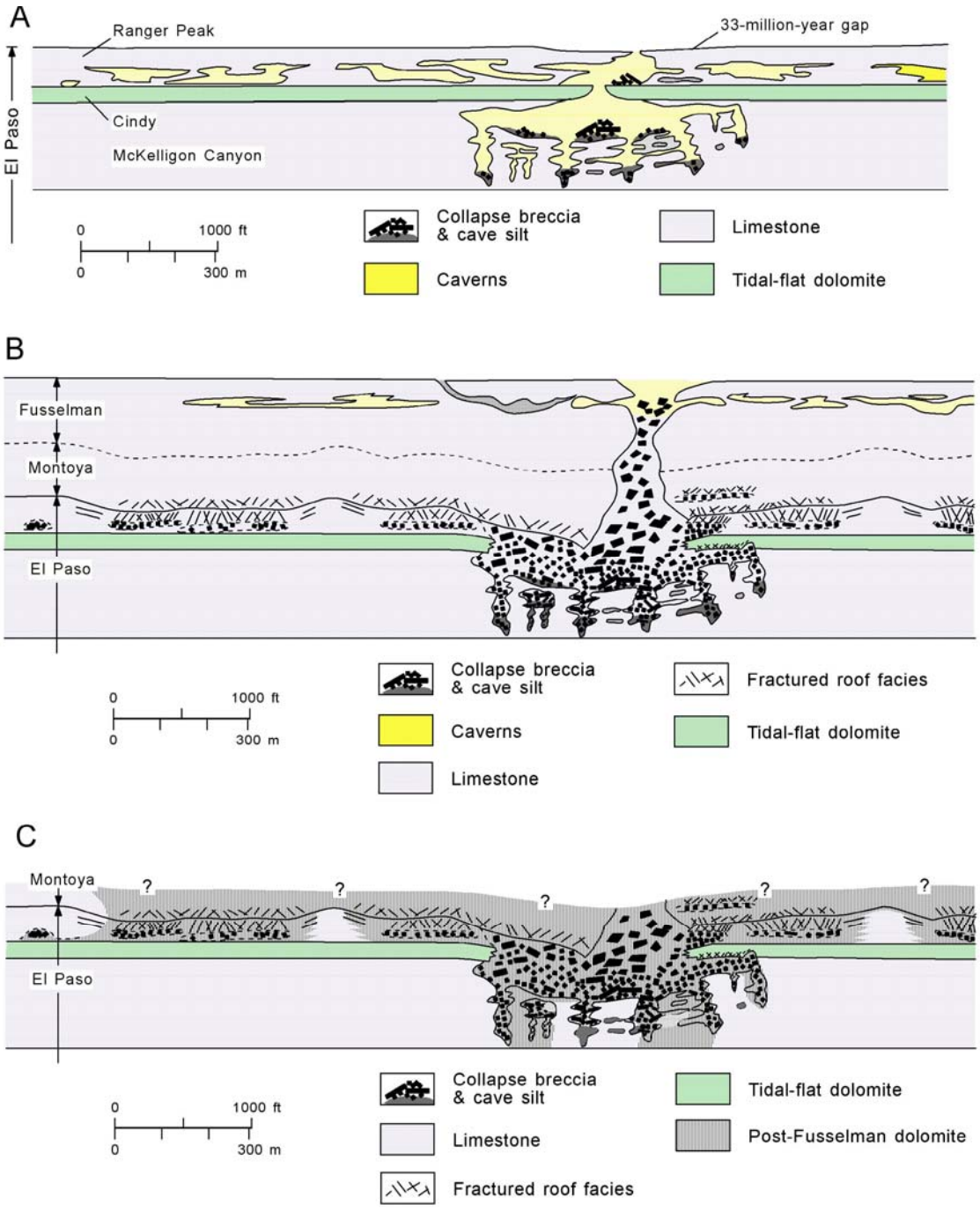

Figure 25. Reconstruction of El Paso paleocave system by Lucia (1995). Figure caption is directly from Lucia (1995). (A) Penecontemporaneous dolomitization of the Cindy Formation and development of tabular, laterally continuous caverns in the Ranger Peak Formation and vertical, laterally discontinuous caverns in the McKelligon Canyon Formation. (B) Collapse of the El Paso caverns showing collapse of the Montoya, development of breccia pipes up into the Fusselman Formation, and development of caverns in the Fusselman Formation. (C) Late-stage dolomitization of the El Paso and Montoya groups controlled by fluid flow through collapse breccia, fractures, and into adjacent carbonates.

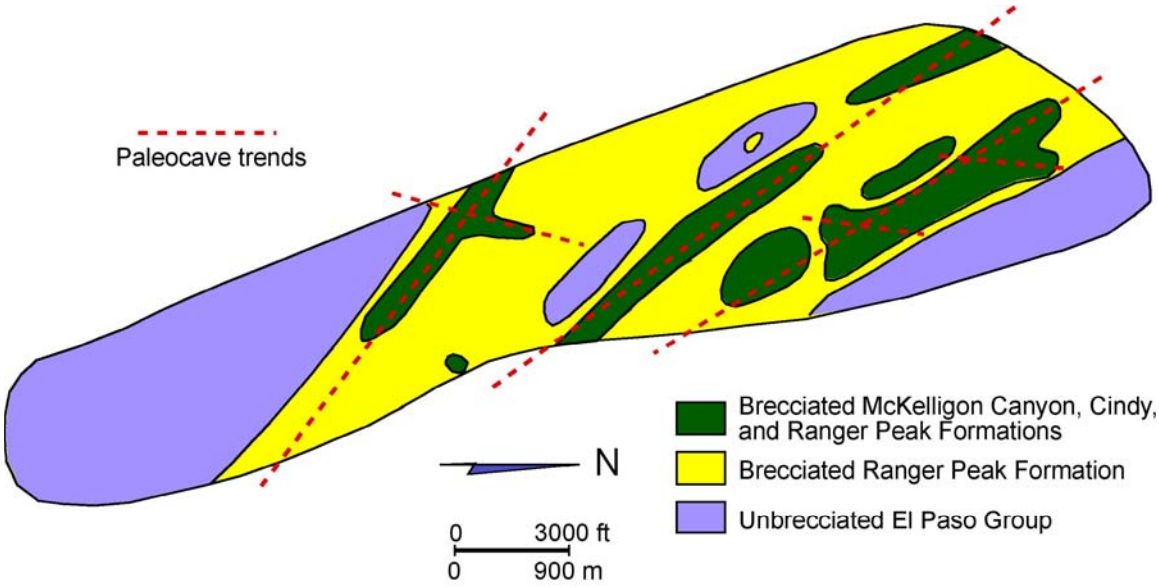

Figure 26. Reconstruction by Lucia (1995) of the different collapsed breccia in the Franklin Mountains, Texas. Paleocave trend lines are by present author.

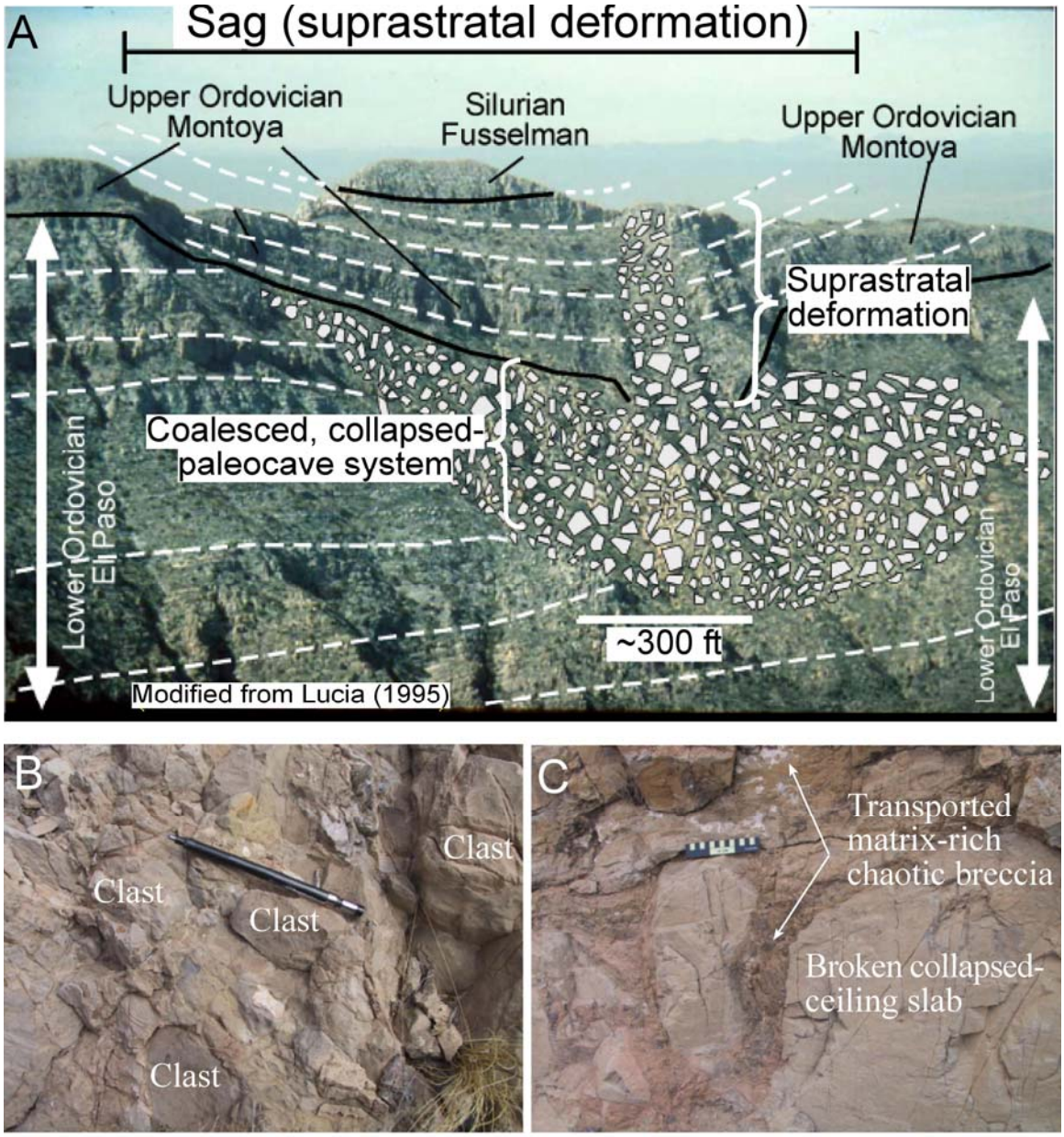

Figure 27. (A) Photograph of the Great McKelligon Sag in the Franklin Mountains of far West Texas. Photograph and general interpretation are from Lucia 1995 but modified by present author. This is an outstanding outcrop example of a coalesced, collapsed paleocave system with associated overlying suprastratal deformation. (B) Transported matrix-rich chaotic breccia. (C) Broken collapsed ceiling slab embedded in transported matrix-rich chaotic breccia.

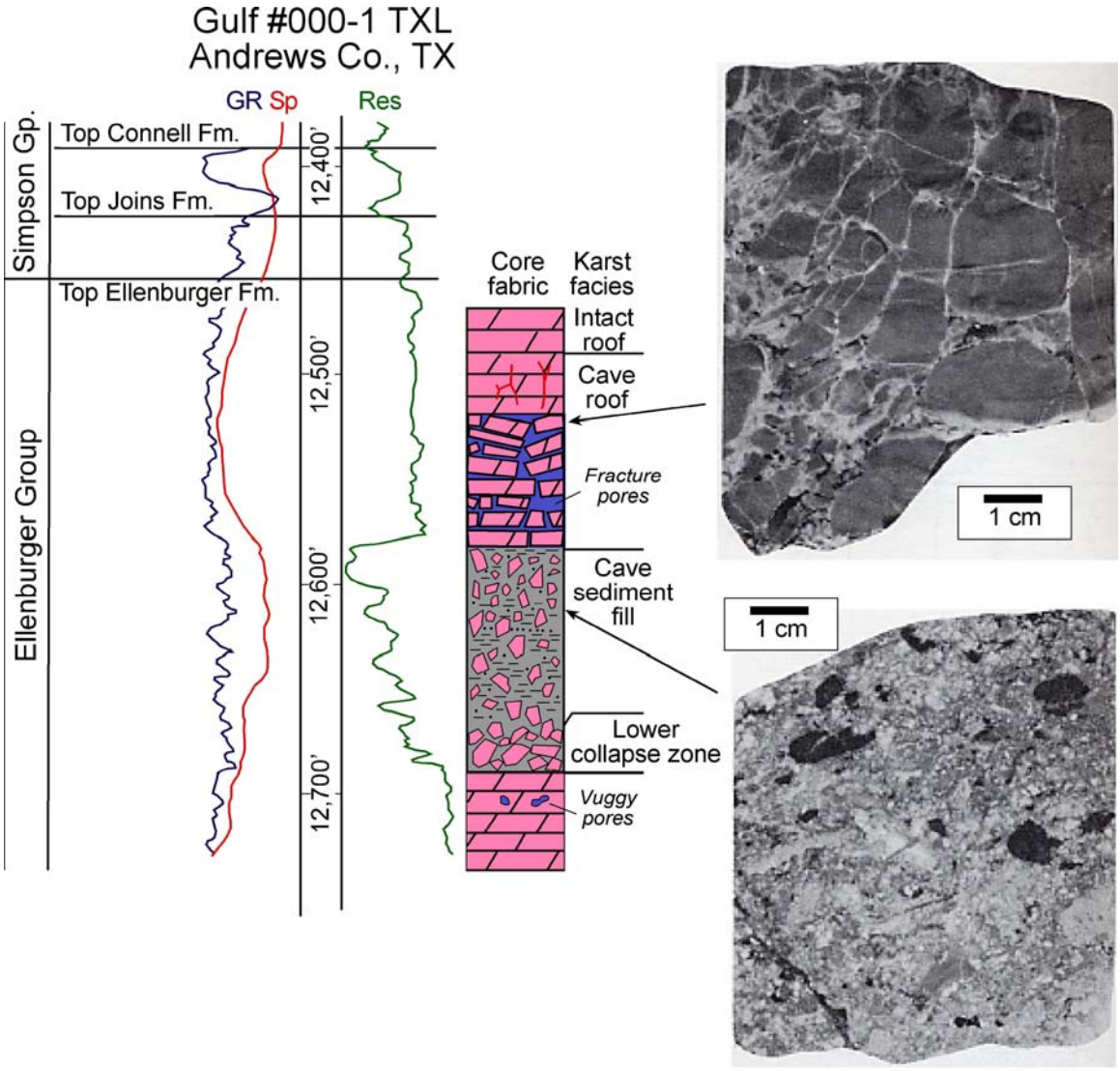

Figure 28. Core and wireline logs form the Gulf #000-1 TXL, Emma reservoir (Andrews County, Texas). Upper photograph from 12,526 ft shows crackle-fracture pores in collapse cave roof. Lower photograph from 12,610 ft shows cave-sediment fill (debris flow) with clasts floating in matrix of chloritic shale and quartz sand. From Kerans (1989).

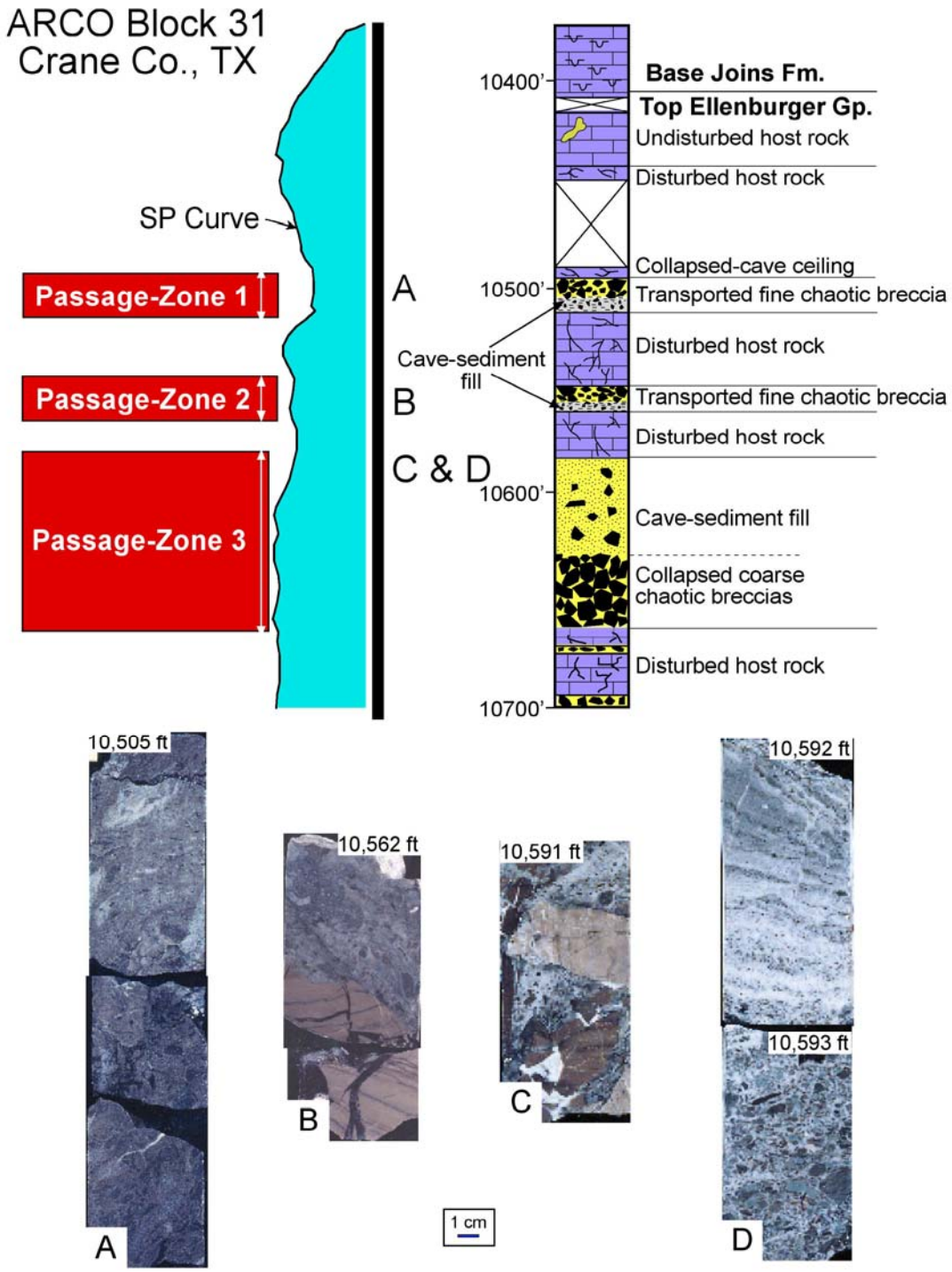

Figure 29. Core description and associated SP log for the Arco Block 31 core in Crane County, Texas. Photograph A is from a debris flow of transported fine chaotic breccia (cave-sediment fill in a passage). Photograph B from a debris flow of transported fine chaotic breccia (cave-sediment fill in a passage). Photograph C is siliciclastic-rich sand and carbonate clast cave-sediment fill (cave-sediment fill in a passage). Photograph D is a debris flow at the base overlain by siliciclastic cross-bedded sandstone (cave-sediment fill in a passage). Modified from Loucks and Handford (1992) and Loucks (2001)

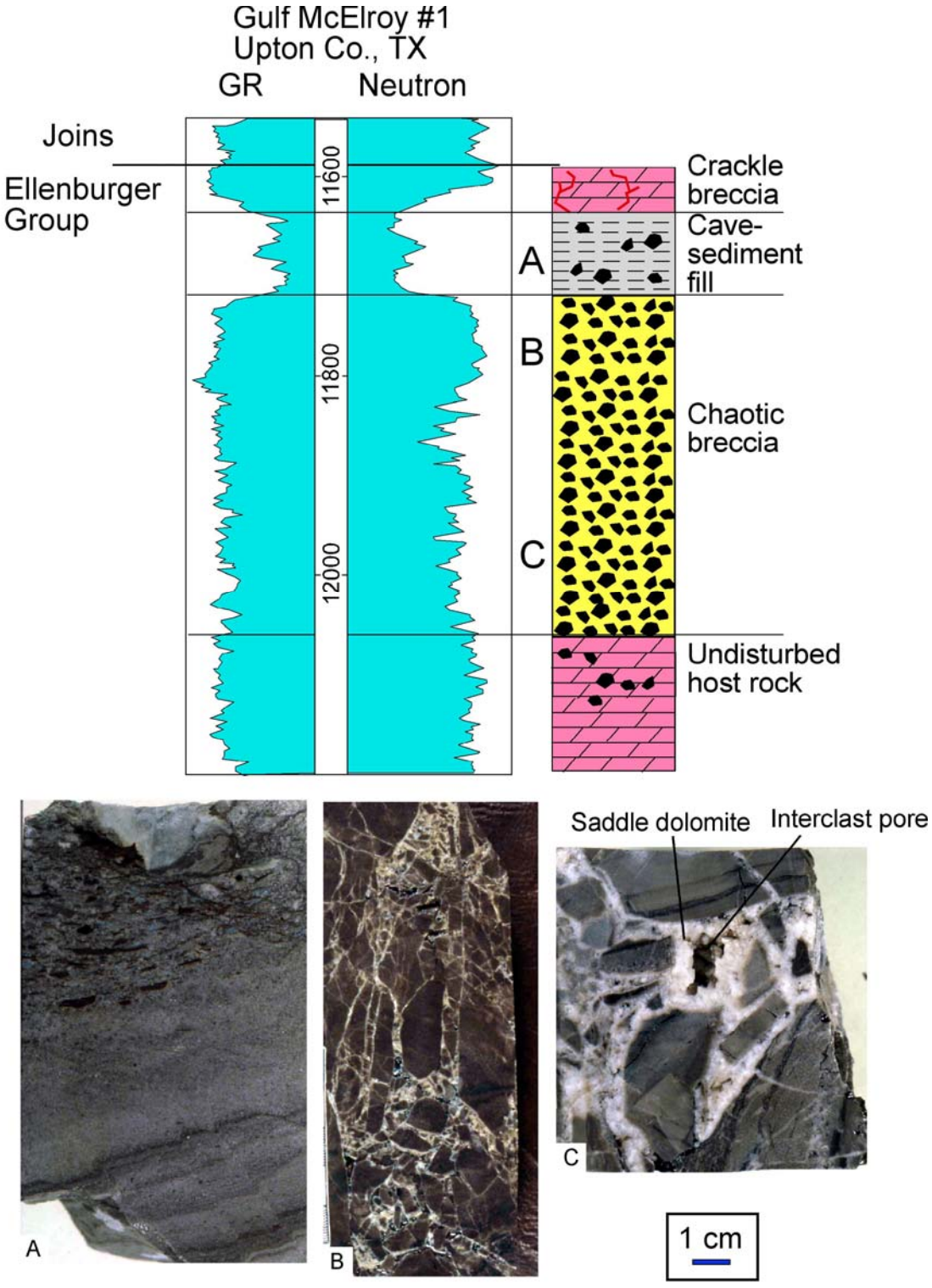

Figure 30. Core description and associated gamma-ray log for the Gulf #1 McElroy core in Upton County., Texas. Photograph A is from the cave-sediment fill in a passage. Photograph B from a chaotic breccia pile in a passage. The clasts show late crackle brecciation. Photograph C from a chaotic breccia pile in a passage. Because of the lack of matrix between the clasts and incomplete filling by saddle dolomite, there are interclast pores present. From Kerans (1989).

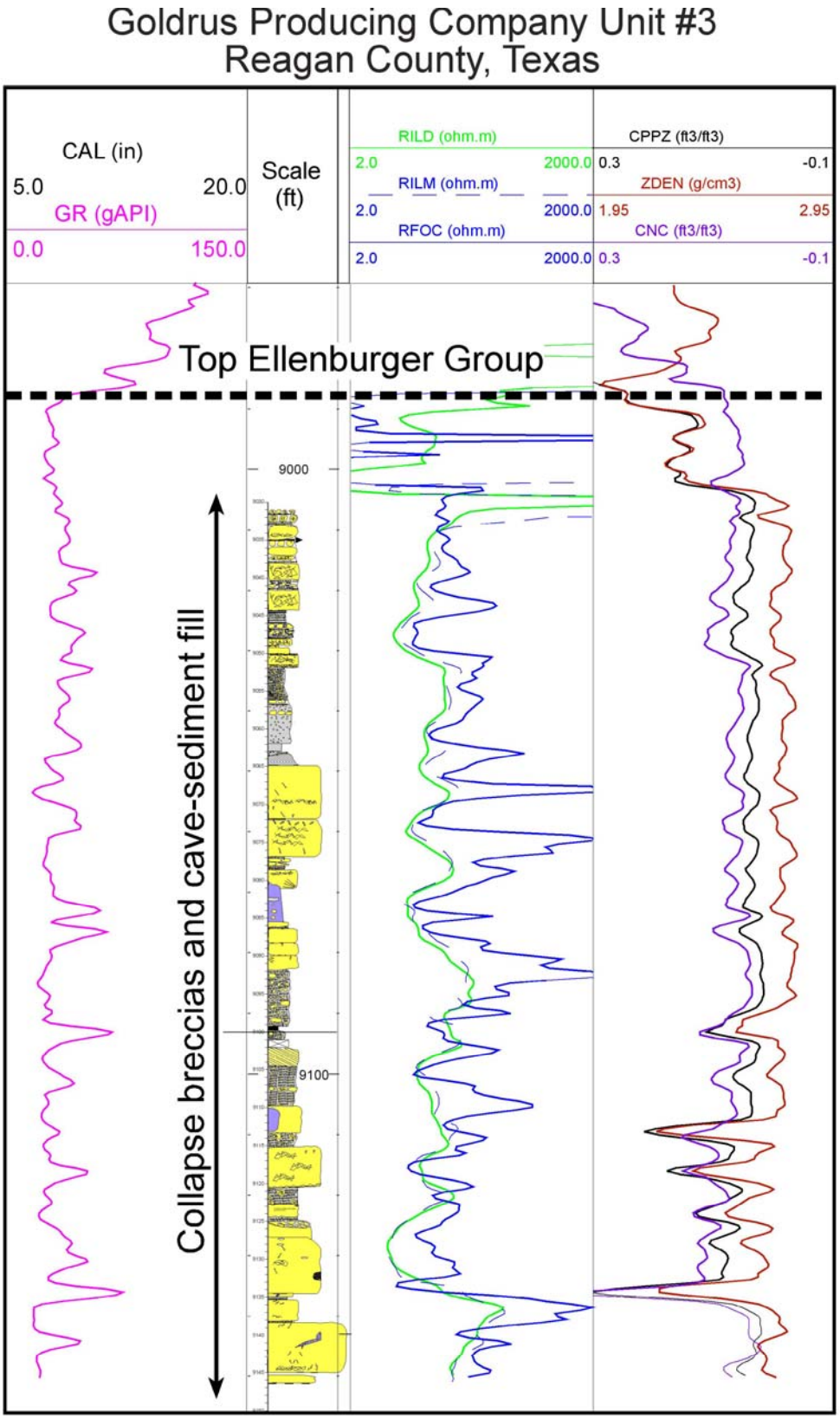

Figure 31. Goldrus Producing Company Unit #3 core and associated wireline logs in Barnhart field (Regan County, Texas) is extensively karsted. See Figure 32 for examples of rock types. From Combs et al. (2003).

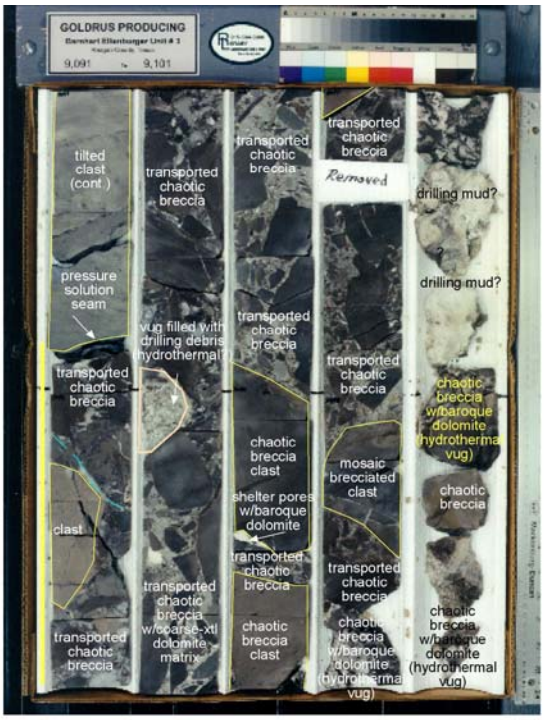

Debris-flow breccia in a paleocave passage. Some of the clasts show crackle brecciation.

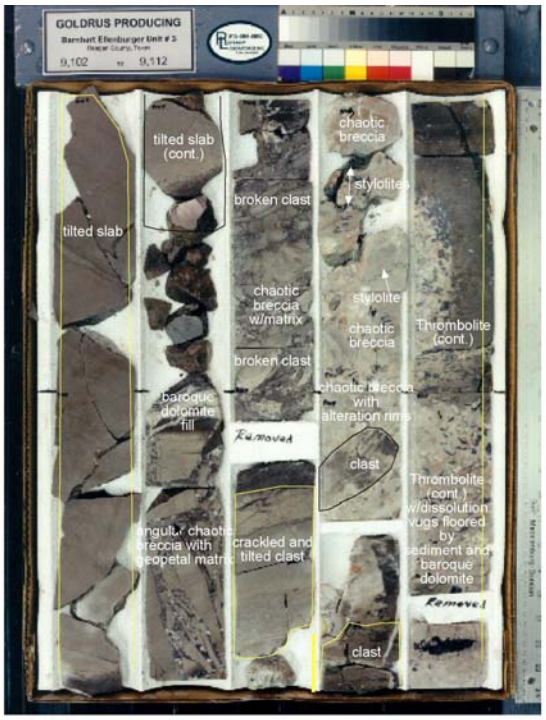

Large deformed blocks with crackle-breccia overprint interbedded with cave-sediment fill.

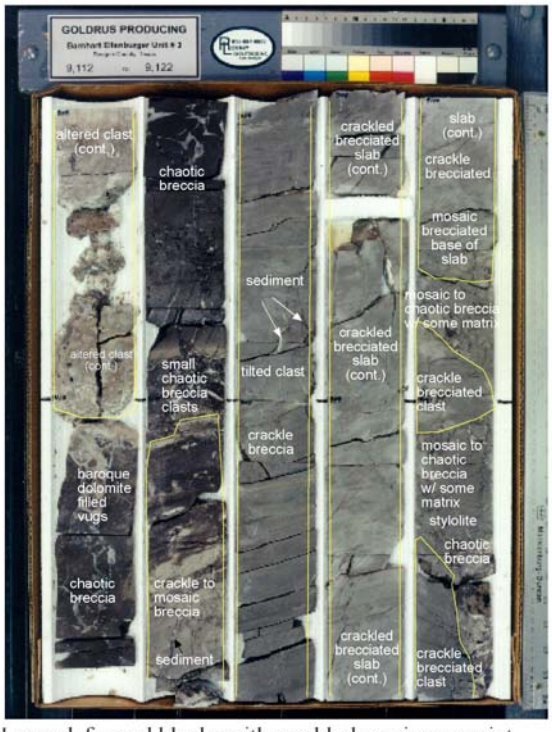

Large deformed blocks with crackle-breccia overprint.

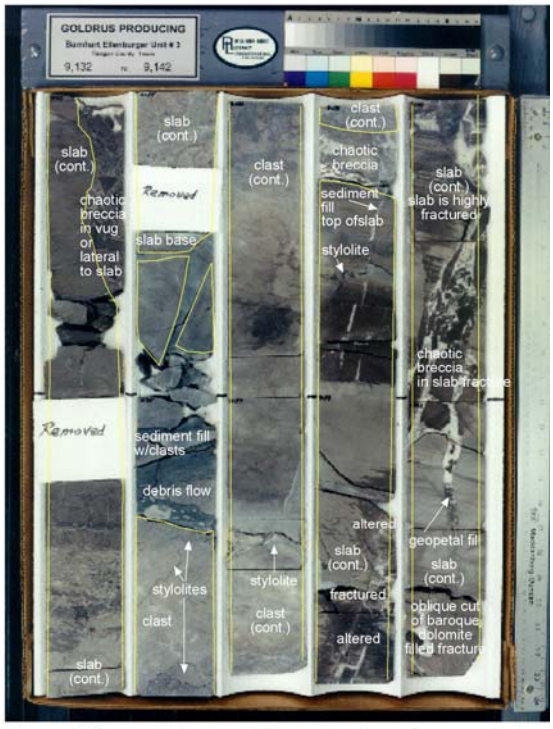

Large deformed blocks with crackle-breccia overprint.

Figure 32. Example of several Ellenburger paleocave facies from the Goldrus Unit #3 Barnhart core in Regan County, Texas. From Combs et al. (2003).

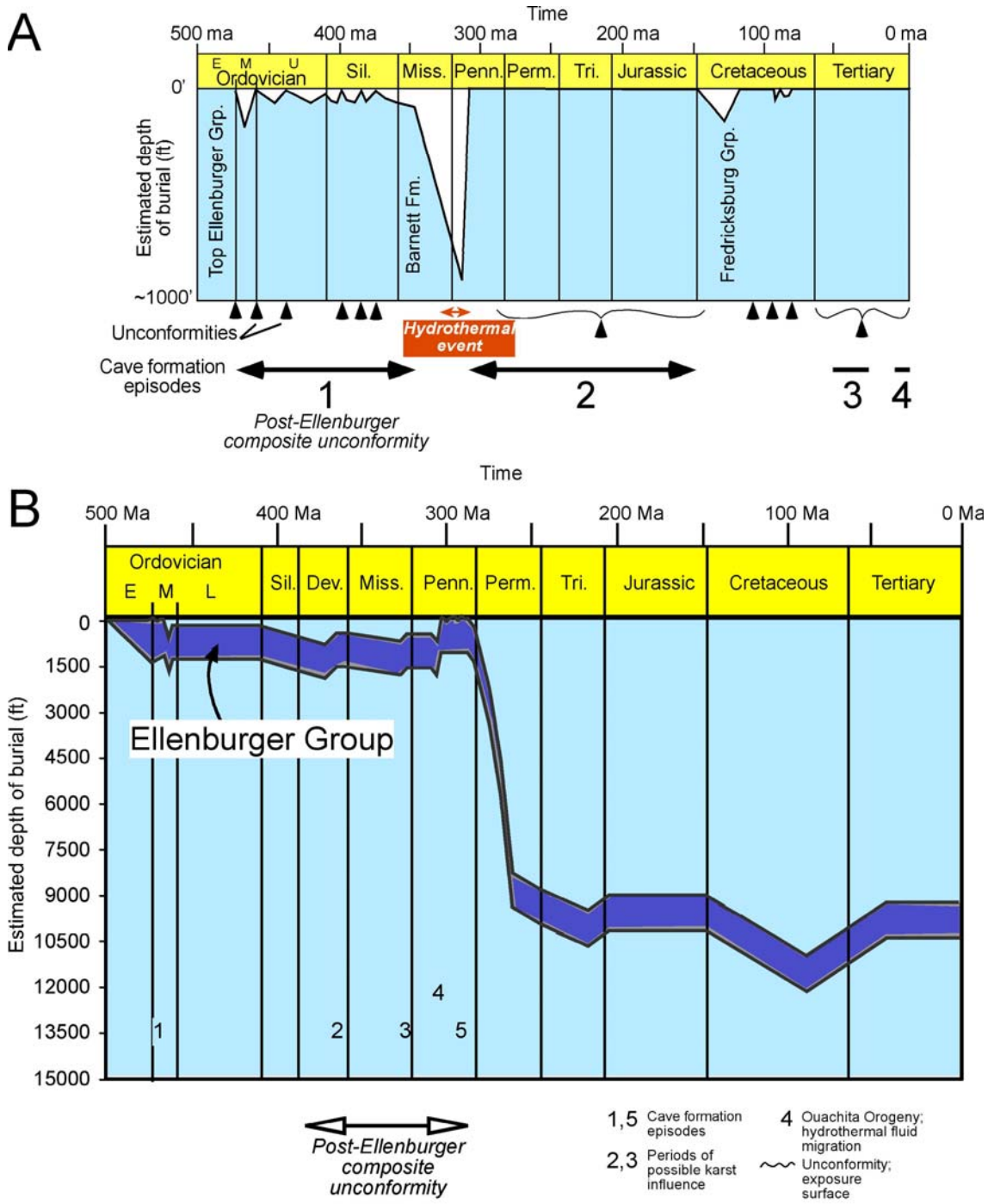

Figure 33. (A) Schematic burial history plot for the Lower Ordovician Ellenburger Group in the Llano Uplift area of Central Texas. From Kupecz and Land (1991). (B) Generalized burial history of the Ellenburger Group within Barnhart field in Regan Co., Texas. Barnhart field underwent several episodes of uplift. At least two of these episodes exposed the Ellenburger Group to karstification and cave formation: (1) Early-Middle Ordovician and, (2) Pennsylvanian times. The Ellenburger Group was also brought close to the surface during the Devonian and Mississippian, and may have experienced some karst influence here. During the Early Pennsylvanian time the Ellenburger Group experienced hydrothermal processes and tectonic uplift related to the Ouachita Orogeny. From Combs et al. (2003).

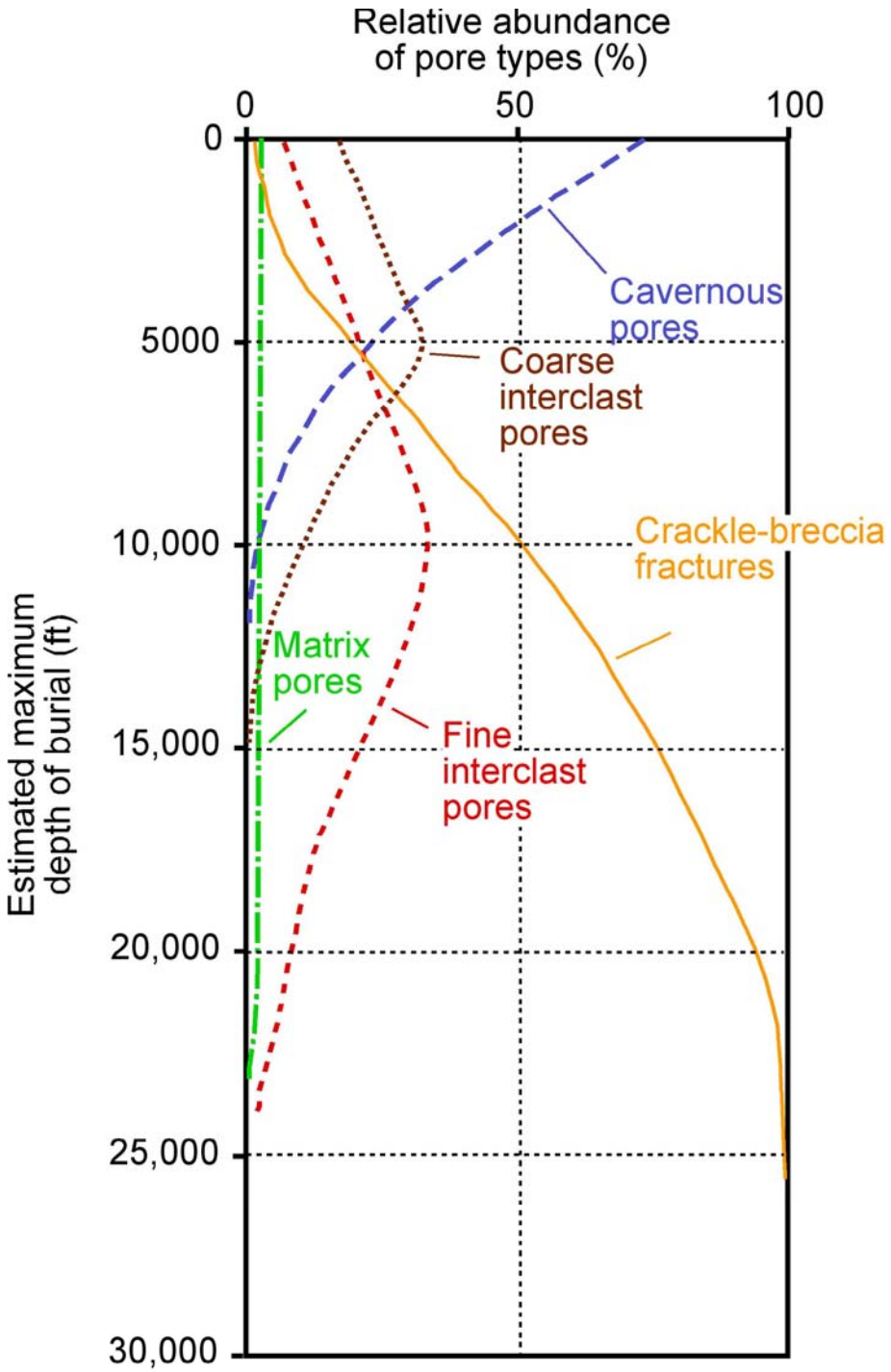

Figure 34. Generalized burial evolution of a cave-system pore network with relative proportions of pore types. The dividing line between fine clast and coarse clasts is 6 cm. The relative abundance of pore types and estimated burial depth are estimates based on review of near-surface and buried paleocave systems presented in Tables 1 and 2 of Loucks (1999). After 20,000 ft of burial, the graph is very speculative. Figure modified from Loucks (1999).

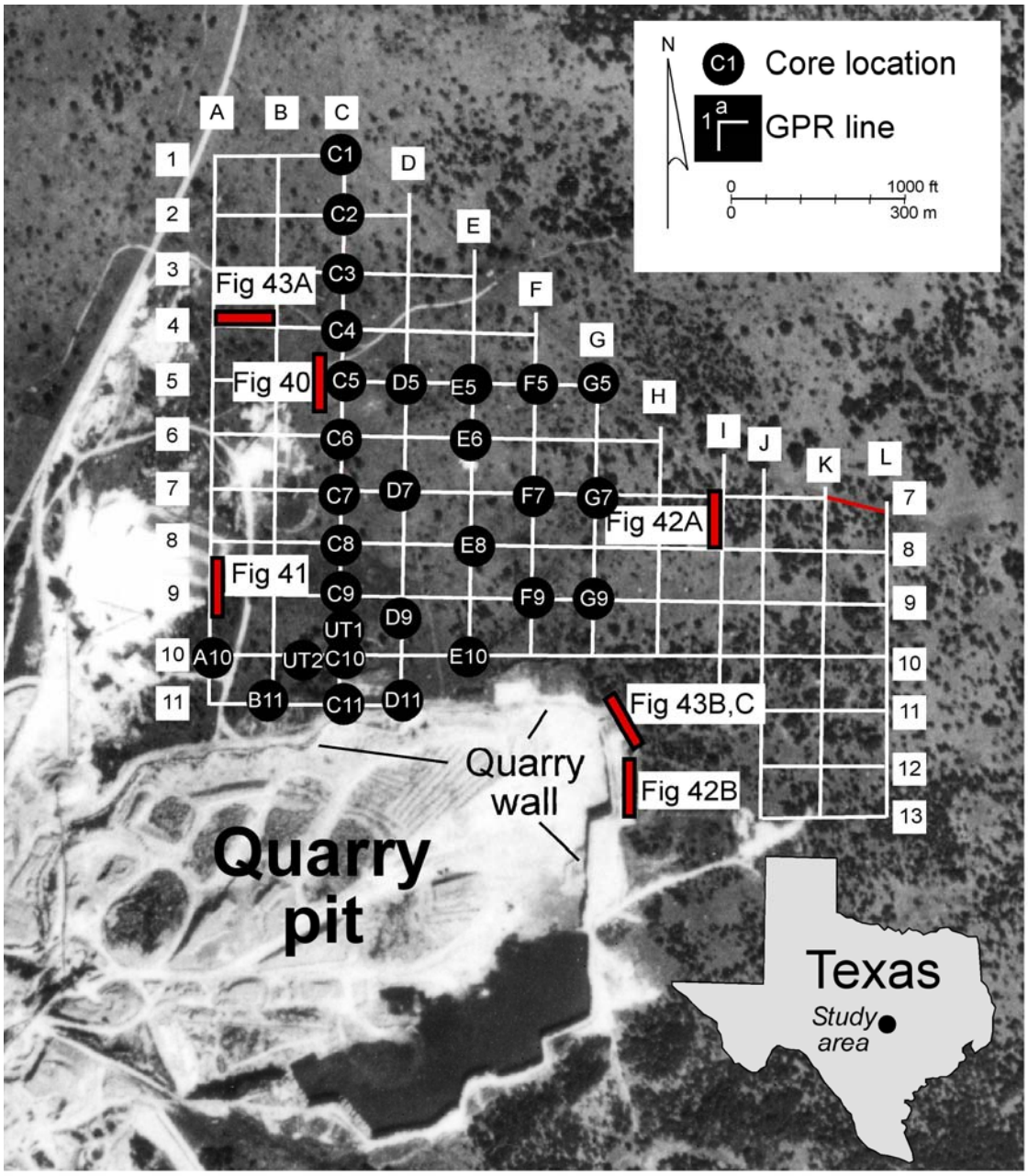

Figure 35. Aerial photograph of Dean Word Quarry showing location of grid of ground-penetrating radar (GPR) lines and cores. Locations of GPR lines illustrated later in the paper are labeled. From Loucks et al. (2004).

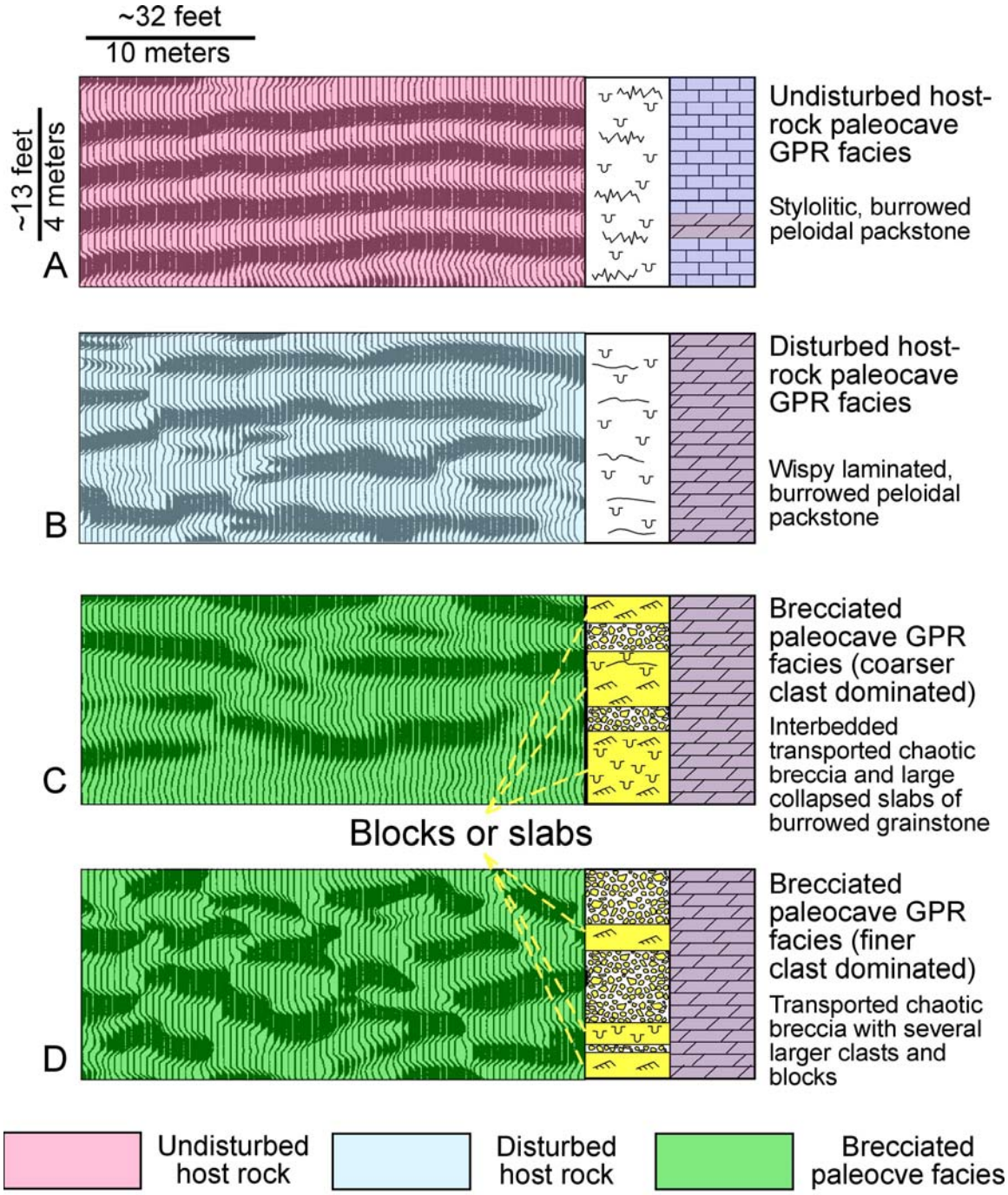

Figure 36. Type ground-penetrating radar reflection patterns for different paleocave facies. Each reflection pattern is matched to core. From Loucks et al. (2004).

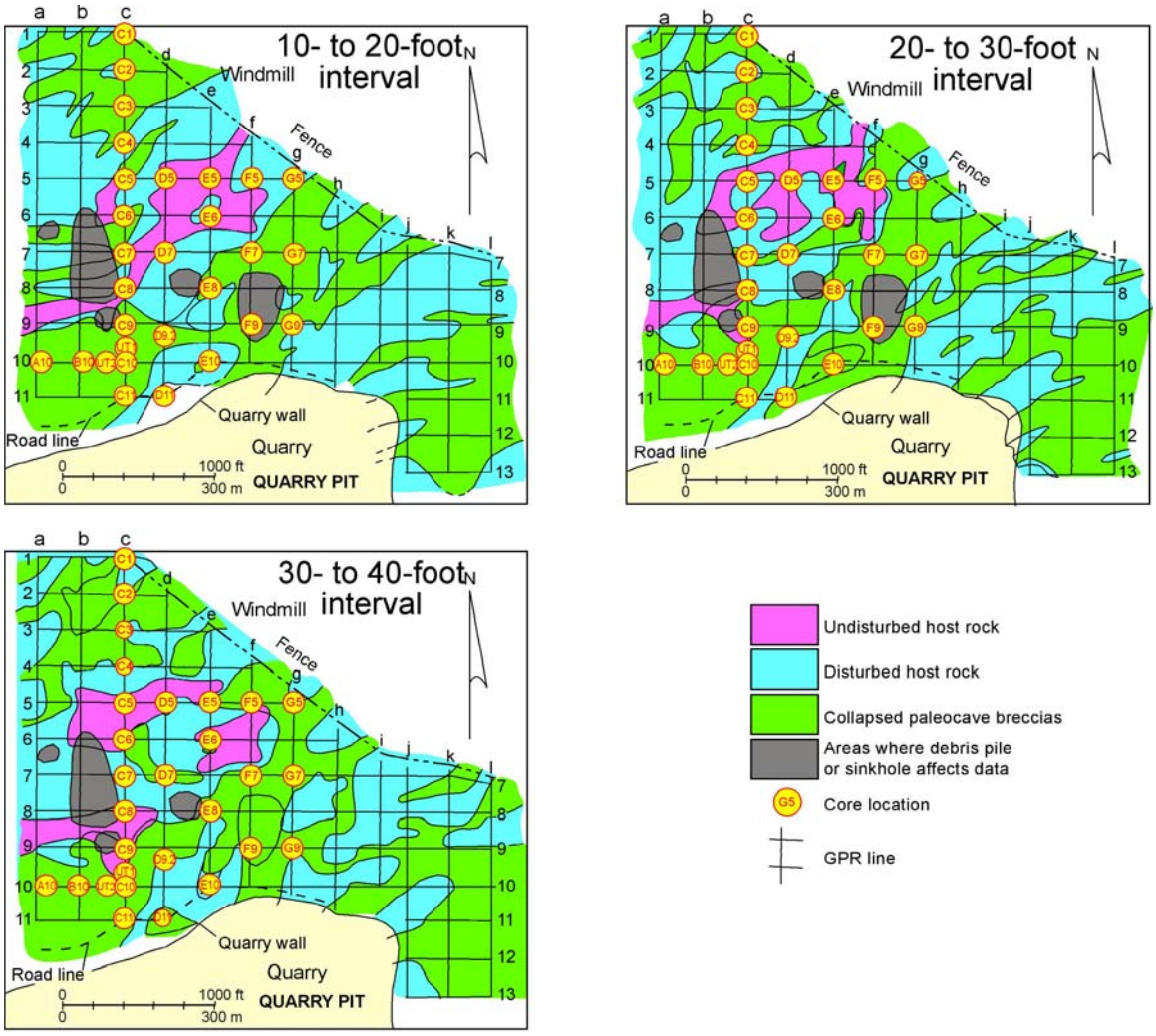

Figure 37. Integration of core and GPR data allows a three-dimensional interpretation of the paleocave system. The mapped volume is divided into three depth zones to display the distribution of paleocave facies. The brecciated bodies, which outline the trends of former passages, are as much as 1100 ft wide. The intervening areas between the breccias are as much as 660 ft wide. From Loucks et al. (2004).

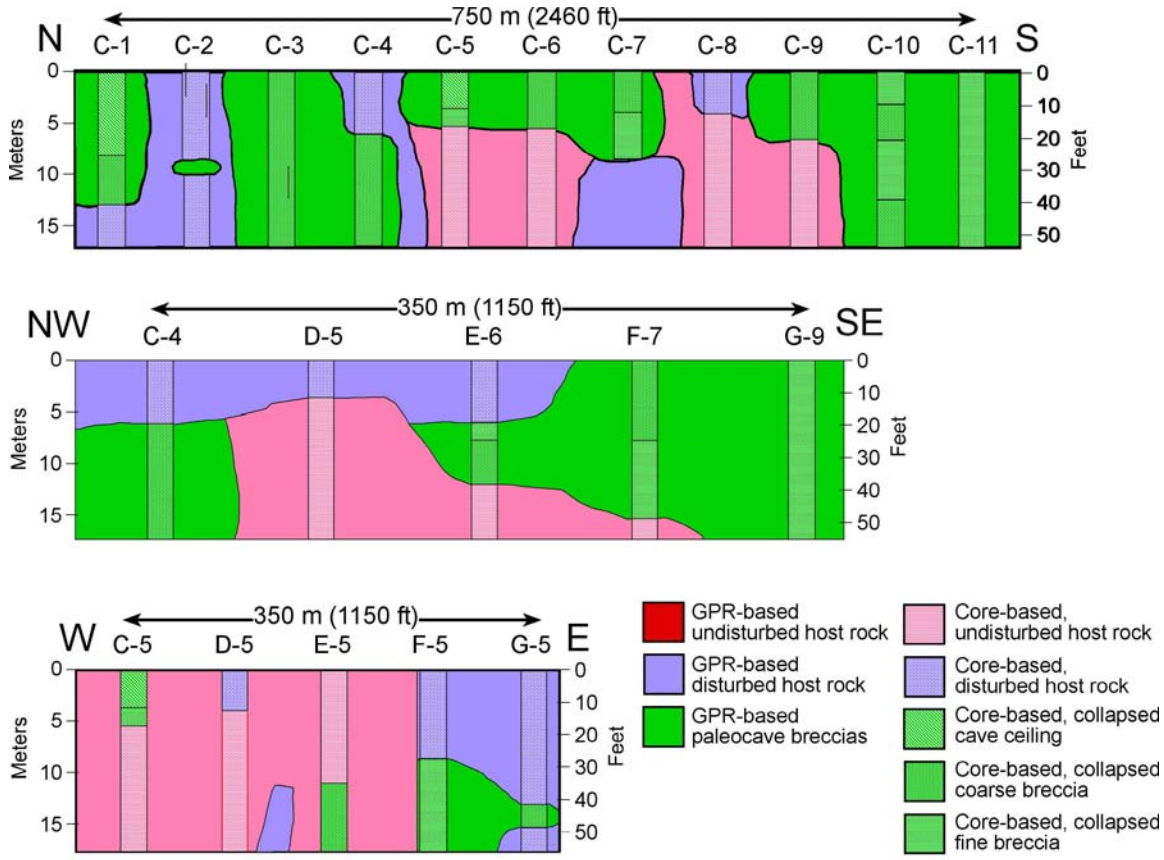

Figure 38. Simplified facies cross sections using core and GPR data. See Figure 35 for location of wells used on lines of sections. From Loucks et al. (2004).

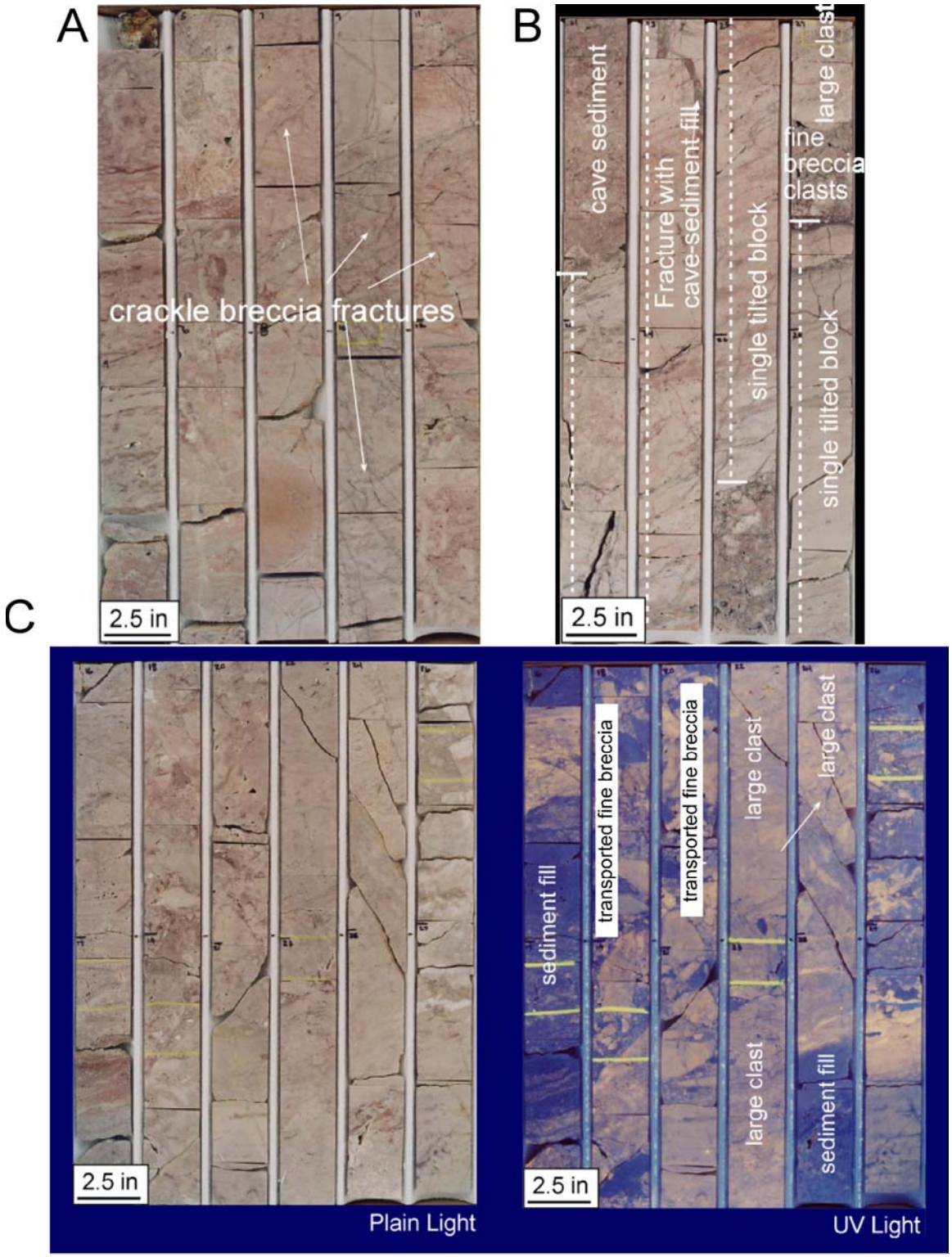

Figure 39. Core examples paleocave facies. (A) Cave roof showing extensive crackle breccia fractures. (B) Cave-passage fill composed of large blocks of chaotic breccia blocks and interbedded cave-sediment fill. (C) Cave-passage fill composed of large blocks of chaotic breccia blocks and interbedded cave-sediment fill. From Loucks et al. (2004).

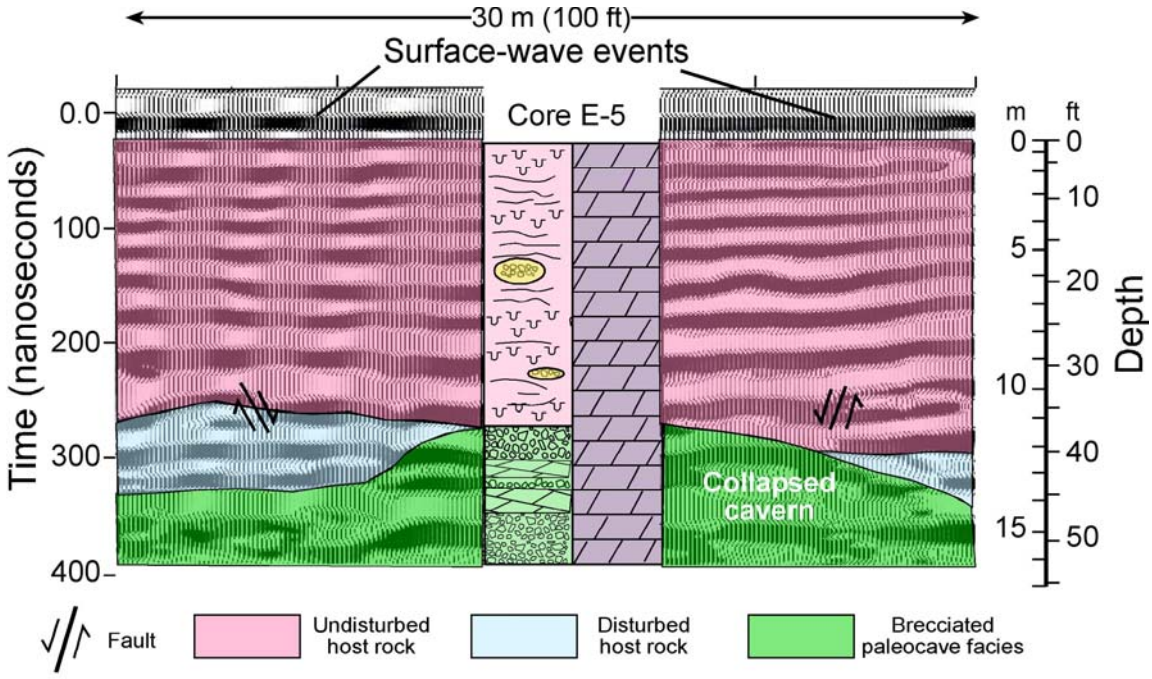

Figure 40. GPR section and core description showing a sequence of cave-fill breccias overlain by undisturbed host rock. A few small faults occur in the host rock above the collapsed cavern. See Figure 35 for location of GPR line and core. From Loucks et al. (2004).

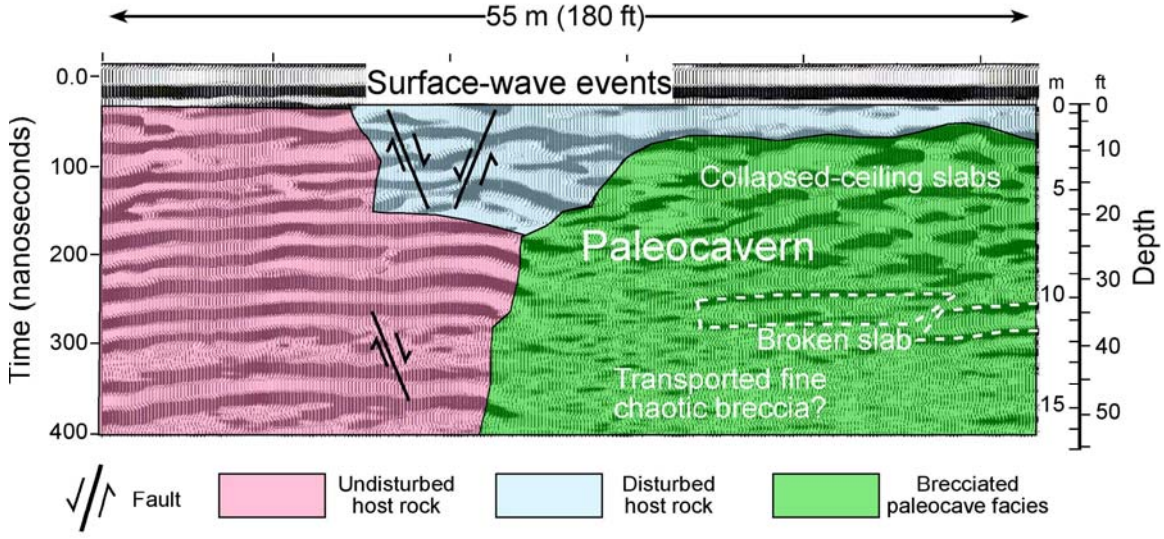

Figure 41. Collapsed paleocavern in contact with undisturbed and disturbed host rock. Several faults occur in the disturbed host rock. Reflection patterns in the collapsed cavern show probable fine breccia in the lower part of the chamber (no reflections) and coarser breccia (slabs) near the top (higher amplitude events). A large broken cave-ceiling slab may also be imaged. See Figure 35 for location of GPR line. From Loucks et al. (2004).

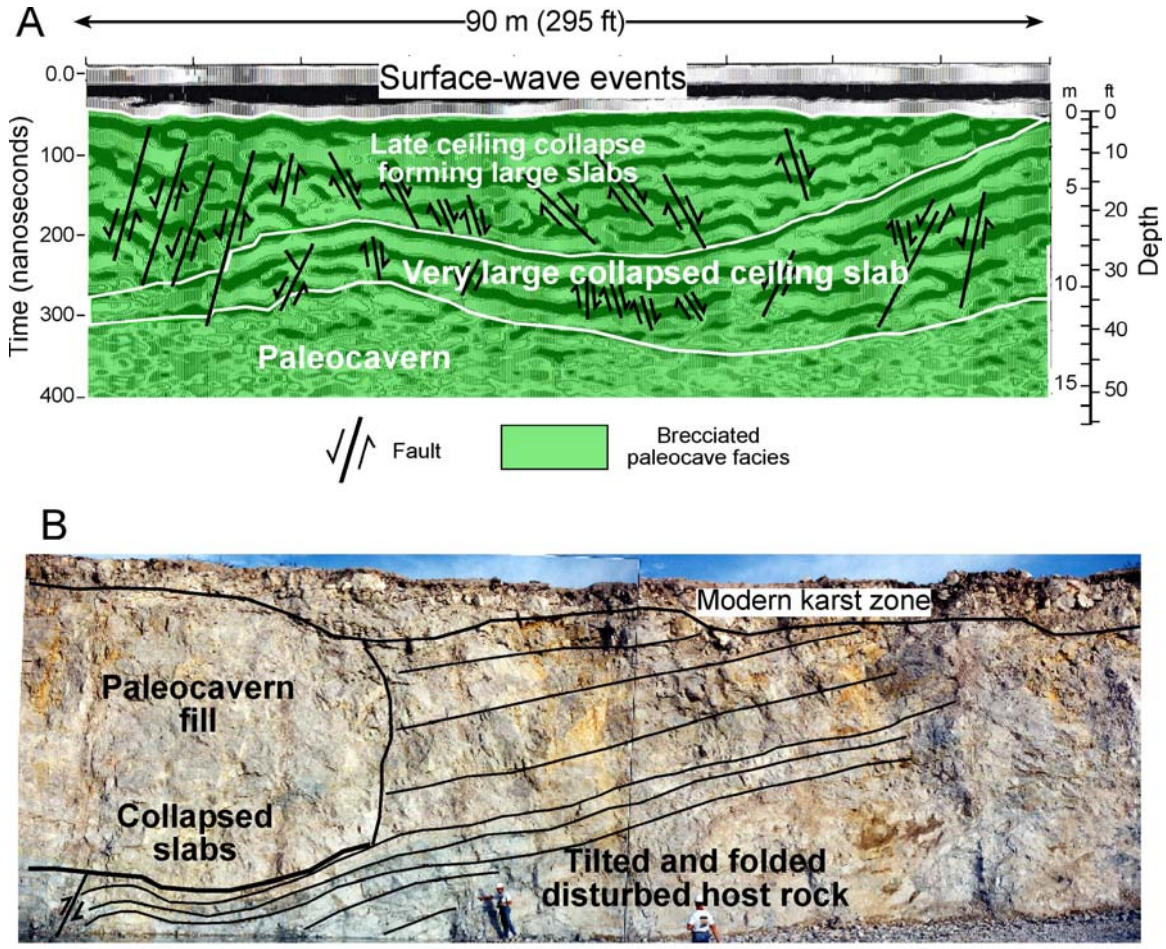

Figure 42. (A) Very large, folded, cave-ceiling slab overlying a paleocavern filled with chaotic breccia. The upper section of the cave ceiling appears to have collapsed after the large slab below on the basis of the onlapping reflection pattern between the two sections. See Figure 35 for location of GPR line. (B) Complex sag and fold feature along east wall in Dean Word Quarry showing features similar to GPR line presented in Figure 42A above. The lower part of the quarry face shows continuous tilted but folded bedding that is interpreted to have sagged or collapsed into a lower paleocavern. The upper part of the tilted block dips into a paleocavern filled with chaotic breccias and slabs. See Figure 35 for location of photograph. From Loucks et al. (2004).

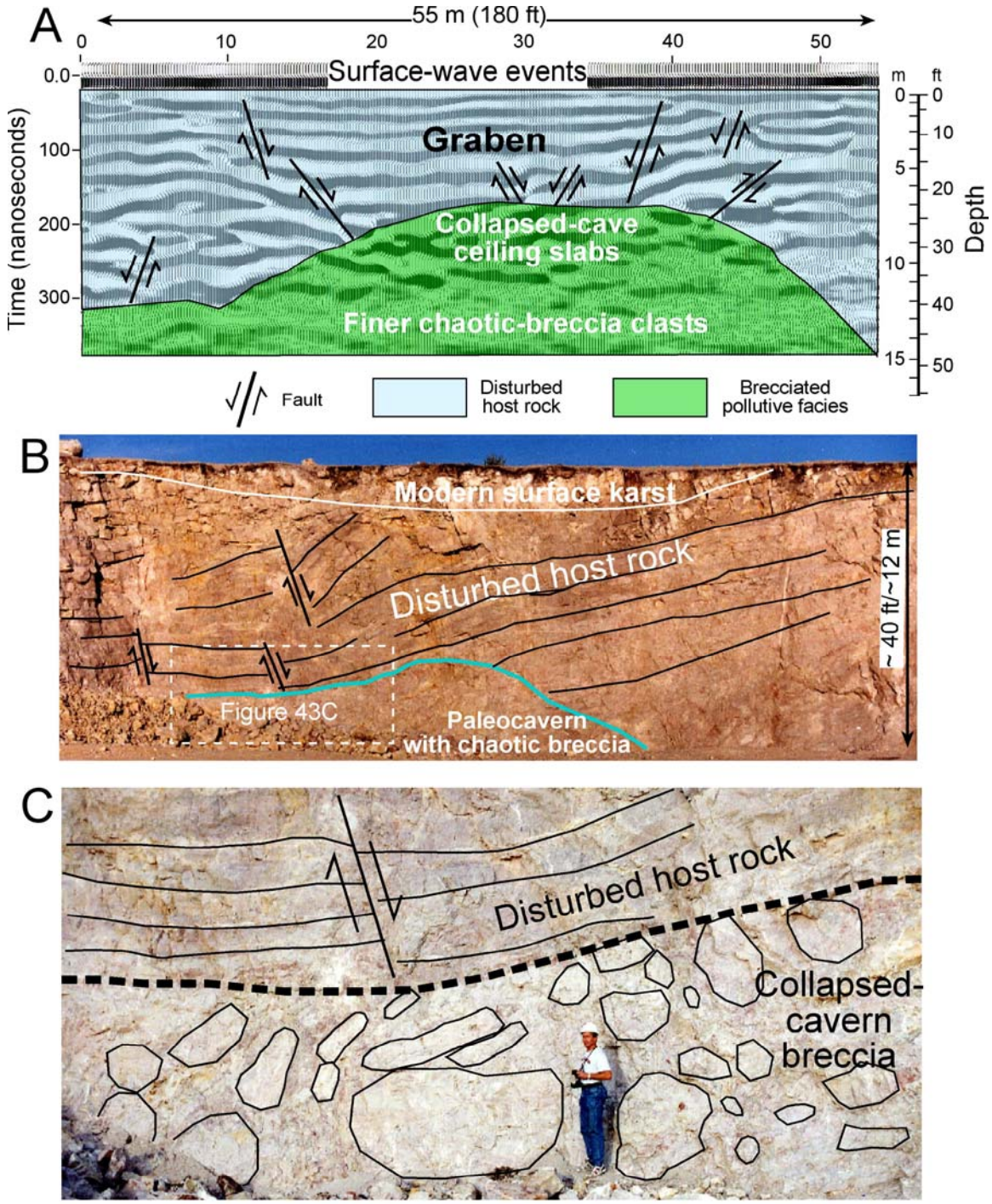

Figure 43. Faults over collapsed paleocaverns. (A) Graben and associated fault system in disturbed host rock overlying a collapsed paleocavern. Within the paleocavern, coarser slabs appear to be at the top and finer breccia at the bottom on the basis of the change in reflection pattern continuity. See Figure 35 for location of GPR line. (B) Example of faulted, disturbed host rock over a collapsed paleocavern similar to GPR line in Figure 43A. Detail of the collapsed paleocavern outlined in dashed box is shown in Figure 43C. (C) Close up of collapsed cavern shown in Figure 43B. Large collapse blocks, up to several meters across, are within the paleocavern (several prominent blocks are outlined). See Figure 35 for location of photographs. From Loucks et al. (2004)

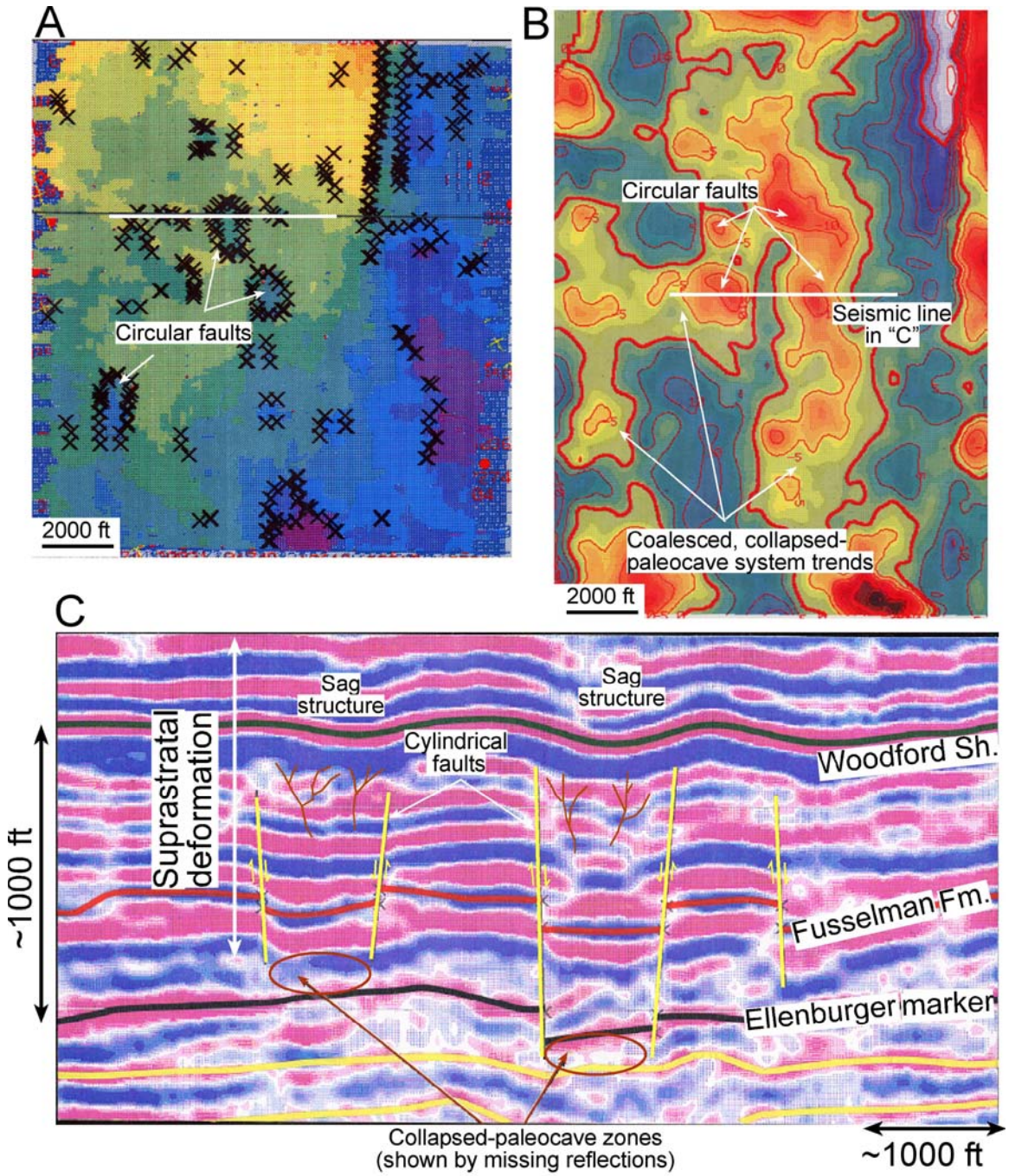

Figure 44. 3-D seismic example over an Ellenburger paleocave system from the Benedune field in West Texas. (A) Structure map on Fusselman Formation showing cylindrical faults produced by burial collapse of the Ellenburger cave system. (B) Second-order derivative map displaying sag zones produced by collapse in the Ellenburger interval. (C) Seismic line showing missing sections (collapse in Ellenburger section), cylindrical faults, and sag structures. Suprastratal deformation is over a thousand feet thick in this section. Modified from Loucks (1999).

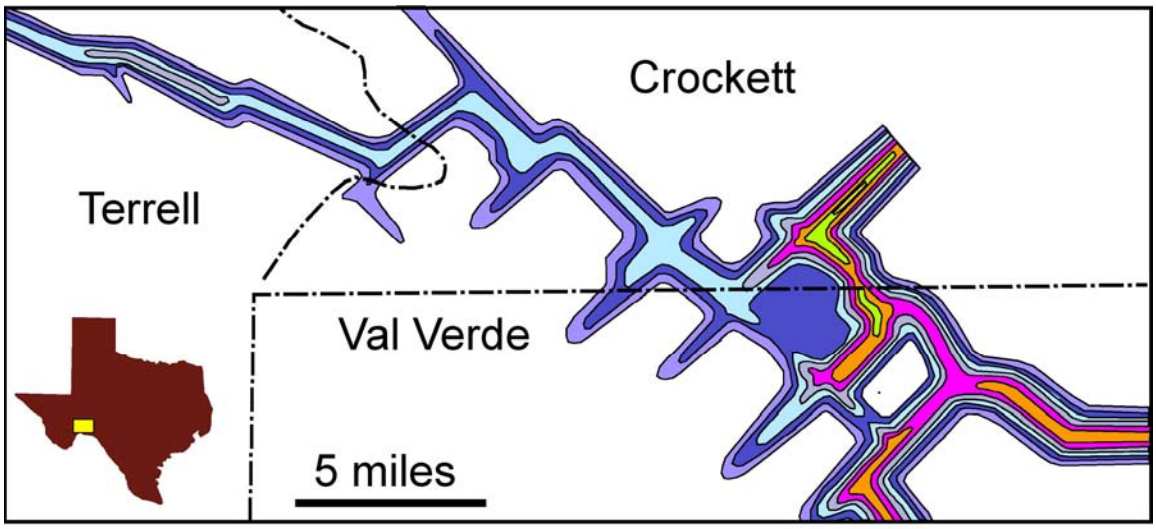

Figure 45. Isopach map of cave-sediment-fill prone interval in Ellenburger Group from wireline logs. The map shows a strong rectilinear pattern that is probably controlled by preSauk unconformity paleofractures. Hot colors are the thicker sections of cave-sediment fill. Figure from Canter et al. (1993).

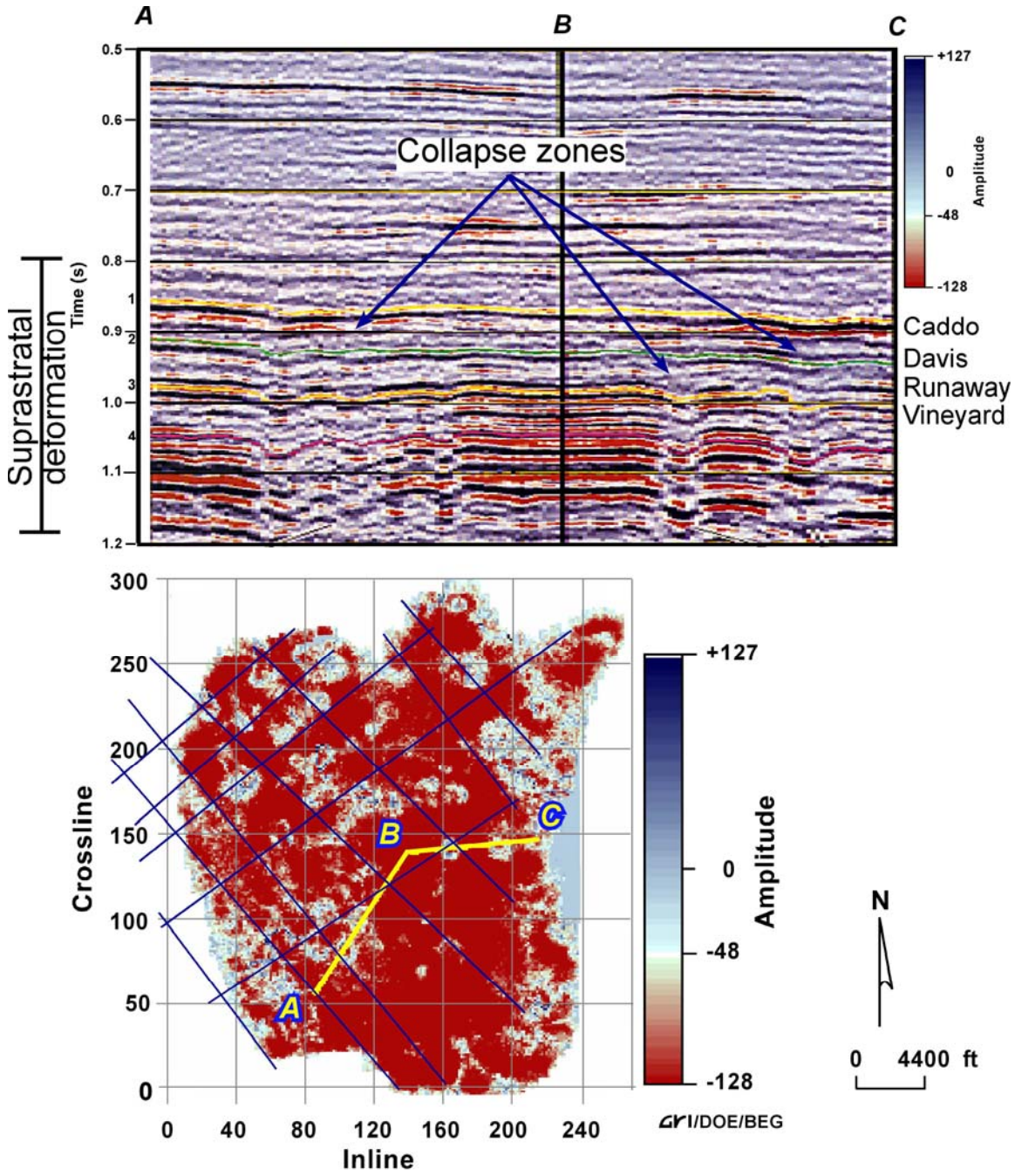

Figure 46. Seismic example of buried collapsed karst features from Boonsville on the line of Jack and Wise Counties in north Texas by Hardage et al. (1996). (A) Seismic profile along line ABC (see figure below), which traverses these collapse zones. Figure was stretched laterally by present author. Zones are up to 2000 ft thick. (B) Seismic reflection amplitude response on the Vineyard surface. The red areas show continuity, whereas the semicircular white areas show disruption of continuity. The white areas are late burial collapse related to karsting of the Ellenburger Group. The blue lines drawn by present author are meant to emphasize the northwest and northeast alignment of the collapse features.

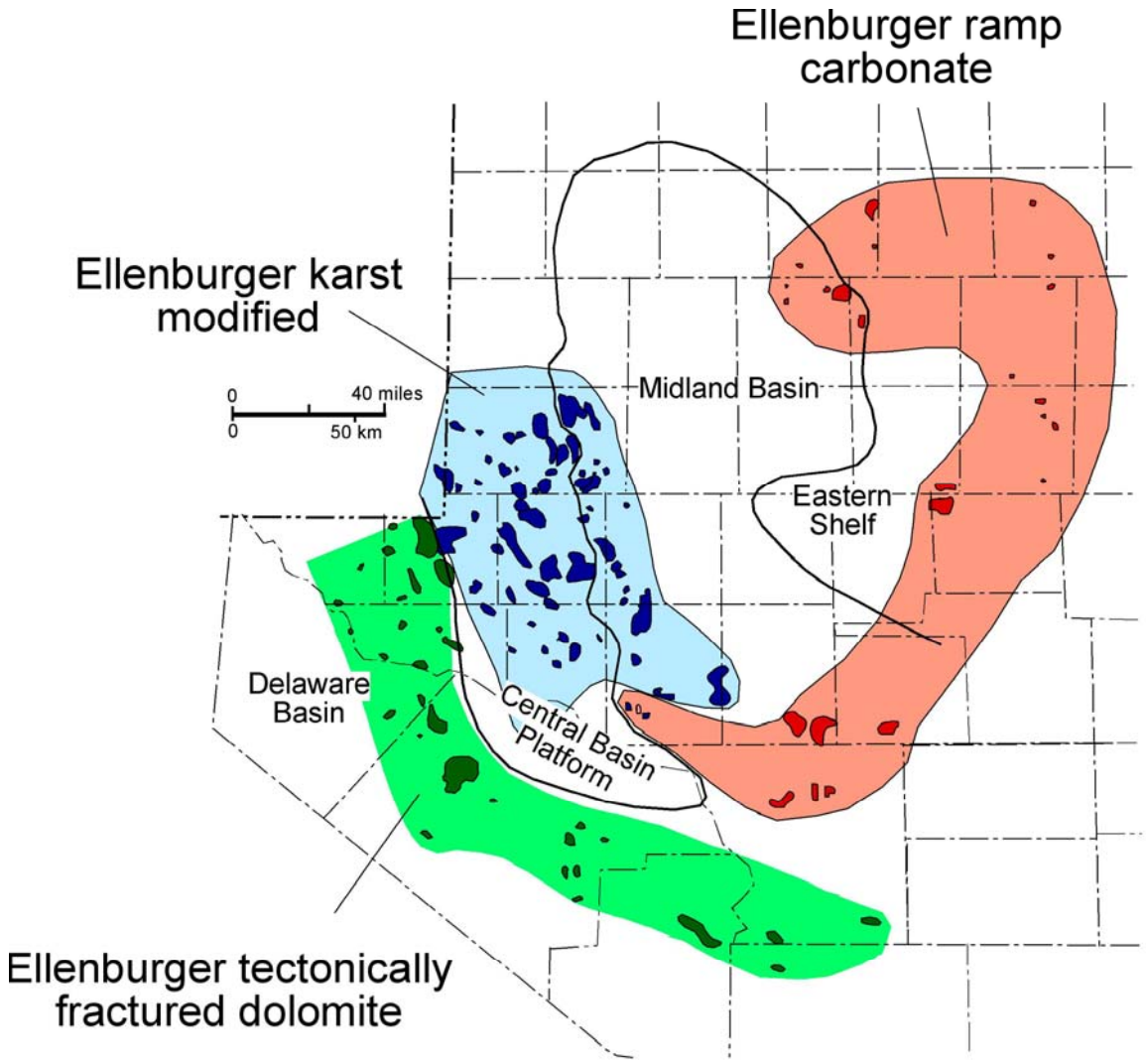

Figure 47. Distribution of Ellenburger Group reservoir types by Holtz and Kerans (1992). Figure modified from Holtz and Kerans (1992).

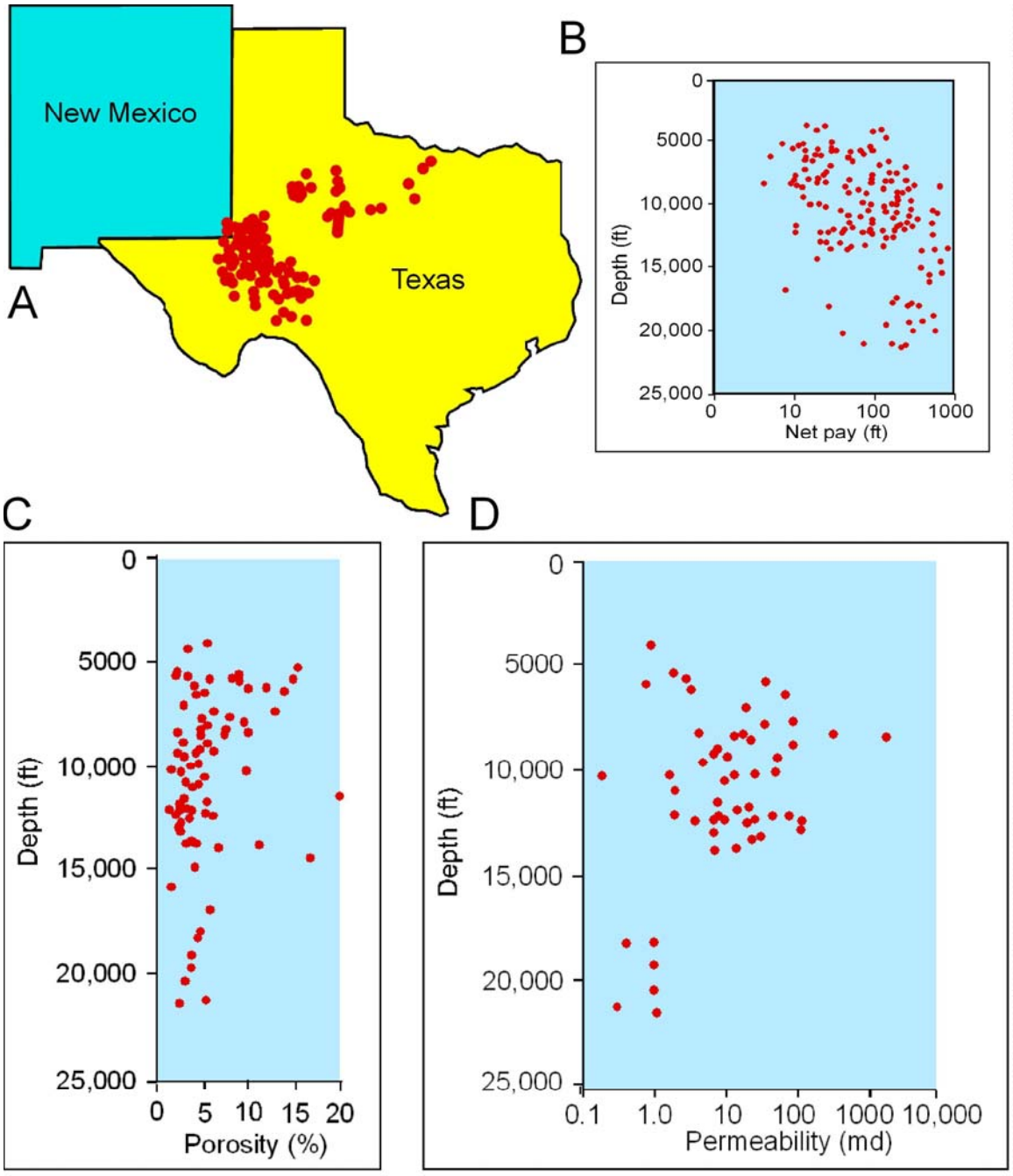

Figure 48. Field data from a 1985 Nerhing database (exact reference not available). (A) Map showing field locations. (B) Thickness of net pay. (C) Average reservoir porosity versus depth. Note most porosity values are 5% of less. (D) Average reservoir permeability versus net pay. Note good permeabilities despite low porosity values.

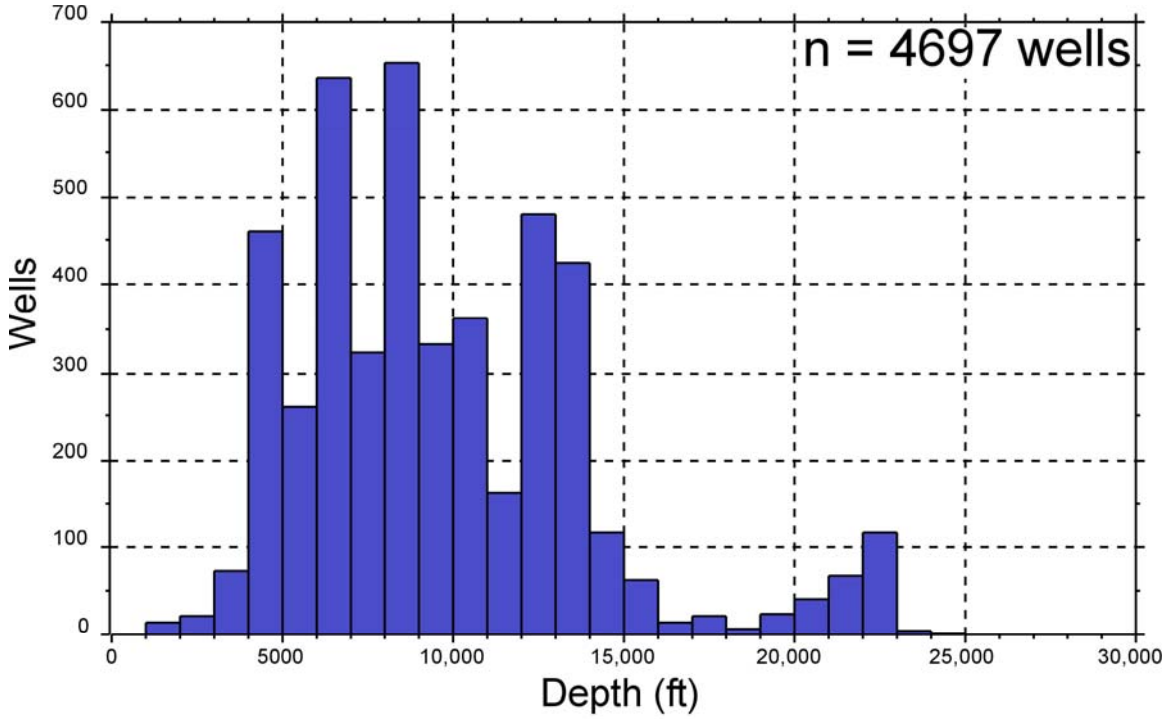

Figure 49. Histogram of productive (past and present) wells drilled into the Ellenburger Group. Producing wells show a range from 856 ft (Originala Petroleum #1 Gensler well in Archer County, Texas) to 25, 735 ft (Exxon Mobil McComb Gas Unit B well in Pecos County, Texas).

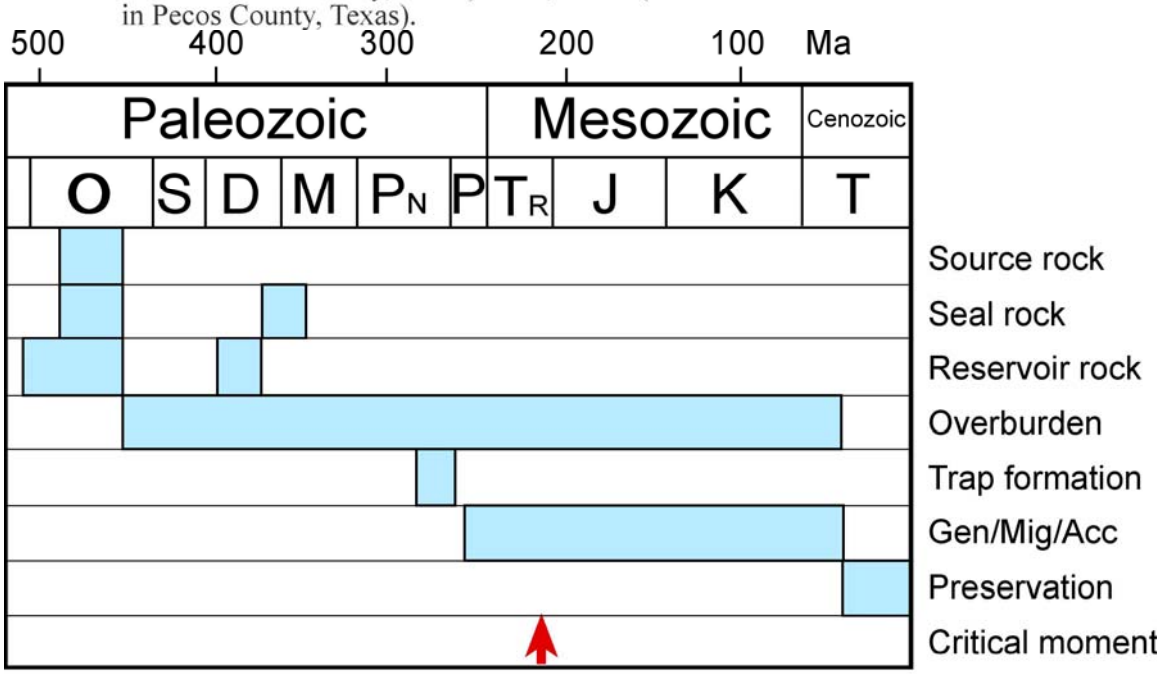

Figure 50. Event chart for the Simpson-Ellenburger petroleum system in the area of the Central Basin Platform showing the temporal relationships of the essential elements and processes. From Katz et al. (1994).

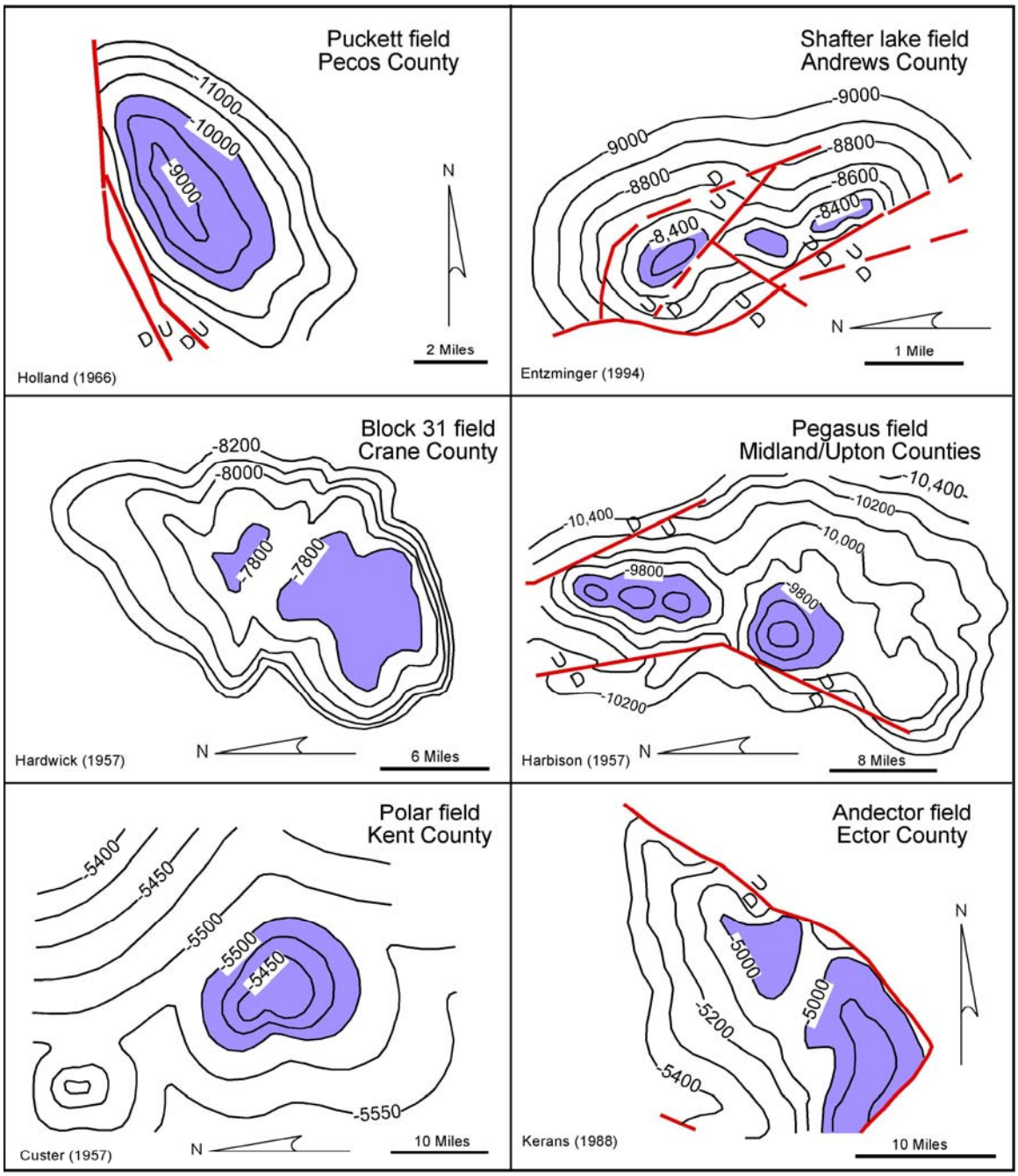

Figure 51. Examples of structural trapping geometries of Ellenburger reservoirs. Structures are relatively simple anticlines or faulted anticlines.

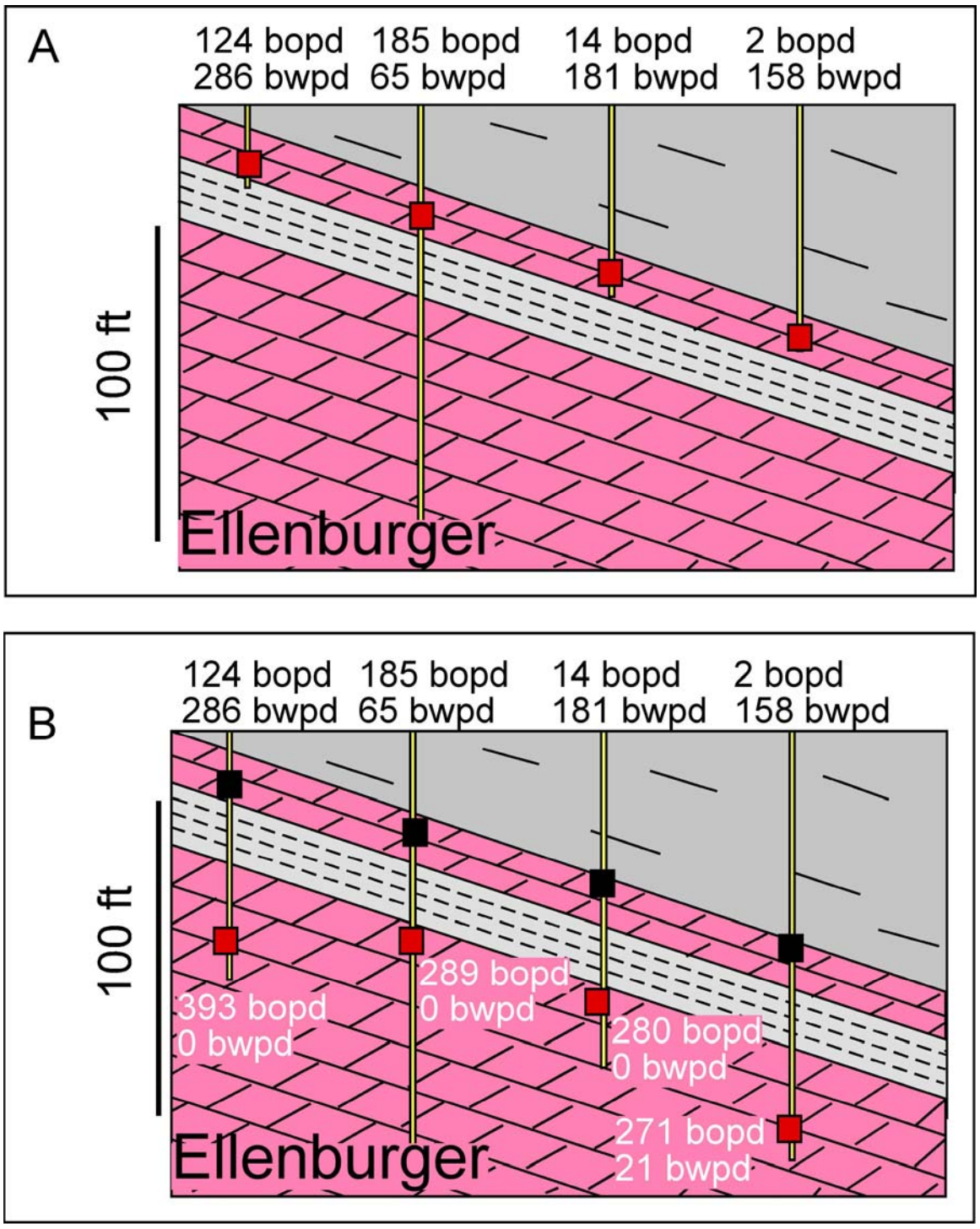

Figure 52. University Block 31 field example form Kerans (1988) that shows permeability barrier within the upper part of the Ellenburger. (A) Initial completions (pre-1977) were above the cave-sediment-prone zone. (B) The wells were deepened after 1977 and new hydrocarbon intervals were encountered.